MINERALOGY AND FLUID INCLUSION STUDY OF THE SAN MATEO VEIN, FRESNILLO DISTRICT ZACATECAS MEXICO

by

Lorie M. Dilley

Submitted in Partial Fullfillment of the
Requirements for the Degree of
Master of Science

New Mexico Institute of Mining and Technology
Socorro, New Mexico
May, 1993

ACKNOWLEDGEMENTS

ABSTRACT

The San Mateo vein is a newly discovered world class bonanza Ag-Au vein located in the Fresnillo mining district, Zacatecas Mexico. Estimated reserves place it second only to the Santo Nino vein, the major producer in the district. The vein contains average grades of 766 g/t Ag, and 1.5 g/t Au and <0.5% base metals. Host rock for the vein is the Chilitos Formation comprising a series of volcanic and sedimentary rocks.

Paragenesis is divided into three stages. Stage 1 is characterized by brecciation and propylitic alteration. Minerals include chlorite, quartz, pyrite, sphalerite, chalcopyrite, and late-stage calcite. Stage 2 is characterized by banding of quartz, pyrite, sphalerite, pyrargyrite, polybasite, chalcopyrite, and galena. Stage 3 is characterized by mineralized breccia fragments. The fragments consist of the same minerals as stage 2 with the addition of native gold and silver, acanthite, marcasite and late stage calcite.

Assay values for Au, Ag, Pb, Zn and Cu were plotted to show metals distribution along the vein. Metal ratios were also plotted. The maps indicate an irregular distribution of Ag and Au along the San Mateo vein. The 425 m. level (lowest level) shows a lower concentration of all metals. Statistical

analysis of assay data indicates that Au and Ag occurs in all 3 stages of mineralization. Linear regression analyses indicate Ag correlates with base metals and Au correlates with Ag and Pb.

Fluid inclusion analysis show that Th's range from 168 ºC to 278 ºC and salinities from 0.0 to 8.2 eq. wt. % NaCl. Measurements were made on inclusions in quartz, calcite and sphalerite. Sphalerite inclusions yielded Th's from 232 ºC to 278 ºC and one salinity of 16.6 eq. wt. % NaCl. Evidence for boiling was observed to be extensive in all stages of mineralization. Plots of Th and salinity versus the paragenetic sequence indicate that each stage of mineralization was accompanied by falling fluid temperatures and increasing salinity. Plots of fluid inclusion histograms against boiling curves indicate that the piezometric head decreased about 300 m.

There is a correlation between the mineralization stages of the San Mateo vein and the stages observed in the Santo Niño vein. The Santo Niño vein consist of four stages of mineralization: stage 1 and 2 are characterized by brecciation, stage 3 by banding and stage 4 by massive calcite. Stage 1 and 2 are ore rich with similar ore minerals. Mineralized stages in the San Mateo are offset. Stage 1 of the San Mateo correlates to stage 2 of the Santo Niño vein, and stage 2 of the San Mateo corresponds to stage 3 of the Santo Niño. Mineralogy is

similar however, gold appears deep in the Santo Niño vein. Gold deposition occurs high in the San Mateo vein and late in the paragenesis.

There appears to be a classic paragenesis in the district with the base metals occurring in the Cerro Proaño area and deep in the Ag veins, and precious metals occurring in the distal margins of the district in the Ag veins. This zoning resulted from an overall lowering of the piezometric head during ore mineral deposition, with fluctuations of the head allowing for the deposition of banded ore minerals and a broad vertical range for the deposition of the precious metals.

TABLE OF CONTENTS

LIST OF FIGURES

LIST OF FIGURES CONTINUED

LIST OF TABLES

PAGE

INTRODUCTION:

The Fresnillo mining district is located approximately 60 km. northwest of the city of Zacatecas in Zacatecas State, Mexico (Fig. 1). It was discovered in the mid-16th century. Mines were worked intermittently in the 18th and 19th centuries, and there has been continuous production since the end of the Mexican Revolution in 1919. Production from 1919 to 1986 is about 10,000 tonnes of Ag, 19 tonnes of Au, 70,000 tonnes of Cu, and more than 700,000 tonnes of both Pb and Zn (Ruvalcaba-Ruiz & Thompson, 1988). Current production is about 60 tonnes of Ag and 0.1 tonnes of Au per month. Most of the exploited ores underlie the Cerro Proaño.

In the mid-1970's exploration southeast of Cerro Proaño revealed several high-grade silver veins, all of which are blind to the surface. Notable among these veins are the Santa Elena, San Ricardo, and Santo Niño, which at present are the principal producers in the district. In 1987, the San Mateo vein was discovered 500-600 meters southeast of the Santo Niño vein. Estimated reserves class the San Mateo as a bonanza Ag-Au vein, second in grade and tonnage only to the Santo Niño vein (Table 1).

Figure 1.   Location of the Fresnillo mining district, Zacatecas, Mexico.

TORREON

SALTILLO

C DEL ORO

GF

DURANGO

RIO GRANDE

SOMBRERETE

FRESNILLO

AIRPORT

ZACATECAS

SAN LUIS POTOSI

AGUASCALIENTES

GUADALAJARA

SCALE

kilometers

MEXICO CITY
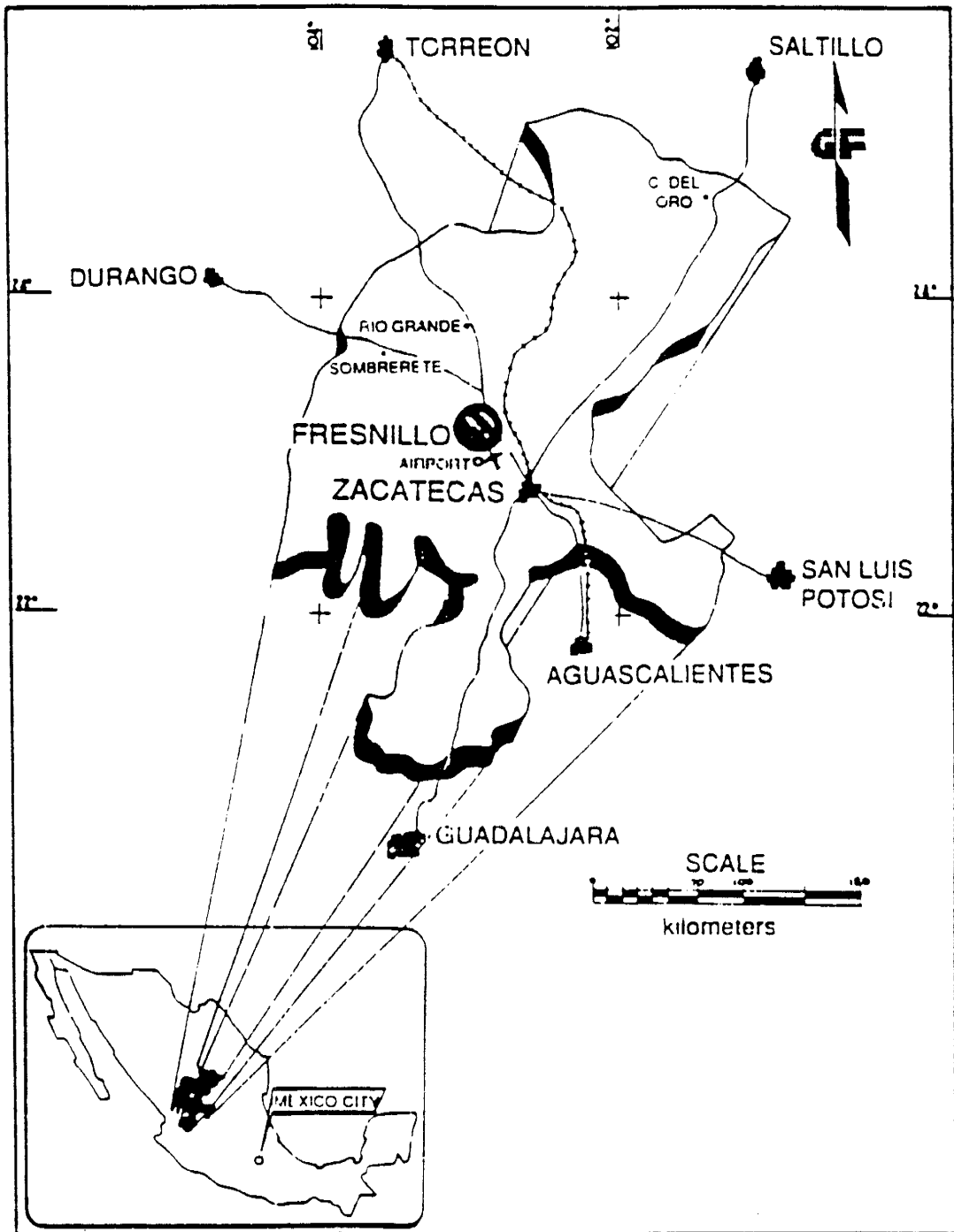
Table 1.   Ore grades and tonnages from reserve estimates and past production.

ASSAYS

VEINS	METRIC TONS	Au (ppm)	Ag (ppm)	Pb (%)	Zn (%)	Cu (%)
SANTO NINO	1,072,800	1.6	756	1.0	1.8	0.06
SAN MATEO	993,000	1.5	766	0.2	0.5	0.02
SAN RICARDO	599,800	0.3	687	0.3	0.6	0.02
SANTA CRUZ	495,000	0.3	955	0.1	0.2	0.01
SAN EMETERIO	452,000	0.8	546	0.2	0.4	0.03
SANTA PAULA	296,000	0.6	977	0.2	0.3	0.02
SANTA INOCENCIA	198,600	0.4	577	0.5	0.7	0.02

<u>Purpose:</u>

The San Mateo vein is a major discovery in the Fresnillo District, and has a mining history of about 2 years. It contains significant gold that has local grades of >10 ppm. The Santo Niño vein has produced little gold until recently, when significantly higher grades were discovered deeper in the vein. Purpose of this study was to conduct detailed geologic and fluid inclusion studies on ores accessible in underground workings augmented by samples from drill core. Objectives of these studies were to determine:

    1. mineralogy and paragenesis of the vein,

    2. the occurrence of gold within the vein,

    3. how the San Mateo vein compares to the Santo Niño vein,

    4. how the San Mateo vein fits into the district.

GENERAL GEOLOGY:

District geology and structural history of the district has been described by several researchers (DeCserna, 1971; Simmons, 1986; Lang et al, 1988; Querol and Palacios, 1990; and Garcia et al, 1991). The Fresnillo district lies on the Mexican Plateau between the Sierra Madre Oriental to the east and Sierra Madre Occidental to the west (Fig. 2). The mine is located in a thick sequence of Cretaceous marine sedimentary and submarine

Figure 2.   Location of the Sierra Madre Oriental and the Sierra Madre Occidental in relation to the Fresnillo mining district. The state of Zacatecas is outlined.

Sierra Madre
Oriental

San Martín   Mexican Plateau

SOMBRERETE

FRESNILLO

ZACATECAS

REAL DE
ANGELES

Pinos

Sierra Madre Occidental

0   50   100
K m.
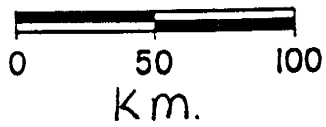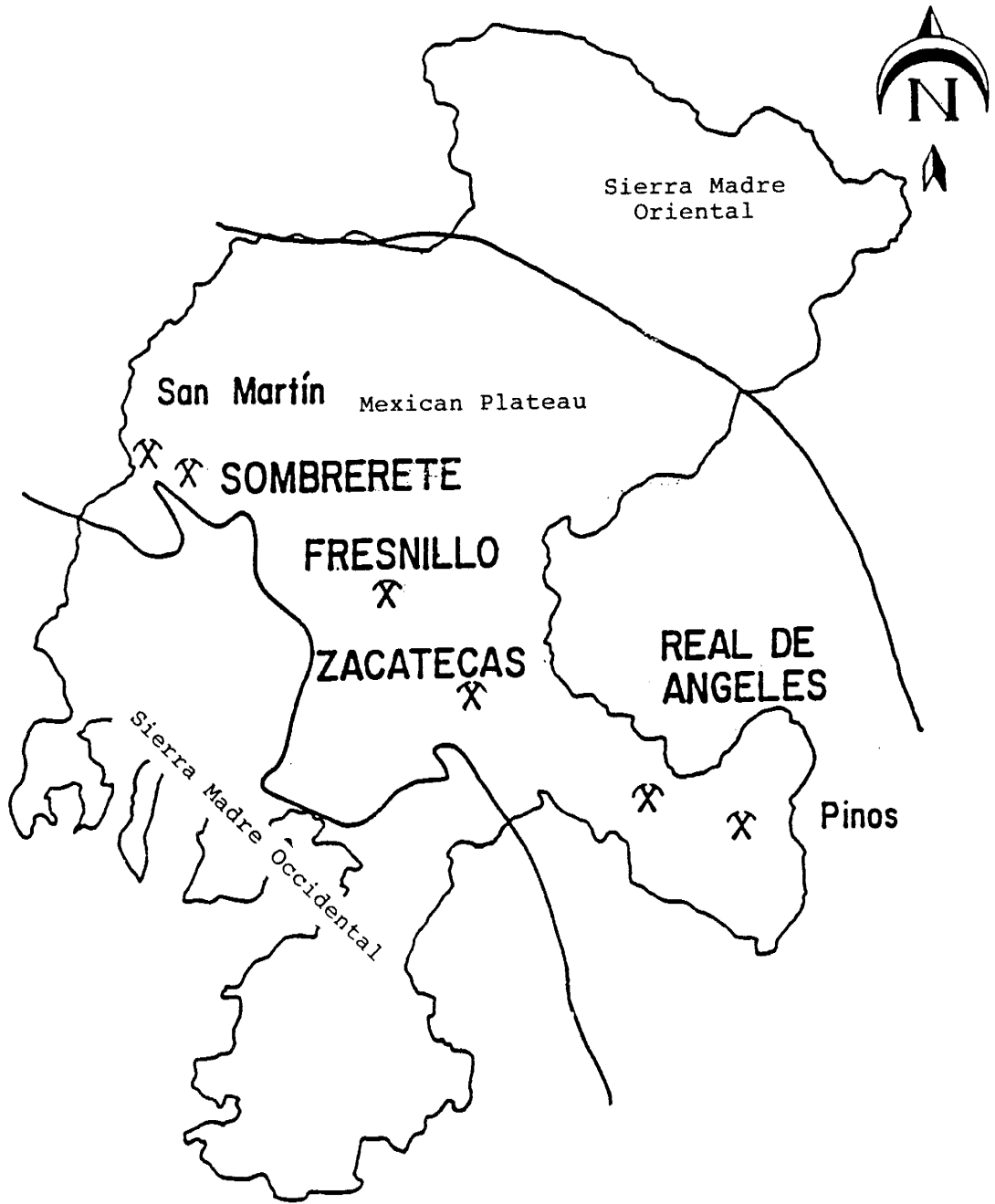
volcanic rocks, which are uncomformably capped by Tertiary felsic volcanics and continental sediments (Fig 3). Outcrops are poor in the district with Quaternary units of alluvium and caliche covering much of the Mesozoic lithologies (Fig. 4). Intrusive rocks in the district consist of a quartz monzonite, granodiorite and quartz trachyte. Andesite and rhyolite dikes are also present in the district.

Stratigraphy:

The Proaño Group (Early Cretaceous) can be subdivided into three mappable units: a lower graywacke, calcareous and carbonaceous shales, and an upper graywacke. The Valdecanas Formation encompasses the lower graywacke unit while the Plateros Formation consists of the other two units. Based on fossil evidence and the lithology of graywackes and shales, a marine origin has been established for the Proaño Group (De Cserna,1976).

The lower graywacke consists of a rhythmic sequence of thinly-bedded, light, greenish-gray graywacke interbedded with thinly-bedded, medium to dark, gray shale (DeCserna, 1976). The shales are carbonaceous and calcareous with discontinuous beds and lenses of dark gray micrite. This formation can only be seen in the deeper levels of the mine and may be over 1000 m thick (Simmons, 1986).

Figure 3.   Stratigraphic column of Fresnillo district.

Stratigraphy of the Fresnillo District

Alluvium & Caliche	0-20 meters
Basalt	30 meters
Felsic Volcanics: Rhyolites & Ash flow tuffs	500 meters
Fresnillo Formation Conglomerates	0-300 meters
Fortuna & Cerro Gordo Limestones	800 meters
Granodiorite 32.2 ma	
Chilitos Formation Andesitic Flow Breccias & Pillow Lavas	400 meters
Proaño Group: Plateros Formation: Upper Graywacke	500 meters
Porphyritic Rhyolite 33.5 ma	
Proaño Group: Plateros Formation: marls & shales	300 meters
Proaño Group: Valdecañas Formation: Lower Graywacke	>1000 meters
Quartz Monzonite 32.4 ma	

TERTIARY

MESOZOIC

Figure 4.   Geologic map of the Fresnillo district (after an in-house report).

Legend:

Tb — Basalt
Tr — Tertiary Rhyolites
Kcc — Quartz Monzonite
Kcc — Cuesta del Cura Formation
KCh — Chilitos Formation
KGs — Proano Group-Graywacke
KLc — Proano Group-Calcareous Lutite

— — — Contacts
——— Veins
=== Roads

0   2.5   5
K m.
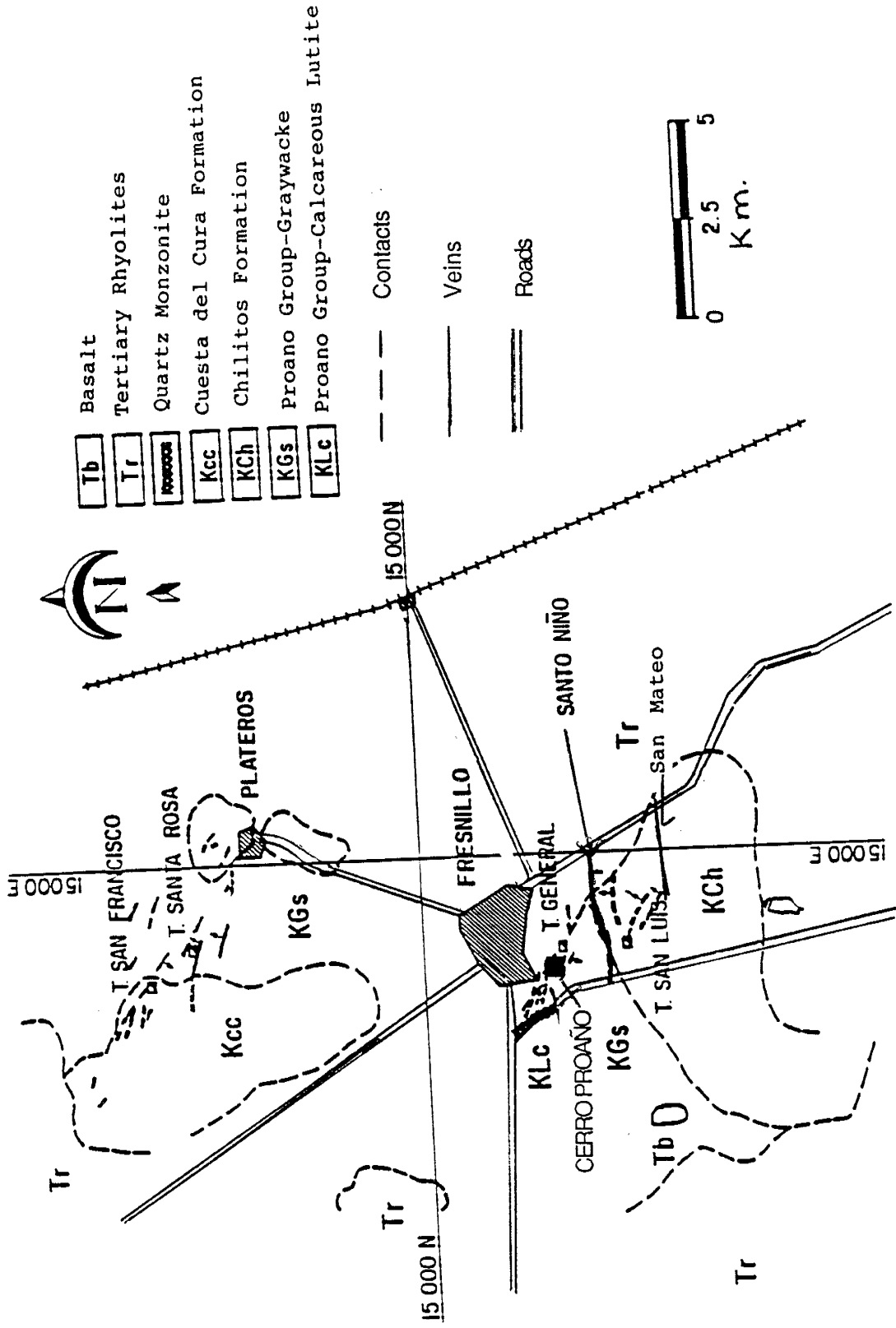
The Plateros Formation consist of a 150-300 m thick sequence of micrites and dark gray, laminated, carbonaceous shales (lutite), and a 200-500 m thick sequence of greenish-gray graywacke alternating with dark gray, carbonaceous and calcareous shales (De Cserna, 1976 and Simmons, 1986). Radiolaria in the upper graywacke are Early Cretaceous in age (Garcia, 1991).

The Chilitos Formation consists of pillowed, greenstone basalts; dark green andesitic flow breccias and clastic marine sedimentary rocks including marls and shales (Simmons, 1986, and Ruvalcabe-Ruiz, 1988). Chlorite, celadonite and calcite have replaced primary minerals in the green, mafic volcanics, indicating hydrothermal alteration (Simmons, 1986). This formation outcrops in the Arroyo Chilitos. Its stratigraphic position is controversial. De Cserna,1976, correlates the Chilitos Formation with Upper Triassic greenstones in Zacatecas, however, andesitic flow breccias which host part of the Santo Niño vein and all of the San Mateo vein, lie conformably above the upper graywacke of the Plateros Formation (Ruvalcaba-Ruiz, 1988, and Garcia, 1991).

The Cuesta del Cura Formation is correlative with the Fortuna Limestone and the Cerro Gordo Limestone (Ruvalcaba-Ruiz, 1988). These limestones outcrop in the district but are not present in the mine. The Fortuna Limestone is a 500-m thick sequence of thin to medium-bedded, dark gray carbonates

(Ruvalcaba-Ruiz, 1988). The Cerro Gordo is a 300 m sequence that is lithologically similar.

The Fresnillo Formation unconformably overlying the Chilitos Formation consists of a continental conglomerate that grades upward into an arkose and tuff unit. The conglomerate is dominated by angular to subangular fragments of lower Mesozoic rocks, including limestones, shales and graywackes in a sand and silt matrix (Garcia, 1991, De Cserna, 1976).

A 500-m thick unit of volcanics overlies the Fresnillo Formation. Volcanic breccias, tuffs and pyroclastic flows comprise this unit (Garcia, 1991). A small unit (30 m thick) of olivine basalt overlies the felsic volcanics (De Cserna, 1976). The whole-rock K-Ar ages for the basal unit (a welded tuff) and the uppermost felsic unit (a porphyritic rhyolite) was determined to be 38.3 ± 0.8 Ma and 27.4 ± 1.5 Ma, respectively (Lang et al, 1988). Quaternary deposits of allivium and caliche up to 30 m thick cover much of the area.

Intrusive Rocks:

The intrusive rocks in the district consist of quartz monzonite, porphyritic granodiorite and quartz trachyte. Quartz monzonite can be seen in the Fortuna mine and as a poor outcrop. It lies adjacent to the manto and chimney bodies in the lower graywacke at the 1030 m level (Simmons, 1986). A minimum age

of 32.4 ±0.8 ma has been determined for the quartz monzonite from whole-rock K-Ar age dating method (Lang et al, 1988).

A small amount of porphyritic granodiorite cutting the Fortuna Limestone is exposed northwest of Plateros (Fig. 4). It consist of a medium grained hornblende and other ferromagnesian minerals (DeCserna, 1976). Variable degrees of hydrothermal alteration associated with quartz-sulfide bearing veins can be seen in the intrusion (Simmons, 1985). A K-Ar whole-rock minimum age of 32.9 ±0.7 ma has been reported (Lang et al, 1988). Southwest of Plateros, porphyritic quartz trachyte occurs in dump material that has a reported whole-rock, K-Ar age of 33.5 ± 0.8 (Lang et al, 1988). Andesite dikes up to 1 meter in thickness are exposed in Fresnillo mine workings (Ruvalcaba-Ruiz, 1988). In addition, several rhyolite dikes crosscut the Mesozoic rocks in the district and are thought to be related to the Tertiary rhyolitic pyroclastic flows (De Cserna, 1976).

Structure:

Folding and faulting as a result of compressional forces associated with the Laramide orogeny, deformed the Cretaceous rocks in the Fresnillo district (Campa & Coney, 1983). The main structure that resulted is an anticlinorium trending N 10º E which plunges to the south (Garcia, 1991).

During the middle to late Tertiary, block faulting occurred

causing a regional southward tilt. The Fresnillo fault which forms the contact between the Fresnillo Formation and the upper graywacke unit and Chilitos Formation (Gemmel et al, 1988) is a result of this deformation.

Following these events, extensive faulting and fracturing occurred. Two major orientations, N 45º E and ENE to ESE, stand out as hydrothermal fluid conduits (Garcia et al, 1991).

Ore Deposits:

The ore deposits in the district have been classified as: stockwork, disseminated, manto, chimney and vein. Both in tonnage and grade, the major source of ore has been from narrow veins (Querol & Palacios, 1990). The Cerro Proaño area hosts all types of ore that occur in the district; the major types are stockworks and disseminated deposits. The Fortuna area is host to many mantos and chimneys while the bonanza veins are concentrated in the Cerro Populo area (MacDonald et al, 1986).

The stockwork deposit covers an area of 700 by 200 m with an average depth of 60 m. (Garcia et al, 1991). This is formed by seven vein sets that each have a width of 10-150 m. and a strike length up to 300 m. (Querol & Palacios, 1990). Host rocks are the Chilitos Formation and the upper graywacke member of the Valdecanas Formation. Silver sulfosalts, native silver, cerargyrite and native gold are the principle ore minerals. Gangue

mineralization includes quartz, feldspar, clays, sulfide minerals and calcite (Garcia, 1991).

Mantos and chimneys are replacement bodies occurring in the calcareous shale beds of the Valdecanas Formation and tend to occur in fold crests. The Fortuna zone contains at least 6 mantos and two chimneys spatially related to the quartz monzonite intrusion. Average thickness is 10 m., with widths up to 100 m. and depths of 150 m. (Macdonald et al, 1986). The largest manto is the Cueva Santa Branch, produced 1.1 million tonnes of ore at a grade of 65 ppm Ag, 2.2% Pb, 3.3% Zn. Ore minerals are pyrite, sphalerite, galena, chalcopyrite, pyrrhotite, argentite, pyrargyrite, tetrahedrite and magnetite. Chimneys have similar ore but average silver values are 20 ppm higher.

Over 100 mineralized veins are known. There are "heavy" sulfide or Pb-Zn veins, and the "light" sulfide or Ag veins. The Proaño Group graywackes host the majority of the veins; however, they also occur in the Fresnillo Formation and the Chilitos Formation (Garcia et al, 1991). "Heavy" sulfide veins are comprised of pyrite, sphalerite, galena, pyrrhotite, chalcopyrite and arsenopyrite. Silver is present as inclusions of polybasite and pyrargyrite in galena at Ag/Pb ratios of 30 ppm Ag/1% Pb (Table 1) (Querol & Palacios, 1990). The Cueva Santa and 2137 are the most important Pb-Zn veins and have a strike length of about 1 km.

"Light" sulfide veins typically have Ag/Pb ratios of 735 ppm Ag/1% Pb (Table 1). Minerals include pyrite, galena, sphalerite, chalcopyrite, native silver, pyrargyrite-proustite, polybasite and electrum (Querol & Palacidios, 1990). There is a vertical zoning of silver, lead and zinc content, with an increase of lead and zinc at depth. Historically the Ag veins are most productive between the 240 and 425 meter levels. Santo Niño, San Ricardo, Santa Elena, 2270, 2125, Agripo, and Esperanza veins are the important producers in this group (Garcia et al, 1991). San Mateo vein is one of the Ag veins occurring in the southeastern part of the Fresnillo district; its relationship to other veins is shown in Figure 5. Lead-zinc veins are similar to Ag veins on the upper levels. Stone and MacCarthy (1942) report a change in grade from low silver grades at depth to high silver values in the upper levels of the Cueva Santa and 2137 veins between levels 340 m. and 425 m.

Alteration:

Five alteration types are identified in the Fresnillo district: silicic, potassic, phyllic, argillic and propylitic. Alteration is irregular and occurs in narrow zones along the silver-rich veins but is not evident along the veinlets that split away from the main veins (Ruvalcaba-Ruiz, 1988). However, in the Fortuna area and the Cerro Proaño area, alteration is extensive due to

Figure 5. Schematic showing the relative positions of the light sulfide ore bodies in the district. (After an in house map, courtesy of Compania Fresnillo).
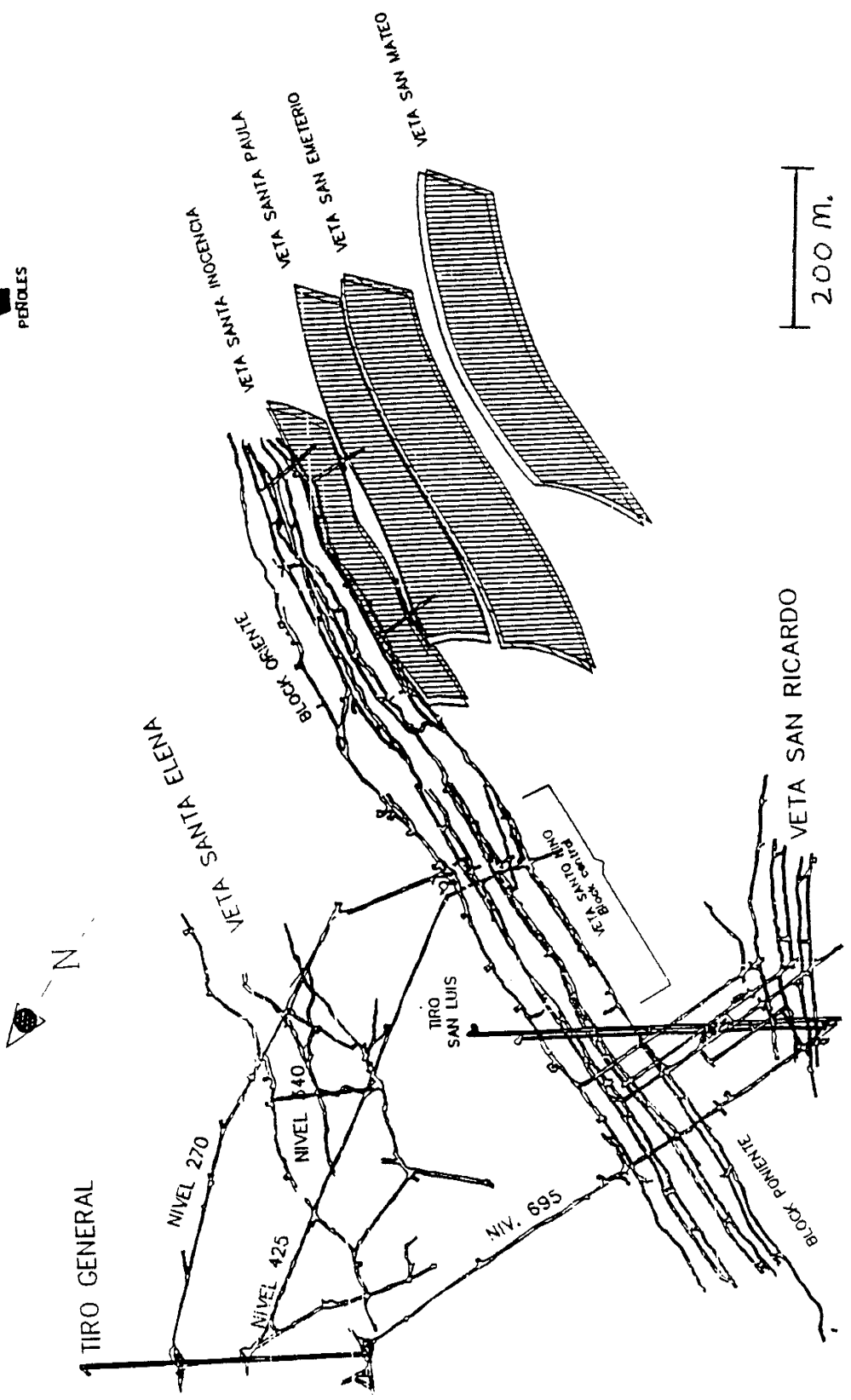
proximity of the quartz monzonite stock and closely spaced fractures and stockwork mineralization in the respective areas (Ruvalcaba-Ruiz, 1988 & Simmons, 1986). The quartz monzonite intrusion is intensely epidotized with associated chlorite, magnetite and disseminated pyrite where it is in contact with manto and chimney bodies. Sediments in contact with the intrusion are intensely silicified (Ruvalcaba-Ruiz, 1988). In the Cerro Proaño area, bleaching and argillic alteration are well developed along veins and grade outward into zones of silicification (Simmons, 1985). Argillic alteration consisting of kaolinite and montmorillonite with pyrite and minor halloysite, sericite, chlorite and epidote, affects andesitic flow breccia, graywacke, and shale units. The width of argillic zones varies from 0.05 to 10 meters.

Phyllic alteration occurs in the immature sandstones that have an abundance of K-feldspar. It is characterized by sericite and pyrite with minor amounts of illite, kaolinite and montmorillonite. The phyllic halo occurs adjacent to silver-rich veins and has a width of 0.01-1.0 meters. Potassic alteration is rare and is characterized by adularia crystals (Ruvalcaba-Ruiz, Thompson, 1988).

Most widespread is propylitic alteration, characterized by the presence of calcite, epidote and chlorite. Depending on intensity and host-rock composition, variable amounts of pyrite, montmorillonite and kaolinite occur. Where it is the sole type,

propylitic alteration exists adjacent to the veins, however, when other alteration assemblages are present, propylitic alteration can occur as much as 4 meters away from the vein (Ruvalcaba-Ruiz & Thompson, 1988). The Chilitos Formation is far more reactive to mineralizing solutions. Chlorites are Mg-rich in breccia fragments in this formation due to propylitic alteration (Gemmel et al, 1988).

Age of Hydrothermal Activity:

A mid-Tertiary age of 46-26 Ma has been suggested by Clark et al (1982) for precious and base metal deposits throughout the Sierra Madre Occidental. Based on whole-rock K-Ar dates, radiogenic ages of 38.4 to 27.5 Ma have been determined for volcanic activity in the Fresnillo area. The pre-32 Ma ages represent an earlier volcanic event. Altered material gives radiogenic ages between 29 and 31 Ma. Fresh volcanics that directly overlie hydrothermally altered rocks have a whole-rock K-Ar ages of 27.5 to 27.7 Ma indicating termination of hydrothermal activity in the Fresnillo district (Lang et al, 1988).

Previous Geochemical Studies:

Previous work considered fluid inclusions, metal zonation and isotopic compositions in order to understand controls on

mineralization (Stone & McCarthy,1948; Chico, 1986; Macdonald et al, 1986; Albinson, 1988; Gemmel et al, 1988; Ruvalcaba-Ruiz & Thompson, 1988; Simmons et al, 1988; Benton, 1991). Simmons et al, 1988, identified three distinct fluids based on oxygen and hydrogen isotopes; a quartz-saturated solution evolved from exchange reactions between country rock and meteoric waters, a calcite-saturated solution derived from a distinct source region and a sphalerite-saturated solution that composed a brine. Helium isotopes suggested the presence of dilute mantle helium. Benton, 1991, stable isotope data suggest an exchanged meteoric fluid and a magmatic fluid were involved in the mineralizing process. Oxygen and sulfur fugacities determined from gases in quartz-hosted fluid inclusions indicate a combination of boiling and mixing of a low salinity fluid with a high salinity fluid.

Fluid inclusion studies on the Fresnillo district (Table 2) include those by Simmons, 1986, on the Santo Niño vein, Ruvalcaba, 1980, and Albinson, 1988, on the Santa Elena, MacDonald, 1978, on the 2200, and Kreczmer, 1977 on chimneys and mantos, and in 1975 on the Cueva Santa 2137. Data indicate that mantos, chimneys, and deep veins formed at higher temperatures (230-444 ºC) and salinities (4-12 eq wt % NaCl) than the Ag veins (190-300 ºC and 0-12 eq wt % NaCl). Fluid inclusion data from the Santo Niño vein indicate drastic changes in the position of the water table during ore deposition (Simmons, 1991, 1986). A total peizometeric change of 200 m. was

Table 2. Summary of Th values and calculated salinities from Tm measurements of inclusions from several ore bodies in the district.

ORE BODY	LEVEL	RANGE IN Th (°C)	SALINITY (eq. wt. % NaCl)	AUTHOR
2200	385-470	260-310	----	MacDonald, 1978
Cueva Santa 2137	875-965	300-360	----	Kreczmer, 1975
Santa Elena	270-425	207-298	0-1.1	Ruvalcaba, 1980
Santo Nino	270	190-250	0-3	Simmons, 1986
Santo Nino	425	220-300	4-12	Simmons, 1986
Santa Elena	425	210-241	0.3-12.5	Albinson
Chimneys & Mantos	------	230-370	4-12	Kreczmer, 1977

determined for the Santo Niño vein. Reconstruction of the stratigraphic column indicate at least 350 m. from the top of the mineralized zone to the paleosurface (Albinson, 1988).

METHODS OF INVESTIGATION:

Samples were collected from underground exposures in the two working levels of the vein at approximately 10 m. intervals along the strike length on the 320 m. level, and at 6 m. intervals along strike on the 425 m. level. At each sampling location 2 or 3 samples were collected representing the footwall, center and hangingwall of the vein (Appendix 1). Each was examined in hand sample and by reflected light microscopy in order to determine mineralogy and paragenesis. Several samples of pyrargyrite, polybasite and sphalerite were analyzed by the SEM (scanning electron microscope) in order to determine if there are variations in chemical composition in those minerals. Concentrations of Ag, Au, Pb, Zn, and Cu and their ratios from assay values were graphed in order to determine areas of high concentrations and validity of hand sample data. Correlations among elements were calculated.

Homogenization and freezing temperatures of fluid inclusions in selected samples were measured in order to determine the nature of the fluids involved in mineralization and in order to compare them with fluid inclusion studies performed on other

veins. A Linkham THMSG 600 stage was used for the measurements.

DATA:

In order to achieve the objectives of this study, data are presented in four sections: geology, mineralogy, sulfide and sulfosalt geochemistry, and fluid inclusion analysis.

GEOLOGY OF THE SAN MATEO VEIN:

The San Mateo vein is a world class bonanza Ag-Au vein with estimated reserves of 993,000 tonnes and average grades of 1.5 ppm Au, 766 ppm Ag, 0.2% Pb, 0.5% Zn and 0.02% Cu. As of September, 1991 a drift of 150 meters had been exposed at the 320 m. level and a drift of 40 meters at the 425 m. level. Based on drilling, the strike length is approximately 1 km. The general strike is N60ºE with an average dip of 60º NW, and host rock is the Chilitos Formation. The dip decreases as the vein approaches the surface. On the surface a stockwork of small veins and veinlets of quartz and calcite including a small mercury deposit is thought to represent the upward development of the vein. Its average width is 2.5 meters ranging between 1.1 and 3.6 meters at the 320 m. level. At the 425 m. level the width of the vein is

fairly constant with an average of 2.3 meters. No evidence for faulting is seen along the vein. Footwall and hanging-wall contacts vary from a sharp, solid contact to altered breccias. Near the beginning of each drift the vein horsetails across the width and then coalesces to a straight trend. On the 320 m. level the vein structure is that of pinching and swelling with some areas containing cymoidal loops. Structure on the 425 m. level is characterized by a straight trend with minor pinching and swelling (Fig. 6).

Alteration is minimal and confined to within a few meters of the vein. The most conspicuous hydrothermal alteration is confined to breccia fragments. Alteration is principally propylization and silicification of variable intensities. Where well developed, propylitic alteration minerals include chlorite, quartz, pyrite and minor calcite. In local areas of silicification, primary minerals are replaced by cryptocrystalline quartz such that little of the original textures remain.

MINERALOGY:

The San Mateo vein is comprised of varying proportions of gangue, sulfide minerals, sulfosalts and native elements. Mineralization occurs as disseminations within quartz bands, in asymmetrical and symmetrical banded veins, and as breccia fragments.

Figure 6.　Examples of vein textures seen within the San Mateo

vein.　Both photographs represent approximately 2

meters of the vein.

a. Brecciation, banding and cymoidal loop on

the 320 m. level.

b. Brecciation and minor bands on the 425

m. level.

A

B

Three stages of mineralization can be defined from mineral assemblages, brecciation and textural relationships of open-space filling. These are well developed in mineralization observed on the 320 m. level, but less so in workings on the 425 m. level. Paragenesis for the vein as a whole is defined by these 3 clearly repeating cycles of mineralization (stage 1, stage 2, and stage 3). Each stage is a repeat of quartz and minor sulfides followed by introduction of massive sulfides and sulfosalts (when they occur), with a late stage of quartz and minor sulfides and sulfosalts. A paragenetic sequence was developed for each stage from cross-cutting relationships, grain overgrowths and replacement textures seen in polished sections.

Sulfide minerals generally occur in fine to medium crystals but are rarely coarsely crystalline. They include pyrite, sphalerite, galena, chalcopyrite, minor argentite and trace amounts of marcasite. Chalcopyrite occurs as inclusions in sphalerite and pyrargyrite as well as in discrete grains (Fig. 7). Sulfosalts are pyrargyrite and polybasite. Native silver commonly occurs associated with the polybasite. Gold was observed as small grains associated with chalcopyrite and pyrargyrite (Fig. 7). Sulfide minerals occur in all stages whereas sulfosalts are observed only in stage 2 and 3, and the native elements only in stage 3. However, sulfide and sulfosalts minerals always occur in similar paragenetic sequence, with pyrite and sphalerite being deposited initially.

Figure 7.   Photomicrographs of mineral association.

    a. pyrargyrite and sphalerite with chalcopyrite disease. The pyrargyrite grain in the upper left hand corner is 75 μ in diameter.

    b. Pyrite grain rimmed by pyrargyrite with chalcopyrite and galena inclusions. The pyrargyrite is 25 μ in diameter.

    c. Gold in association with chalcopyrite, pyrargyrite, polybasite and galena. The gold grain is 7.5 μ across.

    d. Native silver in association with polybasite. Silver appears to overgrow the polybasite. The entire grain is 10 μ in diameter.

A — Pyrargyrite, Sphalerite, Chalcopyrite

B — Pyrite, Pyrargyrite, Galena, Chalcopyrite

C

Pyrargyrite

Gold

Chalcopyrite

Polybasite

Galena

D

Silver

Polybasite
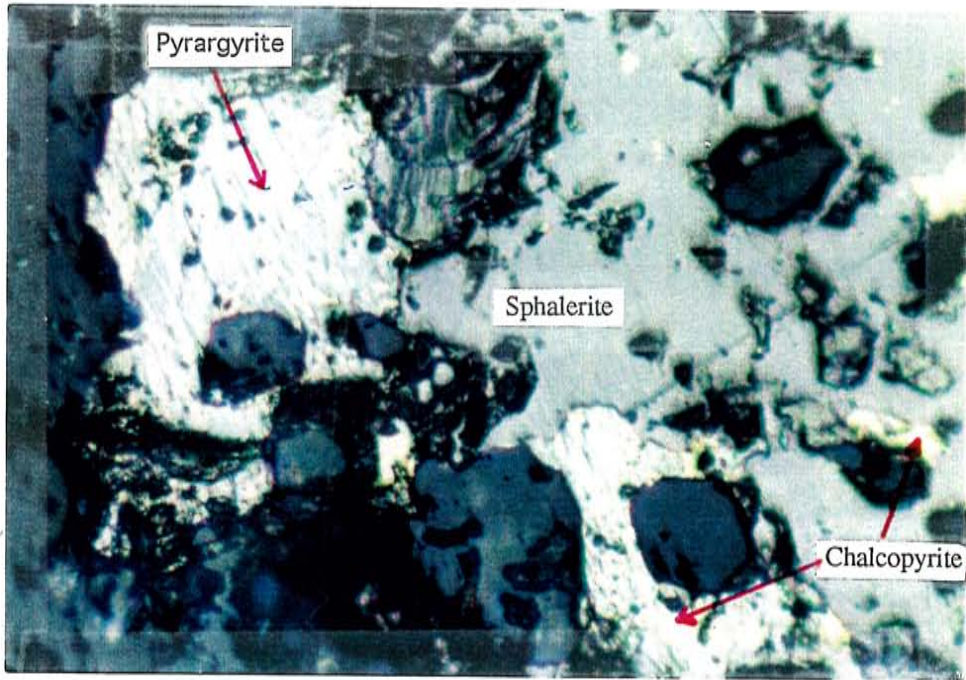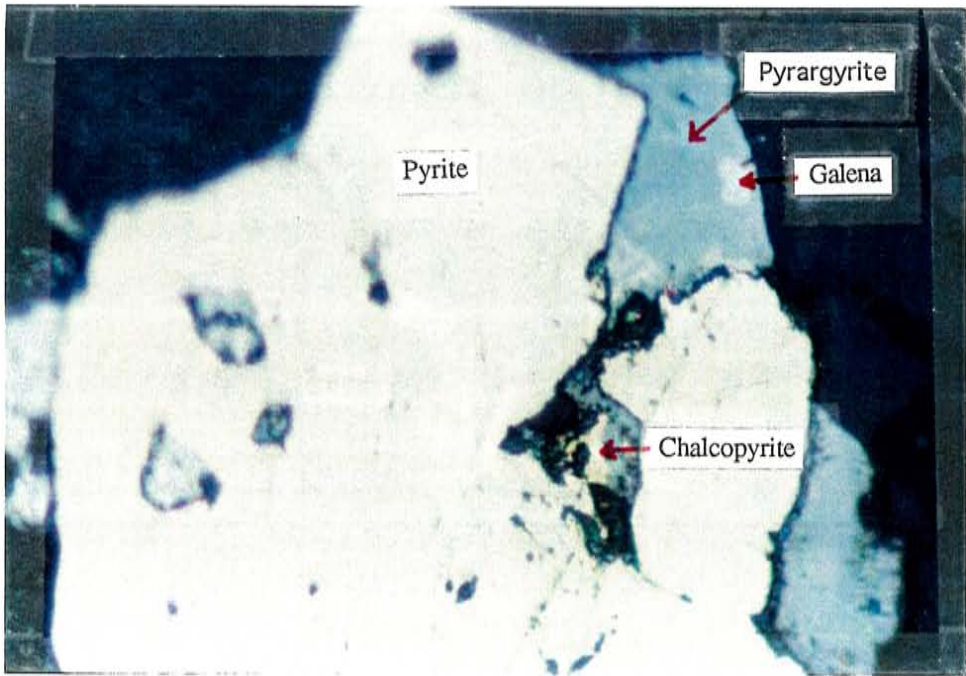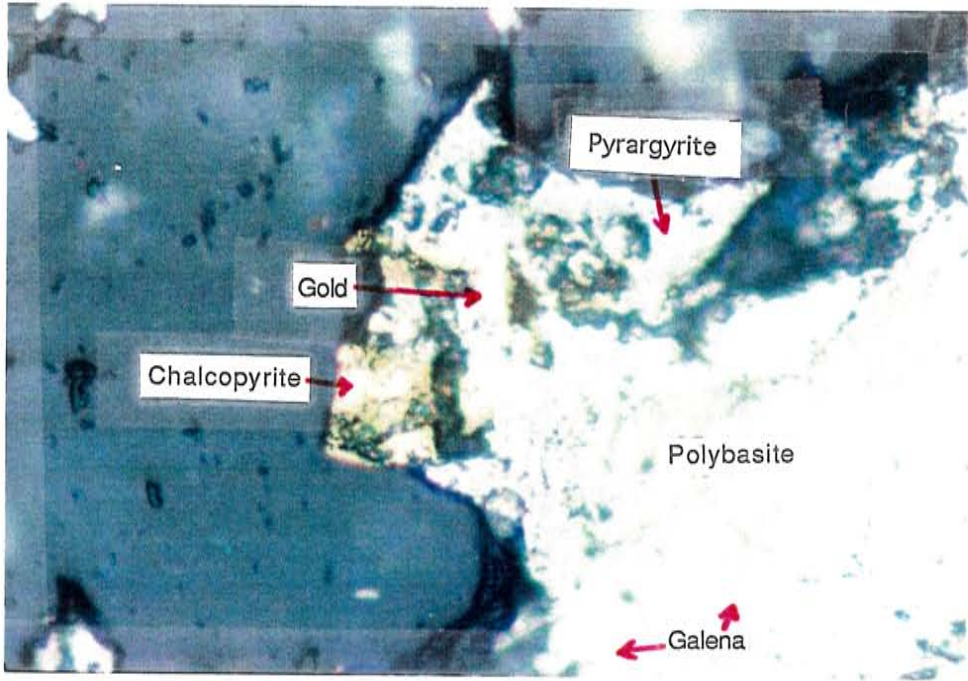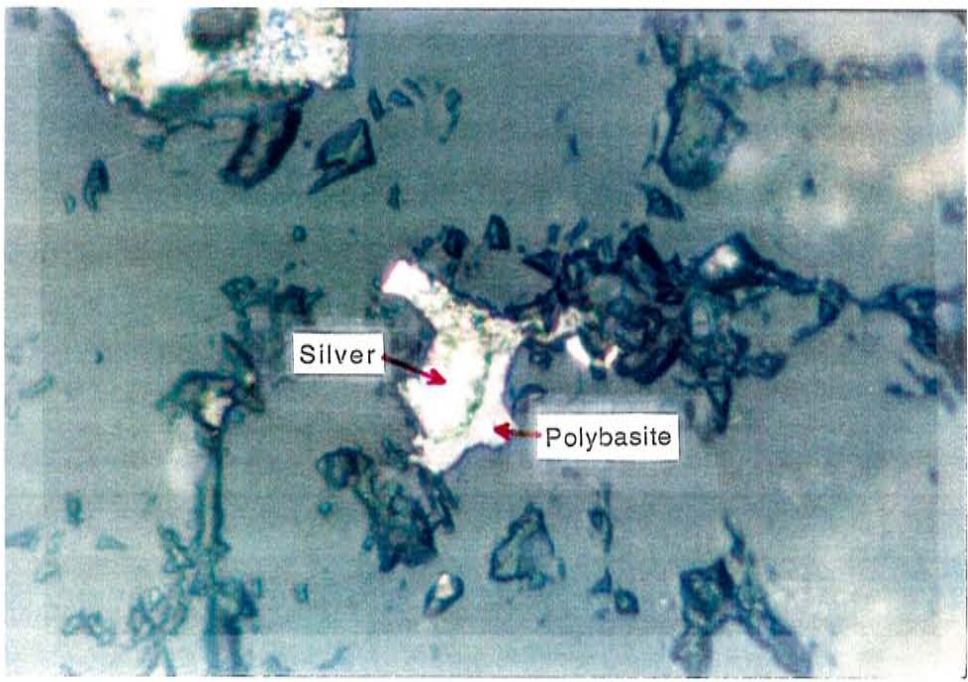
Gangue minerals consist of quartz, chlorite, and minor calcite. There are several varieties of quartz ranging from finely laminated chalcedony to coarse subhedral crystals in colors of white, gray, light blue, amethyst, rose and dark gray. Amethyst quartz is prevalent at the 425 m. level. Light gray to white, massive quartz with disseminated sulfide minerals is more abundant than banded quartz. Bands of quartz are parallel to subparallel to the vein margins and vary from 0.5 mm to 3 cm and are discontinuous laterally and vertically. Chlorite occurs as an alteration product of host rock and as such, occurs as fragments and host to mineralization. Sulfide minerals commonly occur as rims around chlorite fragments. Calcite occurs in yellow and white bands as well as in coarse subhedral crystals as a late stage vug filling.

Stage 1:

Stage 1 (Fig. 8) mineralization is associated with the initial vein opening event and is seen in both levels of the San Mateo vein. It is well developed along the hanging wall on the 320 m. level and on the footwall on the 425 m. level and varies in width from 0.5 m to 2.5 m. In some localities it is the only stage observed.

This stage is accompanied by the fracturing and brecciation of the wallrock. Wallrock consisting of andesite breccia is

Figure 8.   Stage 1 paragenetic sequence. Dotted lines indicate
minor occurrences.

STAGE 1
MINERALIZATION

QUARTZ

CHLORITE

PYRITE

SPHALERITE

CHALCOPYRITE

AMYTHEST

CALCITE

TIME
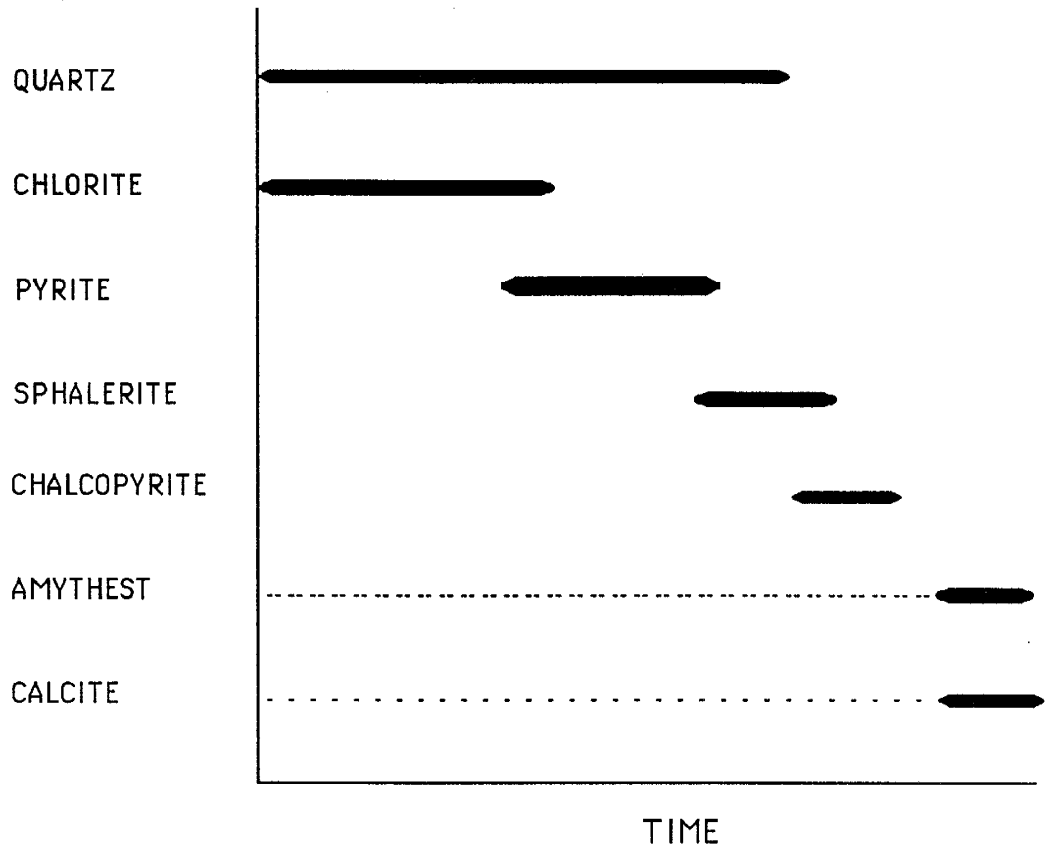
propylitically altered. Fragments of wallrock occurring in stage 1 mineralization are mainly composed of chlorite and quartz. Mineralization interstial to wallrock fragments consists of sulfide minerals within light to dark gray quartz. Sulfide minerals are also disseminated within the chlorite and as small stringers around fragments and along fracture boundaries. Pyrite is the main sulfide mineral and ranges in size from fine grain to medium grained (<1 cm). Sphalerite and chalcopyrite are typically very fine grained. Amethyst is common in this stage on the 425 m. level but restricted to vugs on the 320 m. level. Calcite is only a minor component of stage 1 mineralization and is the last mineral to form.

Stage 2:

Stage 2 is volumetrically the most important stage. It is best developed along the footwall and center of the vein on the 320 m. level and just in the center of the vein on the 425 m. level. It varies in width from 0.0 up to 3.0 m.

This stage is characterized by two types of mineral banding. The early part of this stage consist of symmetrical bands paralleling vein margins. Bands are typically thin (1-5 mm) and generally consist of pyrargyrite with or without pyrite, gray quartz and yellow calcite (Fig. 9). Symmetrical bands occur in

Figure 9.   Photographs of polished sections of hand samples

from the San Mateo vein showing textural

characteristics of the 3 stages of mineralization.

a. Sample from the 320 level. Mineral banding

common to stage 2 mineralization occurs on

the left side of the sample. Breccia characteristic

of stage 3 mineralization is seen on the right side

of the sample.

b. Sample from the 425 level. The dark material is

chlorite characteristic of stage 1 mineralization.

The white bands are quartz replacements of calcite

blades from stage 1 mineralization.

A

Stage 2
Banding

Stage 3
Breccia

0   1   2
inch

B

Quartz
replace
calcite
blades

Stage 1
Chlorite

Stage 1
Chlorite

0   1   2
inch
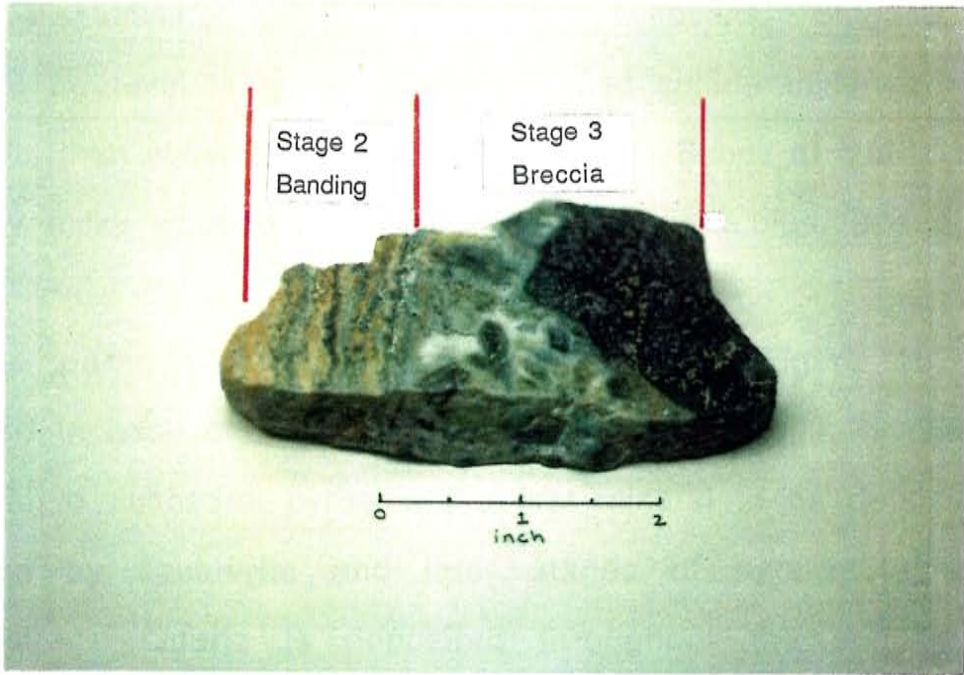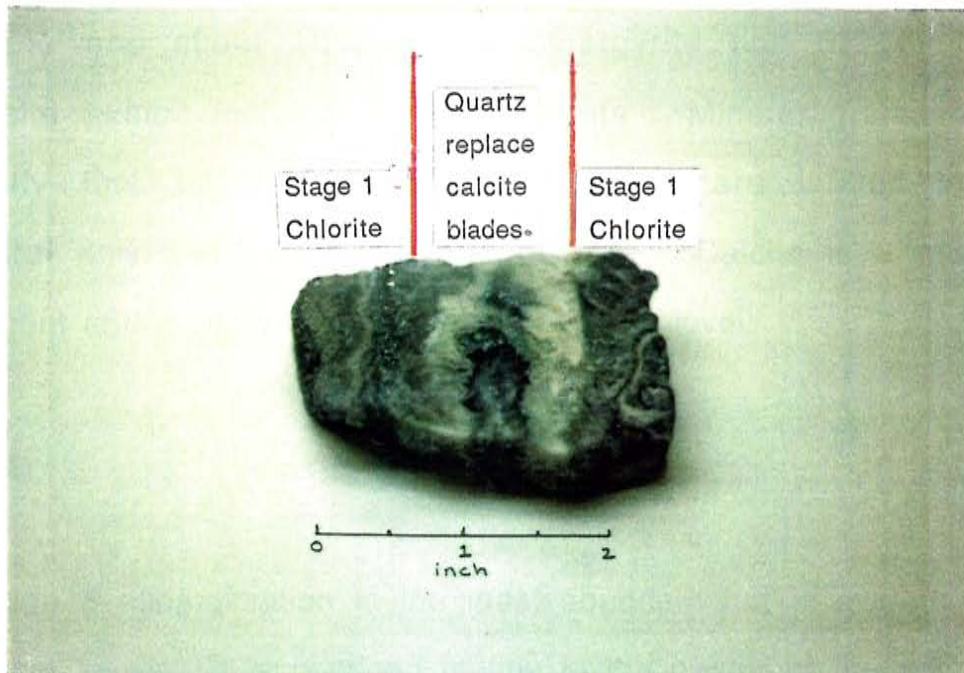
contact with stage 1 mineralization on the 320 m. level (Fig. 9). Later stage 2 mineralization consists of banded quartz with or without disseminated sulfide minerals and sulfosalts. Stage 2 on the 320 m. level is richer in disseminated sulfide minerals and sulfosalts than observed on the 425 m. level. Bands of quartz are typically milky white but can be light gray, light blue, and dark gray.

The paragenetic sequence summarized in Figure 10, is repeated in each of the bands that characterize stage 2. Early euhedral to subhedral pyrite is the first mineral to be deposited followed by sphalerite and later stages of pyrargyrite and polybasite. Quartz is deposited throughout the sequence. Chalcopyrite and galena are the last sulfide minerals in this stage. Chalcopyrite was observed as minor grains within sphalerite, pyrargyrite and polybasite. Approximately 40% of the sphalerite and about 10% of the pyrargyrite and 5% of the polybasite exhibit inclusion of chalcopyrite. Mineral grains are generally fine to medium grained. Vugs are infilled with subhedral amythest or clear quartz crystals. Calcite is a minor component and is observed only on the 425 m. level.

Stage 3:

Stage 3 mineralization is the least abundant but is evident on both mine levels. It is confined mainly to the center of the vein

Figure 10. Stage 2 paragenetic sequence. Notice the presence of sulfosalts in stage 2 as opposed to stage 1 mineralization.

STAGE 11

MINERALIZATION

QUARTZ

PYRITE

SPHALERITE

PYRARGYRITE

POLYBASITE

CHALCOPYRITE

GALENA

AMYTHEST

CALCITE

TIME
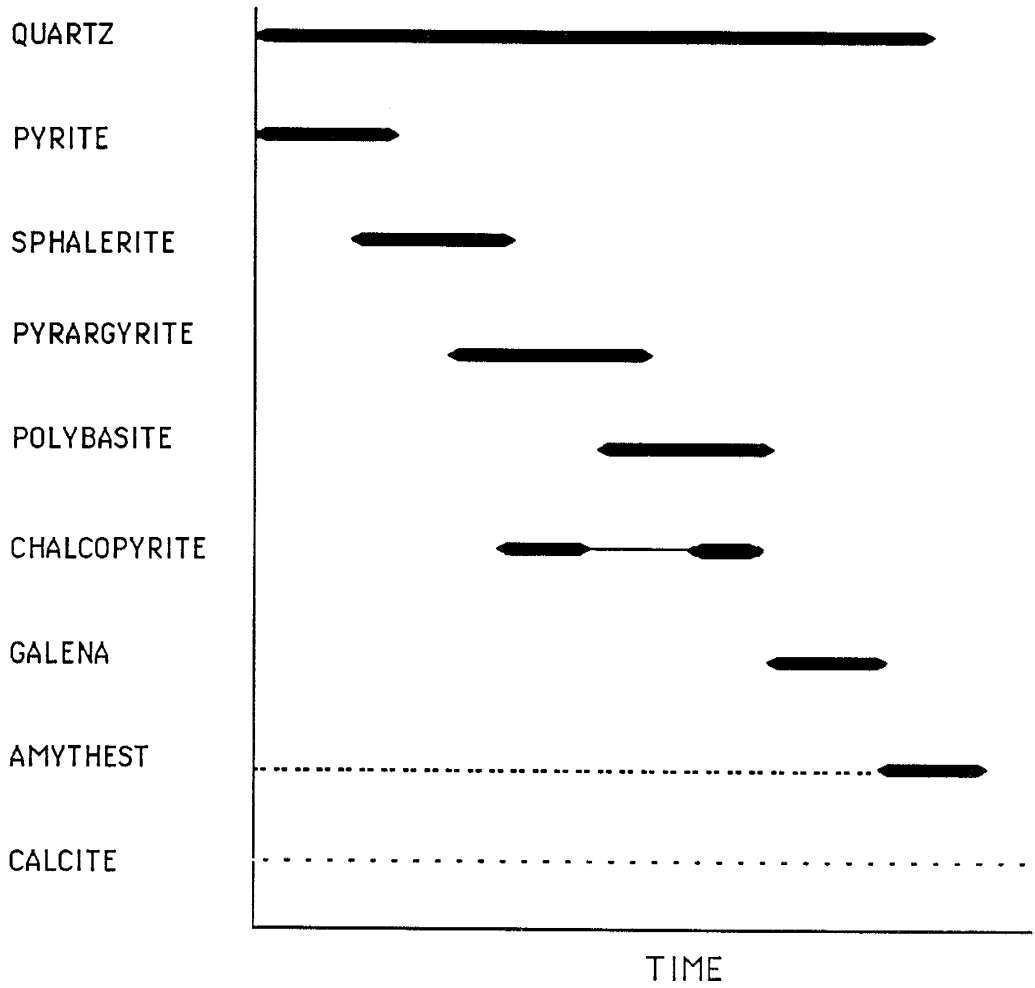
and can be up to 1.0 meters wide. Stage 3 mineralization consists of mineralized light gray to clear, dark quartz that on the 320 m. level contains mineralized breccia fragments. These range in size from 3-40 mm in diameter (Fig. 9). Stage 3 mineralization generally occurs within that of stage 2.

The paragenetic sequence is similar to stage 2, but differs in the occurrence of several more minerals (Fig. 11). Quartz is deposited continuously. Early euhedral to subhedral pyrite is intergrown with sphalerite. pyrargyrite follows sphalerite and both minerals exhibit chalcopyrite disease. About 40% of the sphalerite and approximately 30% of the pyrargyrite has chalcopyrite within the grains. Polybasite was deposited before and concurrently with native silver (Fig. 12). Chalcopyrite is also observed within about 10% of the polybasite. Galena was observed as individual grains and as mymerketic intergrowths in approximately 10% of the polybasite and pyrargyrite (Fig. 13). Gold was observed in one sample as minute grains (<10 μ) associated with pyrargyrite and chalcopyrite. Acanthite was observed in association with polybasite, sphalerite, and was considered to represent a late stage. A few grains of pyrite showed conversion to marcasite. Amythest is a late stage mineral seen only as vug filling. Calcite was seen in hand samples to cross-cut the mineralized fragments.

Figure 11. Stage 3 paragentic sequence. Note the addition of native element minerals as well as the sulfosalts.

STAGE 111
MINERALIZATION

QUARTZ

PYRITE

SPHALERITE

PYRARGYRITE

POLYBASITE

CHALCOPYRITE

GALENA

NATIVE GOLD

NATIVE SILVER

ACANTHITE

MARCASITE

AMYTHEST

CALCITE

TIME
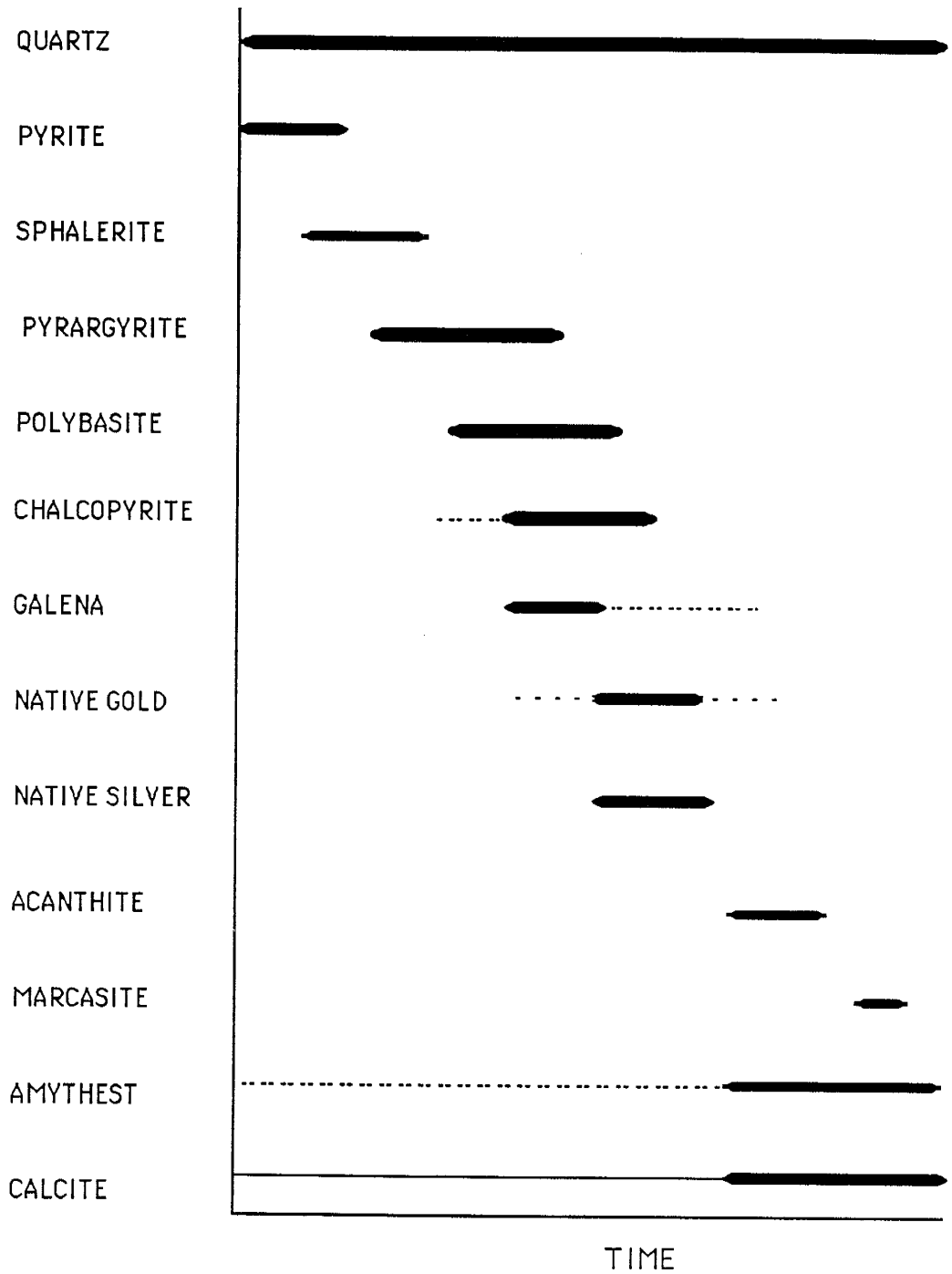
Figure 12.   Photomicrographs showing common mineral

associations.

a. Association of chalcopyrite, pyrite, acanthite,

sphalerite, and polybasite.   The

entire grain is 120 μ across.

b. Native silver in association with polybasite.   The

grains are 50 μ in diameter.

A

Chalcopyrite

Sphalerite

Polybasite

Acanthite

Pyrite

B

Native
Silver

Polybasite
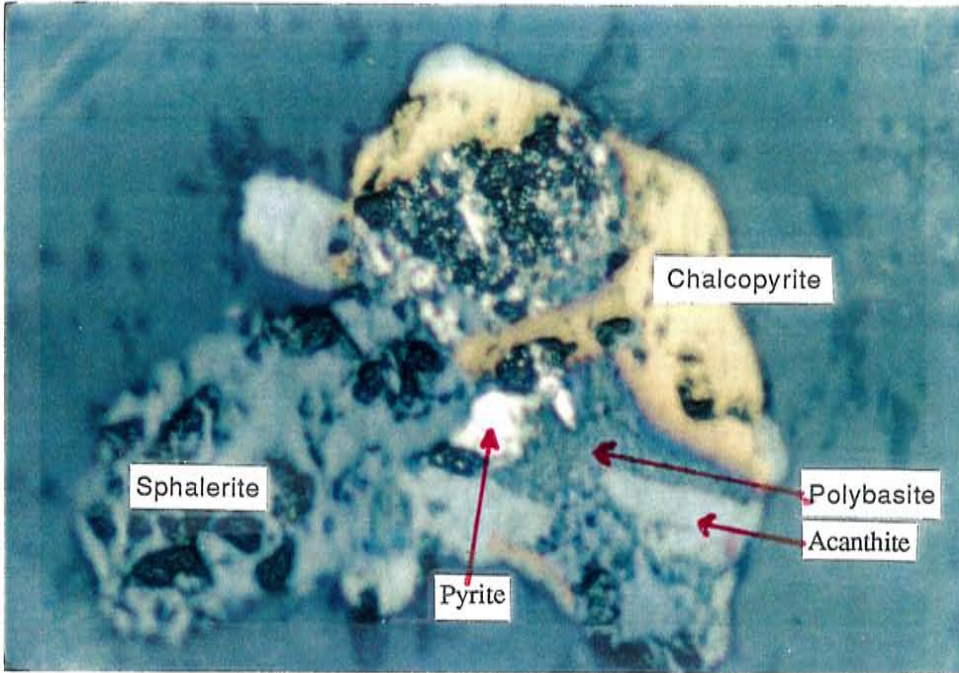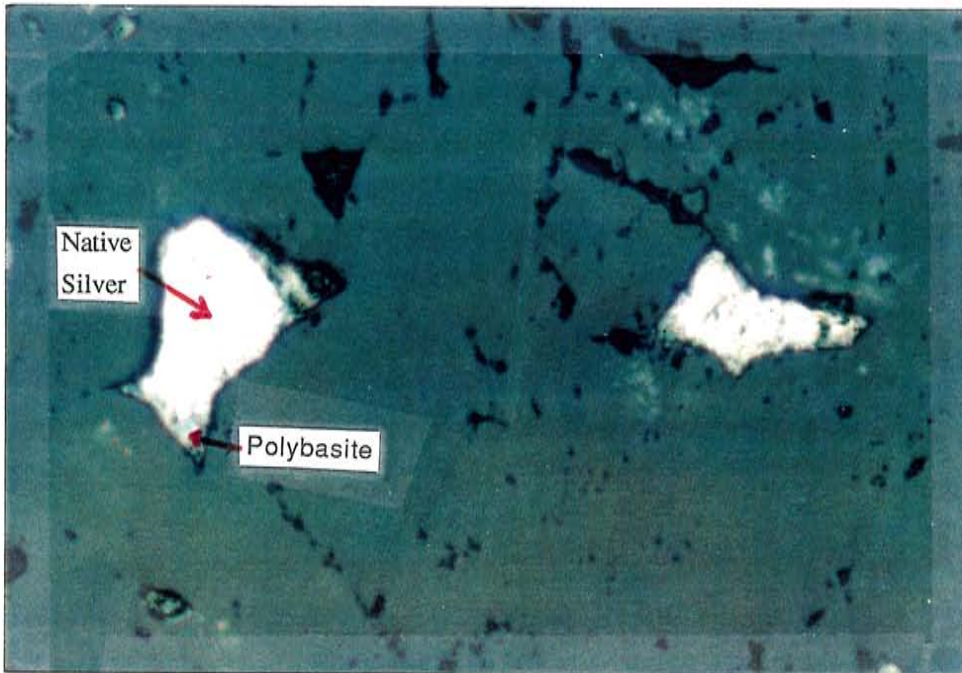
Figure 13. Photomicrographs showing the occurrence of galena.

a. A galena grain, crosscutting sphalerite. The width of the galena grain is 50 μ at its narrowest.

b. Galena as mymerketic intergrowths within pyrargyrite. Galena is the lighter gray material. The pyrargyrite grain is 75 μ in the long dimension.

A

Sphalerite

Galena

B

Pyrargyrite   Galena

Sphalerite

Sphalerite
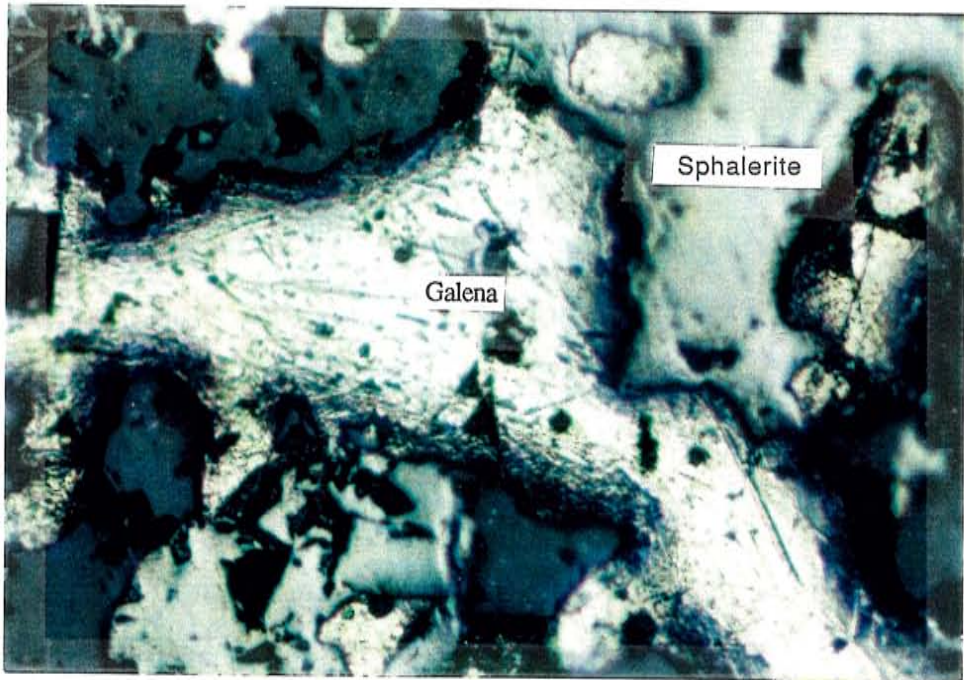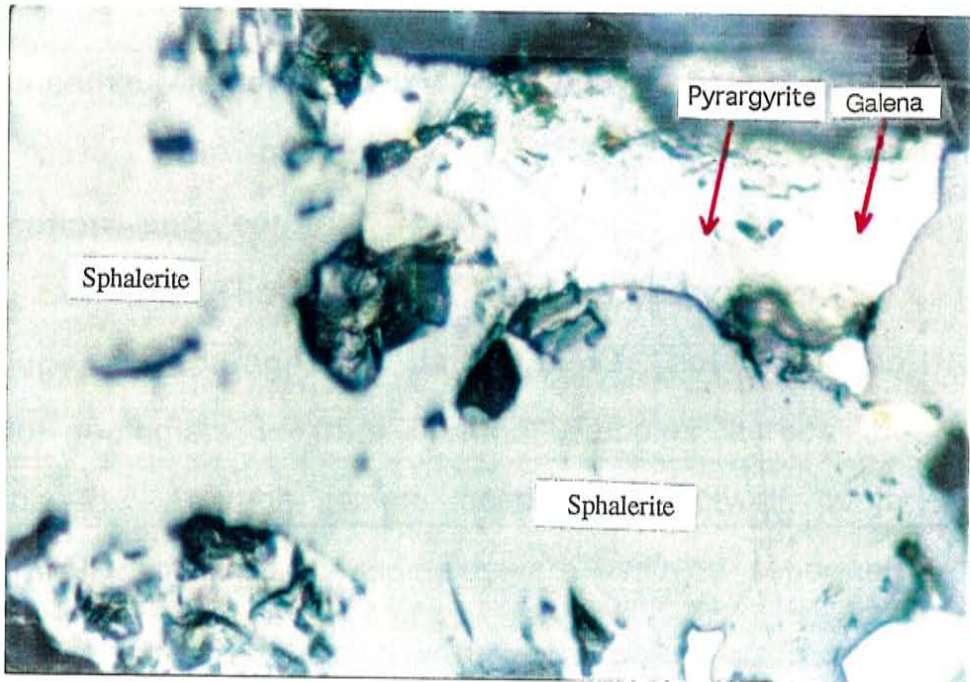
<u>Occurrence of the 3 Stages of Mineralization:</u>

A map of the vein showing the occurrence of each stage of mineralization was produced from field notes and sketches along with descriptions of hand samples (Fig. 14). It indicates the relative abundance of each of the 3 mineralization stages. Stage 2 mineralization is the most abundant at the 320 m. level, whereas at the 425 m. level, stage 1 is the most abundant. Stage 1 mineralization occurs along the hanging-wall at the 320 m. level. Stage 3 mineralization is the least abundant and occurs in pockets in the center and the along the footwall on the 320 m. level and along the hanging-wall on the 425 m. level.

SULFIDE AND SULFOSALT GEOCHEMISTRY:

Qualitative element identification and statistical analysis of assay data was performed in order to verify mineral identification and confirm the mineralogy of each stage of mineralization. The assay data was correlated with the mineralogy and paragenetic data. Assay data acquired from Fresnillo geologists is from channel samples across the vein (Appendix 2). At each sample location the footwall, center, and hanging-wall section of the sample were assayed separately.

Figure 14. Schematic cross section of the occurrence of stages within the vein. Variations in the width of the vein are not shown. The placement of the stages are based on sample descriptions.

STAGES OF THE SAN MATEO VEIN

320 LEVEL
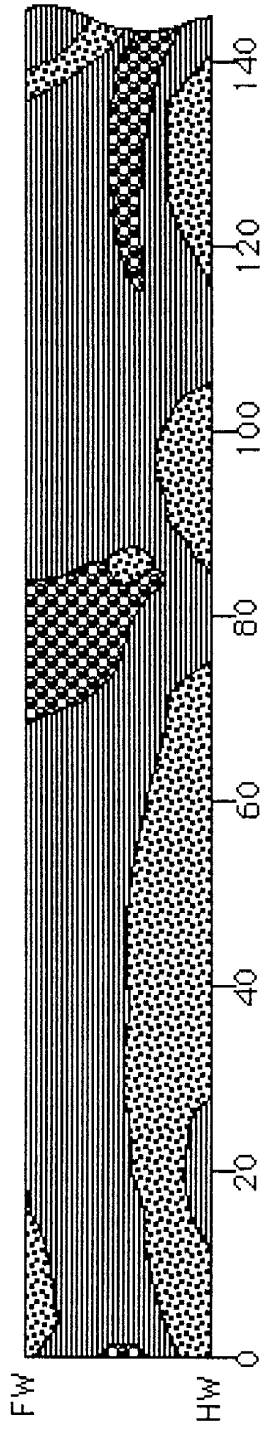
425 LEVEL
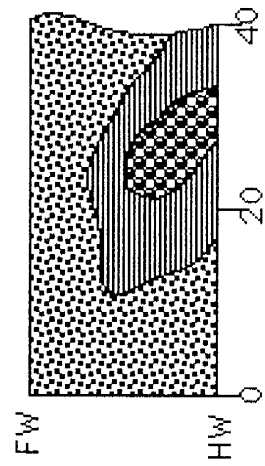
STAGE 1

STAGE 2

STAGE 3

Element Identification:

Qualitative element identification was performed using a scanning electron microscope (SEM). A sample emits X-rays producing characteristic energies from the elements within the sample. Identification of the elements are obtain by comparing these energies in the form of peak heights to X-ray energy tables. The SEM used had a computerized element identification system. Peak heights are proportional to the concentration of the element. Only elements with atomic numbers >11 and concentrations above 1% can be detected (Welton, 1984). By scanning each mineral for a specific length of time the relative proportions of elements within the mineral can be obtained.

Qualitative element identification was performed on three widely spaced samples In each sample several minerals were used for element identification. Determination of the relative iron (Fe) content in sphalerites and relative arsenic (As) and antimony (Sb) content in pyrargyrite and polybasite was made.

Sphalerite minerals range in color from yellow to orange to brown with varying amounts of iron (Table. 3). Samples from 320 m. level all yielded values for Znk_α/Fek_α ratios, indicating low Fe levels. Brown-colored samples from the 425 m. level have lower ratios indicating higher Fe content. Zn to Fe ratios apparently control the color with lighter yellow sphalerites containing less iron and the reddish brown samples containing more iron. This

Table 3.   Summary of SEM data for sphalerites.

Sample No.	Level	Location	Color	$Zn(k_\alpha)/$ $Fe(k_\alpha)$
951C	320 m.	147 m.	orange	3.0
951C	320 m.	147 m.	red	2.5
951C	320 m.	147 m.	yellow	4.0
941B	320 m.	85 m.	orange	3.1
965A	425 m.	24 m.	red-brown	1.8
965A	425 m.	24 m.	red-brown	2.0

relationship was also noted by Gemmel (1988) who used microprobe analysis on samples from the Santo Niño vein. He found that the reddish brown sphalerite contained 10-15% iron, while the light yellow only 5-10% iron. While banding was not observed as in the Santo Niño vein, sphalerites of darker color occurred next to lighter ones with the darker sphalerites appearing petrographically to be earlier during each stage of mineralization. This would suggest that the fluid responsible for deposition of the sphalerites had a high iron content and was depleted over time in each stage of mineralization.

The sulfosalt solid solution series pyrargyrite-prousite (Ag_3 (Sb,As) S_3) and the polybasite-pearcite ($(Ag,Cu)_{16}$ $(Sb,As)_2$ S_{11}) series were observed by reflective light microscopy but positive identification could not be obtained with certainty. Qualitative element identification by the SEM was performed in order to determine the relative antimony and arsenic contents, hence idenitfing the better mineral name to apply to the mineral. On grains thought to be pyrargyrite EDEX data show a prominent Sb peak and a minor peak for As indicating the mineral is pyrargyrite (Table 4). Data for polybasite-pearcite solid solution series was similar with a prominent Sb peak and a minor As peak indicating polybasite (Table 4).

Table 4.　Summary of SEM data for pyrargyrite and polybasite.

Sample No.	Level	Location	$Ag(k_\alpha)$	$Sb(k_\alpha)$	$As(k_\alpha)$
951C	320 m.	147 m.	4.2	0.5	0.1
951C	320 m.	147 m.	4.8	0.5	0.1
941B	320 m.	85 m.	7.2	0.6	0.1
941B	320 m.	85 m.	5.1	0.4	0.1
965A	425 m.	24 m.	7.0	2.0	0.6
965A	425 m.	24 m.	7.5	1.0	0.5

Sample No.	Level	Location	$Ag(k_\alpha)$	$Sb(k_\alpha)$	$As(k_\alpha)$
951C	320 m.	147 m.	7.0	0.8	0.3
941B	320 m.	85 m.	5.8	0.5	0.1
941B	320 m.	85 m.	3.3	0.3	0.1
941B	320 m.	85 m.	7.0	0.4	0.2

Element Distribution:

Assay values for Au, Ag, Zn, Pb and Cu were obtained on channel samples done at 2 meter intervals along the strike length of the vein on each mine level. At each 2 meter interval, channel samples were taken perpendicular to the vein strike. At each sample site, vein width was divided into 2 to 4 segments and a channel sample was taken for each segment. Hence assay data together with Fig. 14 allowed calculation of assays for each stage of mineralization. Weighted averages were calculated for 10 meter intervals in order to smooth the data to visualized changes in metal ratios and grade across vein strike. Values for Ag, Au, Pb, Zn and Cu were plotted against distance along the vein (Fig. 15). Ratios of Ag to Pb, Zn, Cu and ratios of Au to Pb, Zn, Cu were each plotted against distance along the vein (Fig 16).

These plots indicate Ag and Au are irregularly distributed along the vein and that the 425 m. level generally shows lower concentrations of all metals, although they show the same trend as the 320 m. level ore. Silver/lead ratios show a good correlation with Au grade and Ag./Cu correlates well with Ag grade. There are no good correlation between base metal concentrations and precious metal values.

By comparing Figure 14 and Figure 15 and 16 areas of high Ag and Au can be correlated with the occurrence of the stages of

Figure 15   Plots of assay values for Ag, Au, Pb, Zn and Cu along
the width of the vein.

Average Au per Distance

Average Ag per Distance

Average Cu per Distance

Average Zn per Distance

Average Pb per Distance
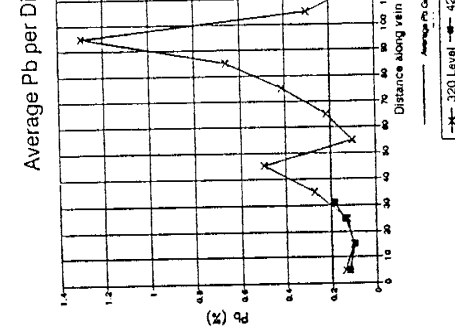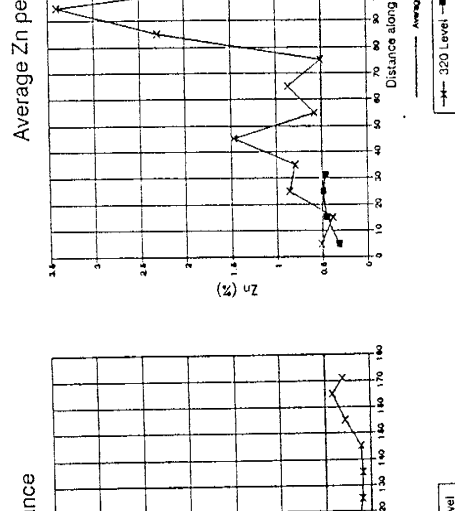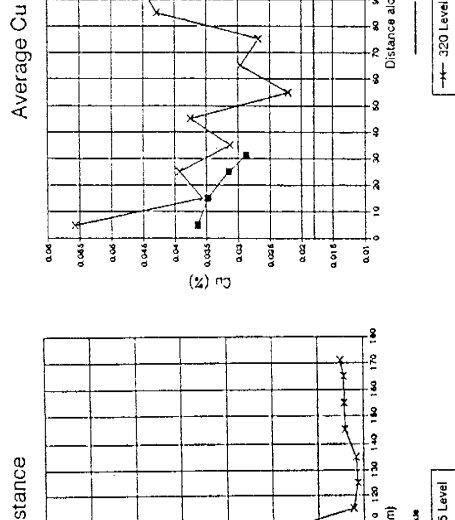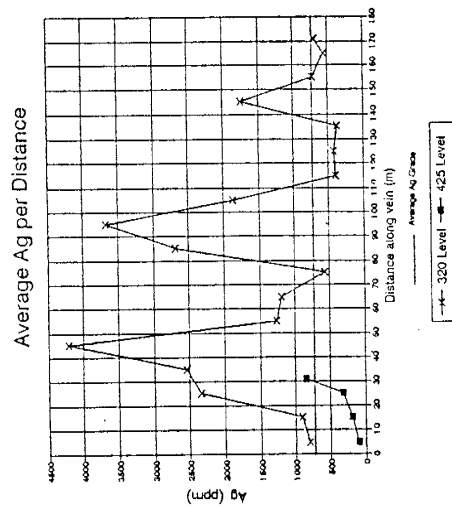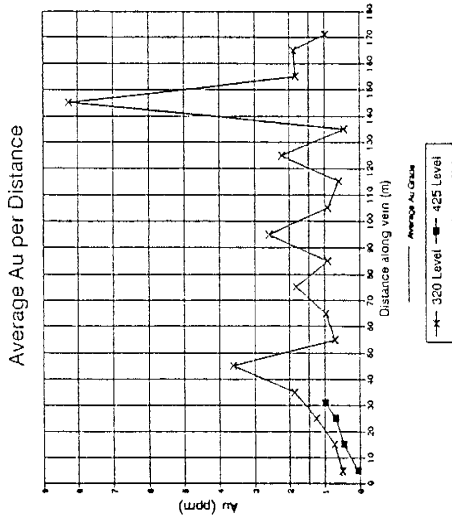
Figure 16.   Plots of ratios of Ag to Pb, Zn, and Cu, and Au to Pb,

Zn, and Cu along the width of the vein.
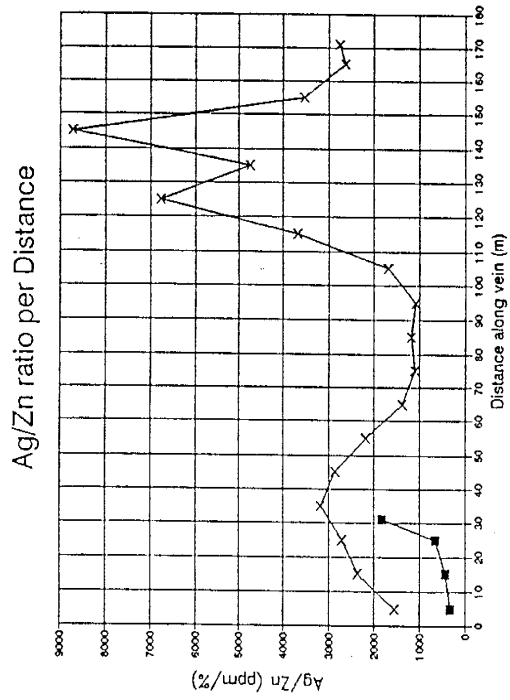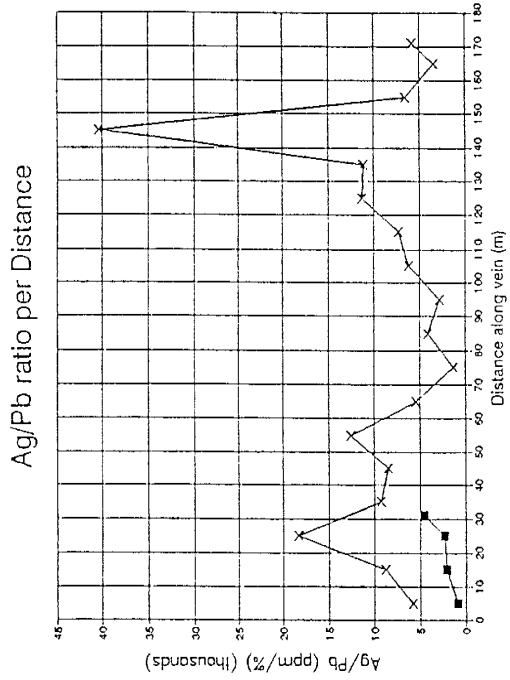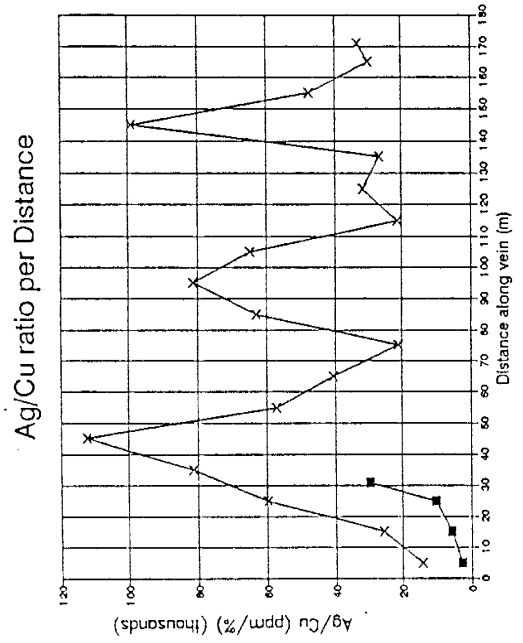
Ag/Zn ratio per Distance

Ag/Pb ratio per Distance
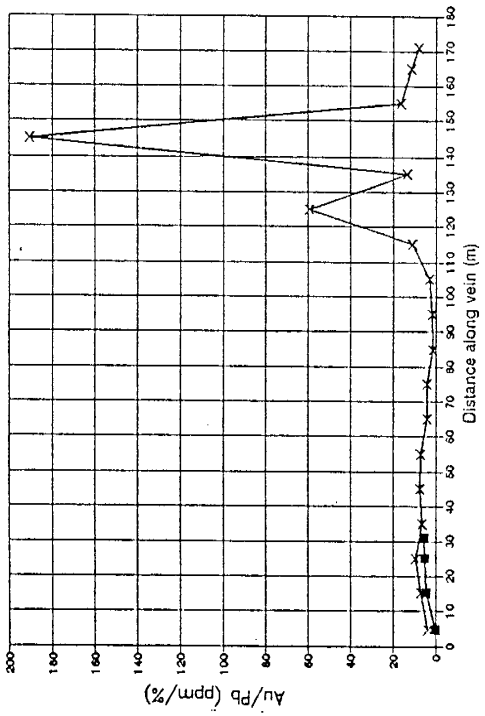
Ag/Cu ratio per Distance

Au/Zn ratio per Distance
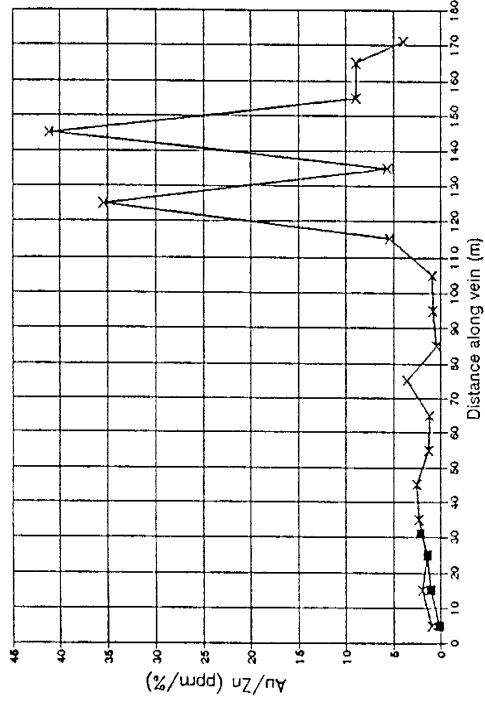
Au/Pb ratio per Distance

Au/Cu ratio per Distance
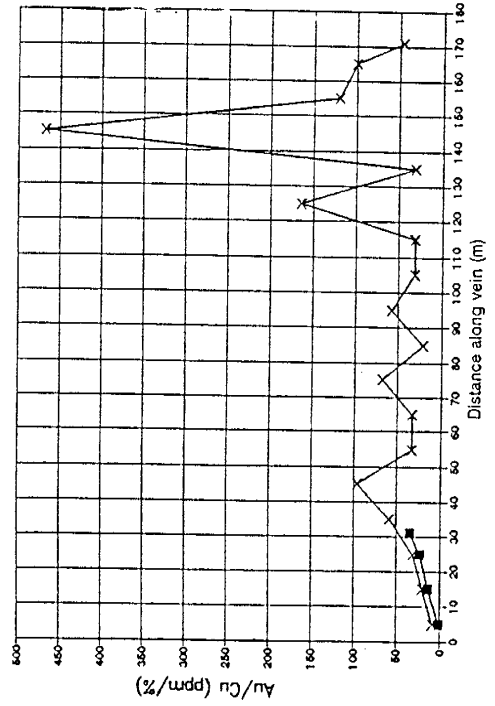
mineralization. The Ag grade on the 320 m. level coincide with stage 2 and 3 mineralization. The Au ratios appears to correlate with stage 3 mineralization. Base metal values are also irregularly distributed, but show no clear relationship with a particular stage of mineralization.

Statistical Analysis of Assay Values:

The mineralization stage represented by each channel sample was determined by use of Fig. 14. For each element, a weighted average based on the width was obtained. These values were used to obtain statistics on each element and to perform a linear regression analysis for each stage of mineralization.

Statistical analysis of assay data is presented in Table 5. It indicates Au occurs in all 3 stages of mineralization. Gold was, however, observed only in stage 3 mineralization, that is indicated to be the stage with the highest amounts of that element. On the 425 m. level gold is indicated to occur mainly in stage 3 mineralization. Silver minerals are only seen in hand specimen to occur in stage 2 and stage 3, however assay values reveal that significant silver occurs in stage 1 ores. Highest silver values are indicated to occur in stage 2 which agrees with the Ag grades plotted on long sections (Fig. 15). Lead and zinc have higher average values for stage 1 and stage 2 mineralization

Table 5. Summary of statistics calculated from assay data.

Mineral	Statistic	320 LEVEL			425 LEVEL		
		Stage 1	Stage 2	Stage 3	Stage 1	Stage 2	Stage 3
Au (ppm)	average	0.53	2.60	3.04	0.09	0.55	1.69
	max	3.60	46.75	17.94	0.70	1.60	4.40
	min	0.00	0.00	0.00	0.00	0.00	0.00
	std	0.85	5.99	4.78	0.18	0.65	1.40
Ag (ppm)	average	1125.23	2134.10	965.89	132.72	232.25	725.12
	max	15410.00	13331.00	5988.00	906.00	592.00	2803.00
	min	4.00	4.00	4.00	8.00	6.00	4.40
	std	2377.63	2888.72	1469.69	191.37	198.54	874.61
Pb (%)	average	0.28	0.29	0.17	0.06	0.13	0.30
	max	4.60	1.40	0.97	0.36	0.50	0.70
	min	0.00	0.00	0.00	0.00	0.00	0.00
	std	0.83	0.41	0.24	0.08	0.17	0.23
Zn (%)	average	0.70	0.98	0.43	0.15	0.47	0.93
	max	8.20	5.77	4.20	0.55	1.53	1.70
	min	0.00	0.00	0.00	0.00	0.00	0.00
	std	1.53	1.37	0.89	0.17	0.52	0.67
Cu (%)	average	0.03	0.03	0.02	0.02	0.04	0.04
	max	0.15	0.11	0.07	0.05	0.11	0.07
	min	0.00	0.00	0.00	0.00	0.00	0.00
	std	0.03	0.03	0.01	0.01	0.03	0.02

on the 320 m. level. High values for these elements occur in stage 3 mineralization on the 425 m. level. Copper has a fairly constant average value in all stages and both mine levels. Average values and maximum values for gold and silver are higher on the 320 m. level than on the 425 m. level for each stage of mineralization.

Linear regression analysis provided correlation coefficients between the elements (Table 6). It can be seen that for stage 1, there are significant values among base metals analyzed especially for samples from the 425 m. level. Silver values correlate significantly with the base metals in all stages except for lead in stage 3. Gold correlates most significantly with silver and lead in stages 2 and 3 at both levels. This was also suggested by the fact that pyrargyrite was seen in association with galena and gold. Although gold was associated with chalcopyrite at the 320 m. level, the correlation coefficients are not significant except on the 425 m. level. This relationship with chalcopyrite may have been a local phenomena. Most important, this data indicate strong correlation between Ag and base metals for that stage rich in sliver, stage 2. This is not evident on long section diagrams because it includes data from all 3 stages, and Ag does not correlate with base metals for stage 1 mineralization. The correlation of Au with Pb also is not evident on long section plots.

Table 6.   Correlation coefficients calculated from assay data by linear regression analysis.   Significant correlations are in boxes.

320 LEVEL

Mineral	Mineral	Stage 1	Stage 2	Stage 3
Au vs	Ag	0.14	0.25	0.22
	Pb	0.07	0.41	0.26
	Zn	0.09	0.01	0.04
	Cu	0.12	0.03	0.14
Ag vs	Pb	0.65	0.52	0.16
	Zn	0.65	0.37	0.65
	Cu	0.37	0.48	0.65
Pb vs	Zn	0.83	0.64	0.39
	Cu	0.47	0.32	0.45
Zn vs	Cu	0.44	0.34	0.70

425 LEVEL

Mineral	Mineral	Stage 1	Stage 2	Stage 3
Au vs	Ag	0.07	0.72	0.11
	Pb	0.07	0.38	0.93
	Zn	0.03	0.26	0.72
	Cu	0.00	0.46	0.40
Ag vs	Pb	0.04	0.65	0.17
	Zn	0.01	0.49	0.29
	Cu	0.00	0.76	0.10
Pb vs	Zn	0.65	0.53	0.79
	Cu	0.49	0.94	0.48
Zn vs	Cu	0.87	0.52	0.70

FLUID INCLUSION ANALYSIS:

A fluid inclusion analysis was performed on 28 samples from along the entire strike length of the vein and both mine levels. Approximately 100 double polished sections were made, however only 62 sections had fluid inclusions that could be measured. Two hundred and fifty-two temperatures of homogenization (Th) were measured and sixty-five melting temperatures (Tm) were measured (Appendix 3).

Nature of Inclusions:

Fluid inclusions were studied in quartz, calcite and sphalerite. Of the 252 Th measurements, 227 were measured in quartz, 20 in calcite and 5 in sphalerite. Sphalerite was observed to contain inclusions but it was difficult to obtain measurements under either white light or infrared light. The 5 measurements obtained were in light colored sphalerite and were obtained under white light. Inclusions could not be seen in pyrargyrite either under white light or infrared light.

Primary, secondary and minor pseudosecondary inclusions were observed. Based on criteria established by Roedder (1984), primary, secondary and pseudosecondary inclusions were distinguished. Primary inclusions occurred along growth zones in quartz crystals and occurred as small groups of isolated

inclusions. In general, these primary inclusions were studied. Some secondary inclusions could not be readily distinguished except by very low Th measurements.

Most inclusions studied were hosted in quartz due to its abundance and transparent nature. Inclusions were typically less than 10μ in length, and finding sufficient populations for study in all mineralization stages was difficult. Stage two mineralization was the most abundant and hence provided the greatest opportunity for study, but care was taken to obtain representative samples from all stages. The greatest occurrence of inclusions was in medium to coarsely crystalline comb quartz. Sphalerite that contain measurable inclusions was from stage 2 mineralization. Measurements were obtained from stage 3 and surface calcite samples.

Fluid inclusions studied ranged from 4 μ to 15 μ in diameter with a few as large as 50 μ in diameter. Both liquid-dominated and vapor-dominated inclusions coexisted spatially in all samples. Degree of fill for inclusions that were used for measurements ranged from 0.95-0.65. Vapor dominated inclusions had a degree of fill of approximately 0.05 (Fig. 17). Attempts were made to obtain measurements on vapor dominated inclusions (>95% vapor), however, homogenization temperatures either could not be obtained or were not reproducible. Daughter minerals were not observed in any inclusions.

In Bodner et al. (1985) several criteria were established for

Figure 17.   Photomicrographs of occurrence of fluid inclusions.

a.   Sample from surface calcite showing primary inclusion.

b.   Occurrence of vapor dominated inclusions.
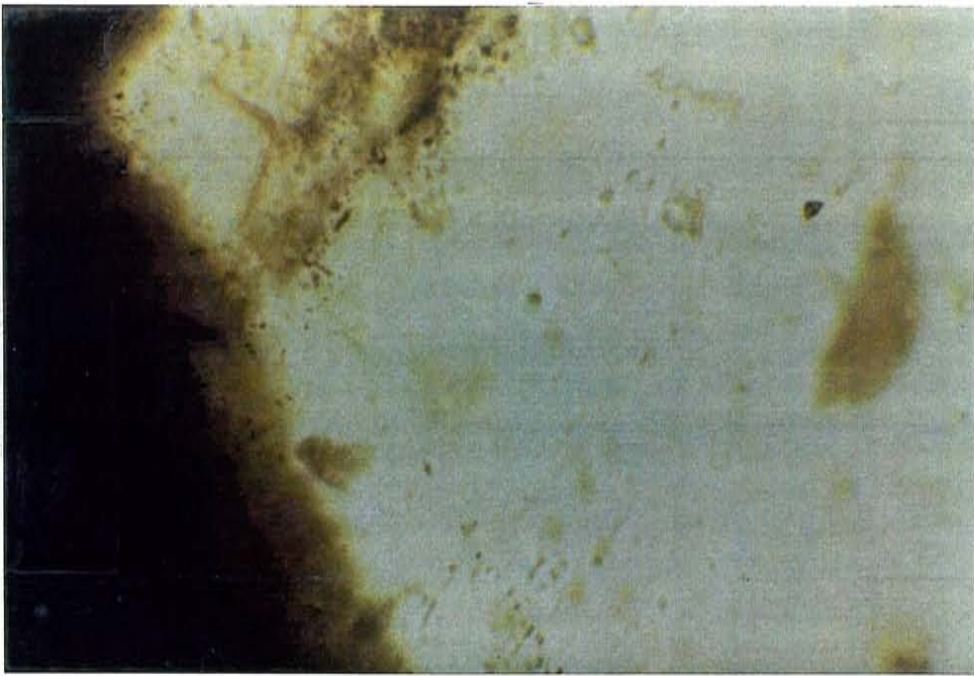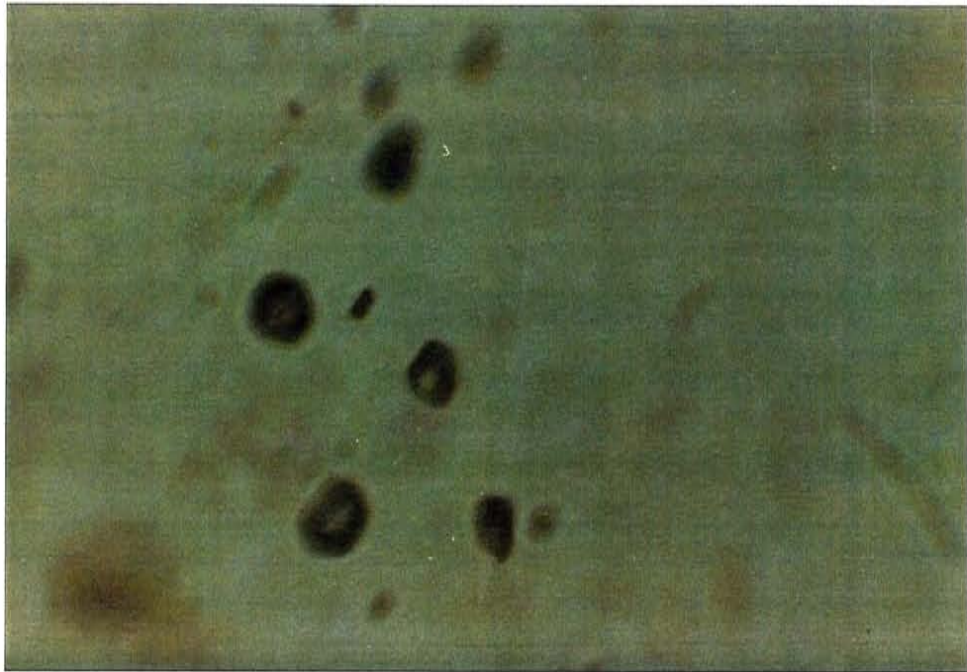
the way fluid inclusions could indicate boiling of hydrothermal fluids, including coexistence of liquid and vapor dominated inclusions and also healed microfractures containing all vapor-dominated inclusions. In the samples from all stages, liquid-dominated and vapor-dominated inclusions appear to be contemporaneous occurring together within individual growth zones. The evidence is strong that fluid boiling occurred throughout all stages of mineralization and on all levels of the San Mateo vein.

Temperatures of Homogenization:

Th values range from 129 ºC to 278 ºC. Temperatures below 159 ºC were only recorded for secondary inclusions. Primary inclusions Th values range from 168 ºC to 278 ºC. Inclusions in calcite from underground workings have Th's ranging from 168 ºC to 233 ºC; Th values for inclusions in surface calcite range from 168 ºC to 203 ºC; for sphalerite inclusion values range from 232 ºC to 278 ºC; and inclusions in quartz have Th values between 168 ºC and 264 ºC.

Histograms of Th measurements were plotted for samples representing each stage of mineralization (Fig. 18 a,b&c). They exhibit an overall decrease in Th from stage 1 to stage 3 quartz and calcite. Quartz and calcite hosted inclusions have similar Th

Figure 18.   Histograms of Th measurements.

a.   Stage 1 mineralization,

b.   Stage 2 mineralization,

c.   Stage 3 mineralization.

A.

TEMPERATURES OF HOMOGENIZATION
STAGE 1
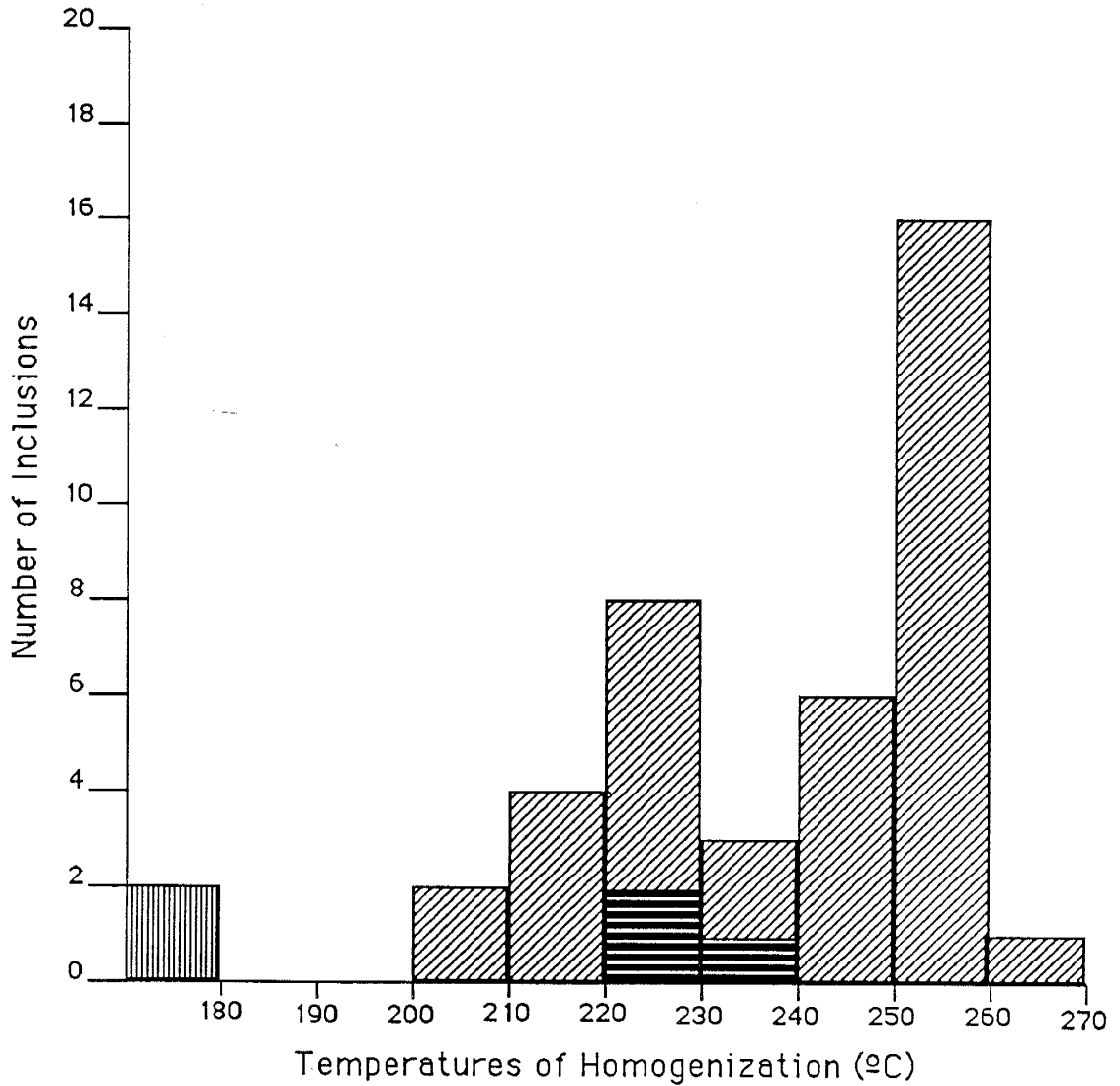
PRIMARY INCLUSIONS IN QUARTZ

PRIMARY INCLUSIONS IN CALCITE

SECONDARY INCLUSIONS

B.

TEMPERATURES OF HOMOGENIZATION
STAGE 2
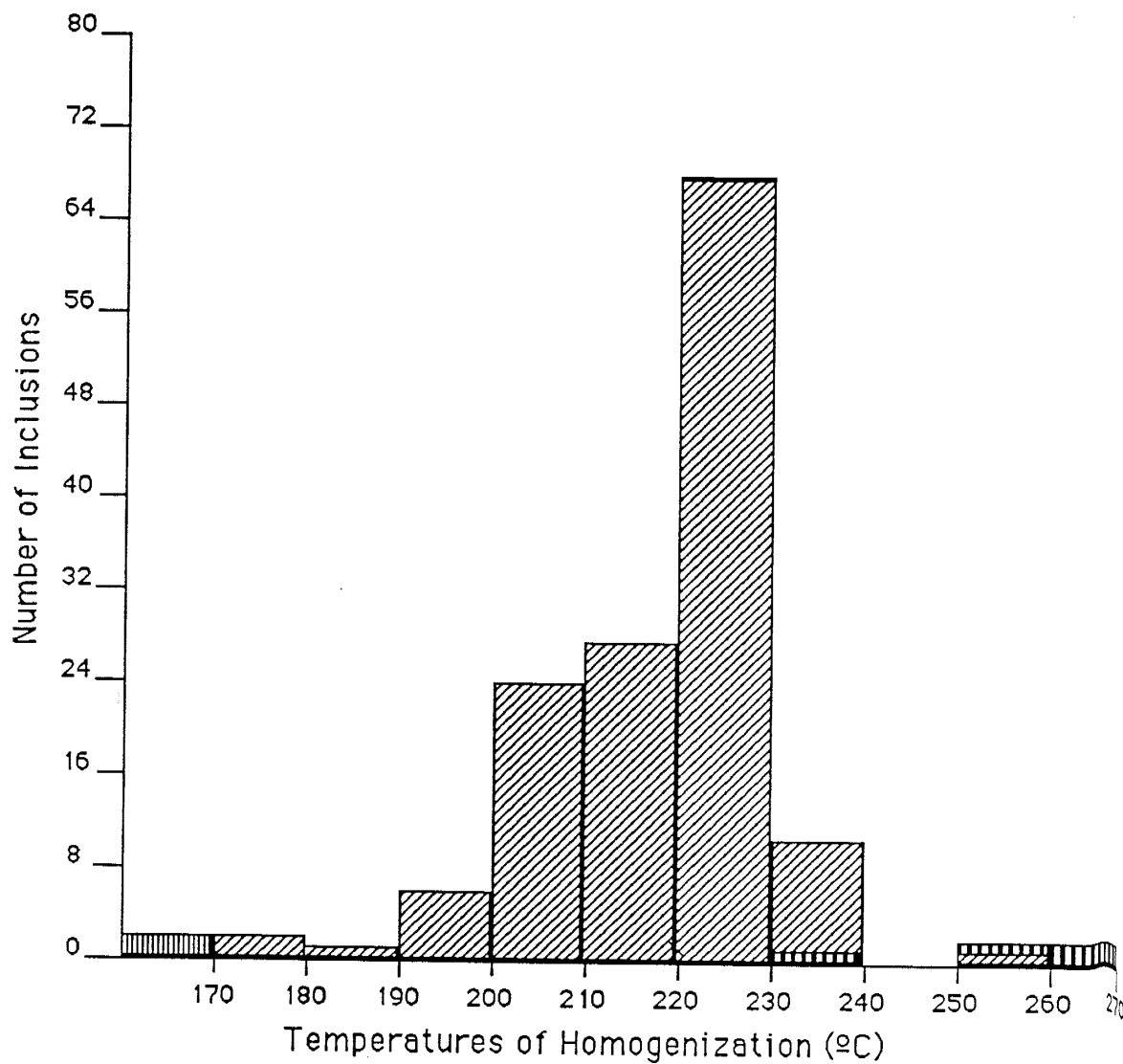
PRIMARY INCLUSIONS IN QUARTZ

PRIMARY INCLUSIONS IN SPHALERITE

SECONDARY INCLUSIONS

C.   TEMPERATURES OF HOMOGENIZATION
STAGE 3
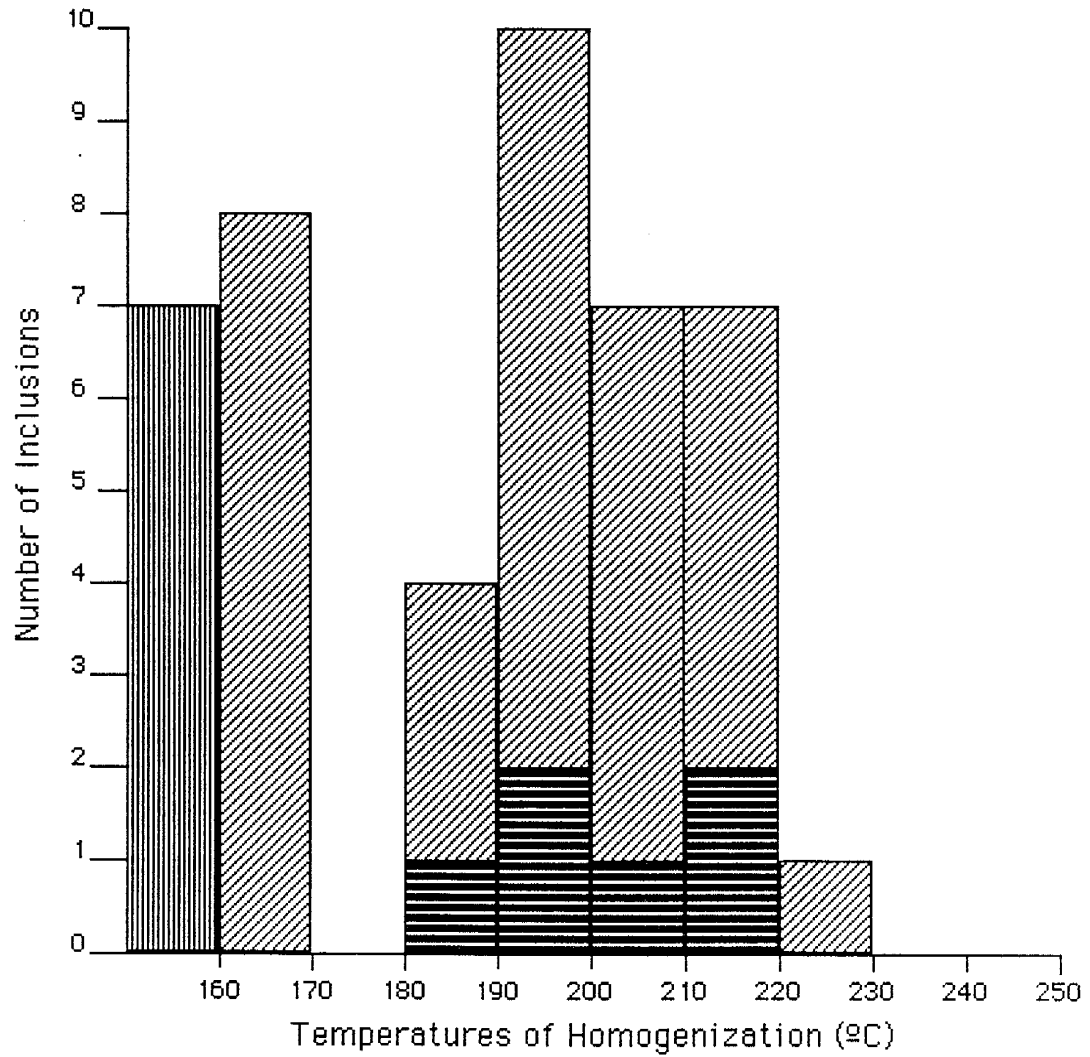
PRIMARY INCLUSIONS IN QUARTZ

PRIMARY INCLUSIONS IN CALCITE

SECONDARY INCLUSIONS

values, but sphalerite hosted inclusions analyzed have higher values than stage 2 quartz and calcite. In stage 3 there is a group of values between 162-170 ºC which are thought to be primary inclusions, however these may have been misidentified.

Histograms representing all stages of mineralization were plotted versus mine level (Fig. 19). The 320 m. level samples and the 425 m. level samples have similar Th distributions. Samples from surface outcrops, however have lower Th values.

Homogenization temperatures indicate minimum temperatures of trapping if there has been no physical change in inclusions. Presence of vapor-dominated inclusions coexisting spatially with liquid-dominated inclusions in all samples studied suggest boiling was extensive. This means that inclusions must have been trapped at or near pressure and temperature conditions where vapor and liquid coexist, hence Th values should represent Tt (trapping temperatures). Paleoreconstruction of the depth of the district during mineralization (Albinson, 1988) indicate lithostatic pressure could not have exceeded 92 bars. Therefore, the maximum pressure correction for trapping under hydrostatic conditions is < 10 ºC (Roedder, 1984). The range of Th values is greater than 10 ºC for a given mineralization stage and level, hence the variation in values represent fluctuating fluid temperatures with time.

Figure 19.   Th values measured in samples from all stages of
mineralization plotted against mine levels.

SURFACE

320 LEVEL

425 LEVEL

HOMOGENIZATION TEMPERATURE, ºC
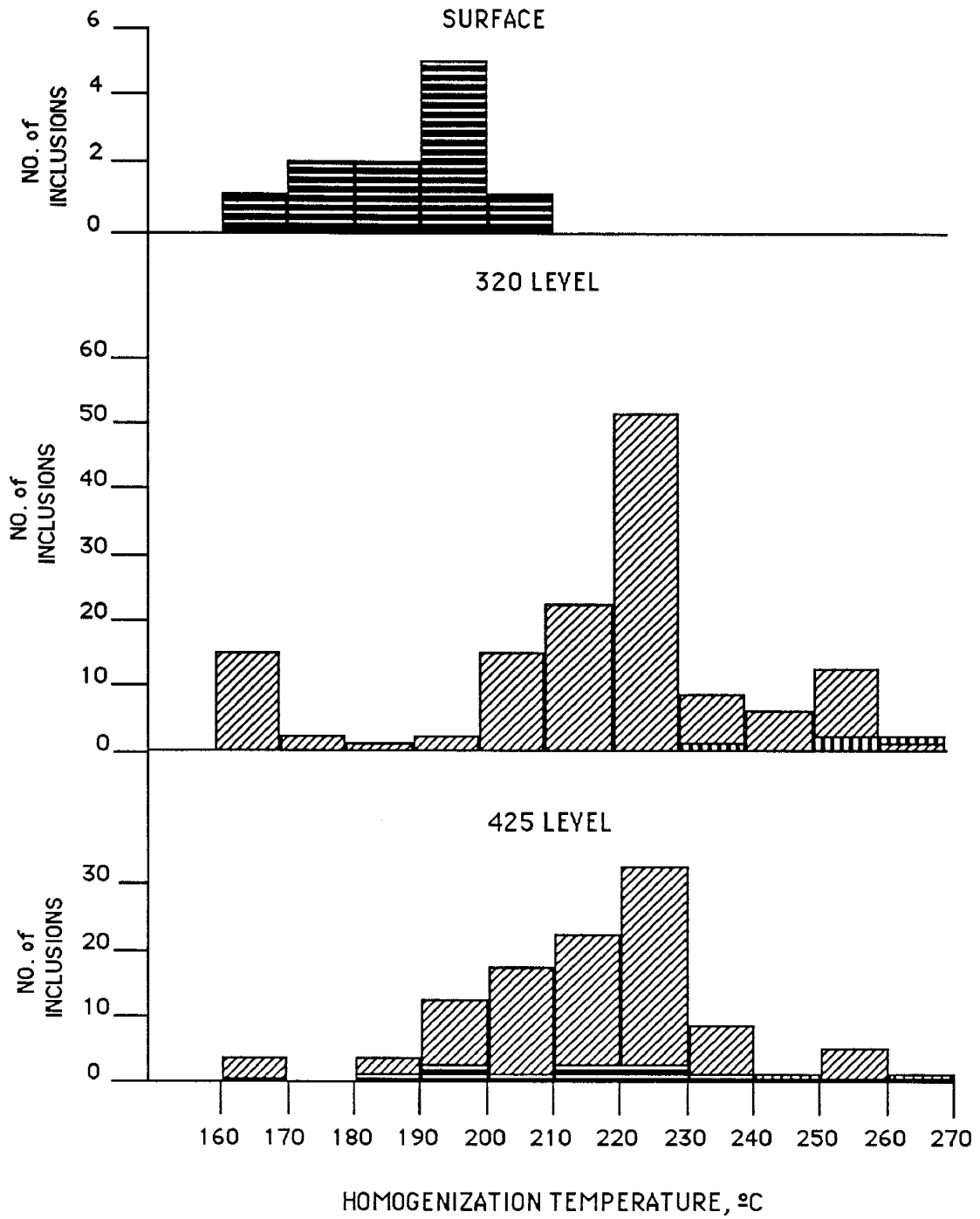
⬚⬚⬚ PRIMARY INCLUSIONS IN QUARTZ

⬚⬚⬚ PRIMARY INCLUSIONS IN SPHALERITE

▬▬▬ PRIMARY INCLUSIONS IN CALCITE

Temperatures of Melting:

Melting temperatures (Tm) values range from -4.2 to 0.0 ºC for inclusions in calcite and quartz. One inclusion in sphalerite has a Tm value of -7.8 ºC. Surface calcite inclusions have Tm values of -0.7 to -1.5 ºC, whereas calcite samples from deeper levels have Tm values of -2.3 to -3.2 ºC.

Salinities were calculated by using Roedder's (1984) equation. A histogram of all salinities except the value from sphalerite was plotted (Fig. 20). Calculated salinities range from 0.0 to 8.2 eq. wt. % NaCl, with the majority of the values lying between 2.0 - 6.7 eq. wt. % NaCl. Calcite samples are divided into two groups. The values below 3.0 eq.wt % NaCl represent surface calcite samples, while the values above 4.0 eq.wt. % NaCl represent calcite samples from deeper levels of the mine.

Plots of calculated salinities versus homogenization temperature for each stage (Fig. 21) were made. The plots show a mixing relationship between a high salinity fluid and a low salinity fluid especially evident in stage 2 mineralization. The sphalerite value of 16.6 eq. wt. % NaCl indicates a high salinity fluid associated with sulfide mineralization. There was no indication of CO_2 trapped within the inclusions, therefore melting temperatures (Tm) represent freezing point depressions by salts within the fluids.

Figure 20.   Histogram of calculated salinities.

CALCULATED SALINITIES
ALL STAGES

Y-axis: Number of Inclusions

X-axis: Salinities (eq. wt. % NaCl)
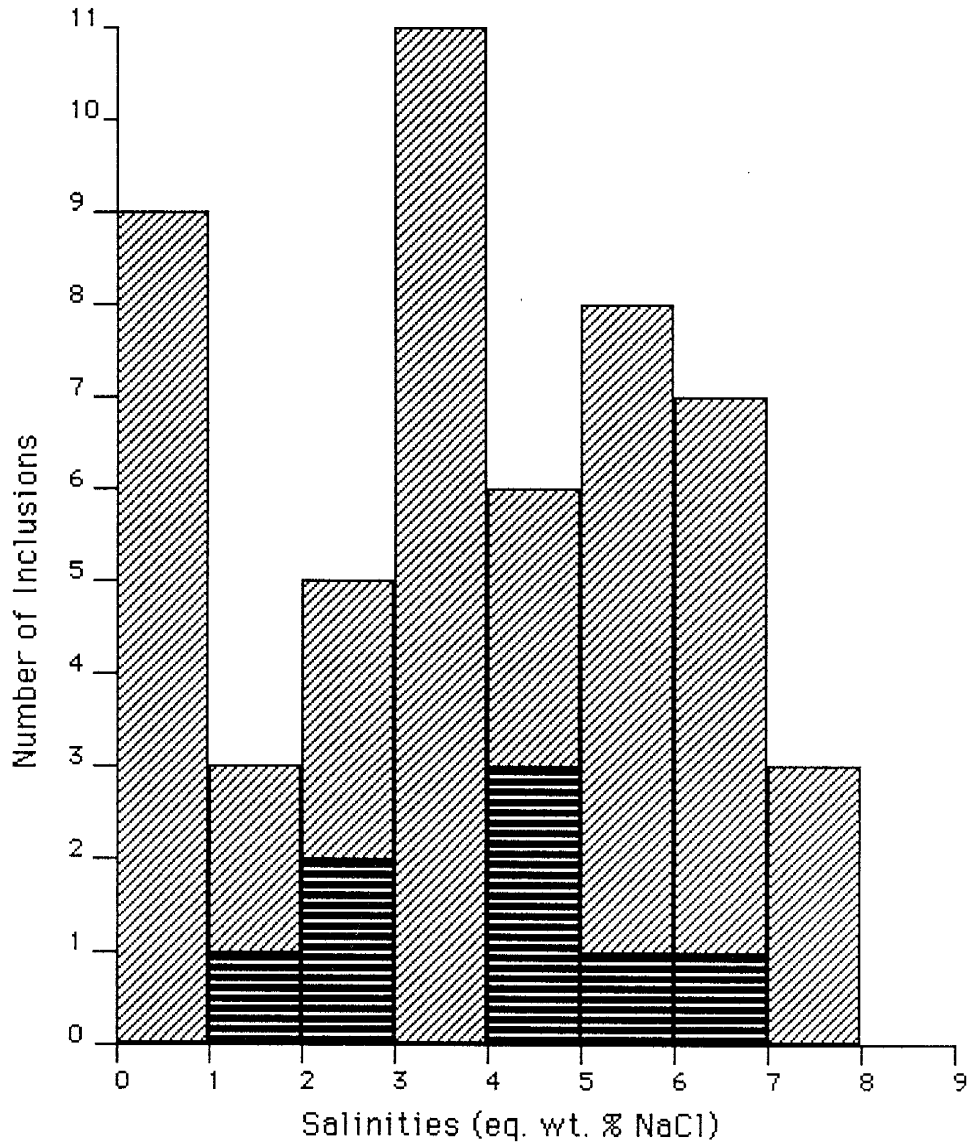
PRIMARY INCLUSIONS IN QUARTZ

PRIMARY INCLUSIONS IN CALCITE

Figure 21.   Calculated salinities versus Th for each stage of
mineralization.

Salinities vs Th
Stage 1
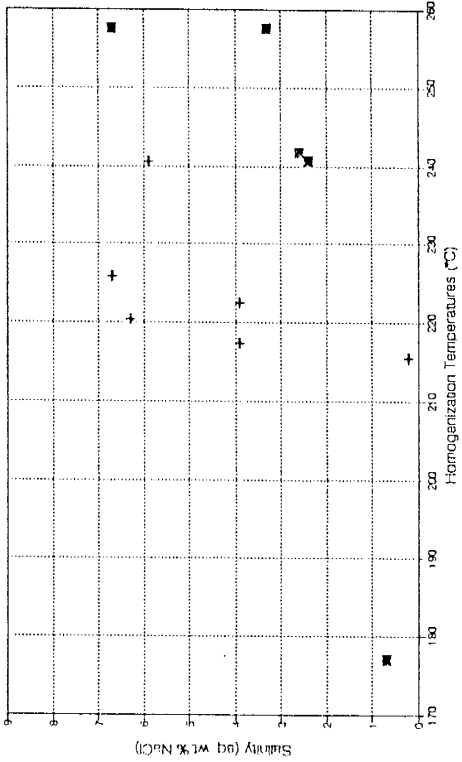
Salinities vs Th
Stage 2
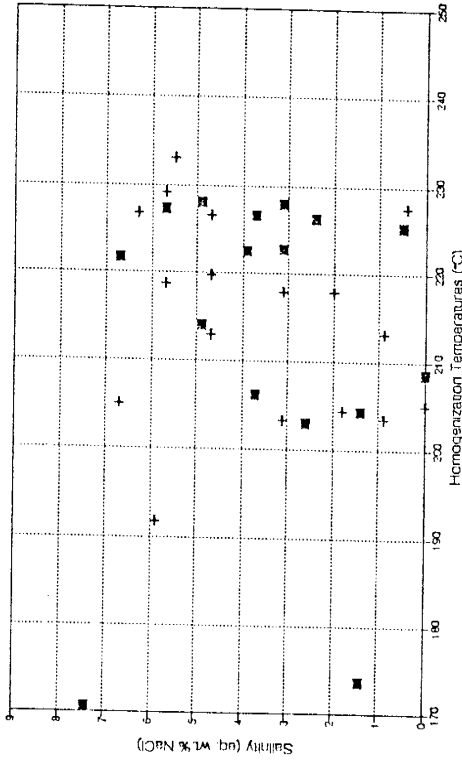
Salinities vs Th
Stage 3
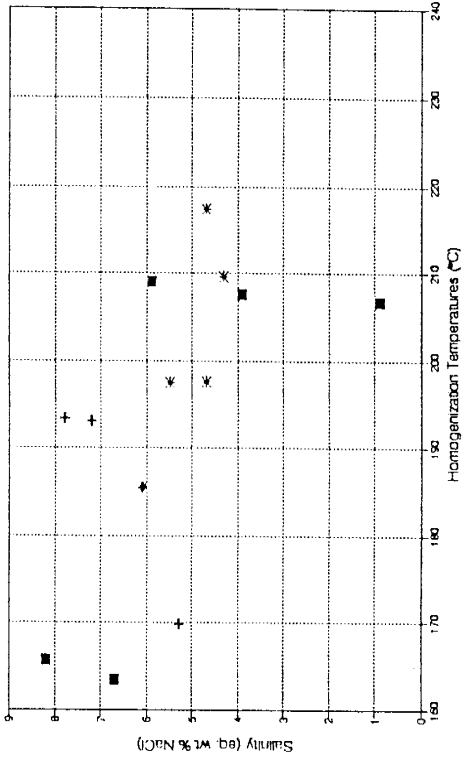
Stage 2 Quartz Bands:

Fluid inclusions were studied in samples from one locality on the 425 m. level that exhibited multiple growth zones of stage 2 quartz. Eight samples that had progressive bands of yellow, white, and clear quartz were studied. Each band ranged from 0.25 to 1.0 cm. wide. Homogenization temperatures decrease from older yellow quartz to the outer clear quartz (Fig. 22). Because of small inclusion size Tm values could not be measured.

Paragenetic Sequence and Fluid Inclusions:

Minor fluctuations in Th occurred between periods of gangue and sulfide-sulfosalt deposition (Fig. 23). In stage 1, the quartz-chlorite mineral assemblage has the highest Th values. In stage 2, the highest Th values are in the quartz-sulfide minerals-sulfosalts assemblage. Stage 3 Th values are similar to stage 2 Th values. There appears to be no distinct pattern between Th values and mineral assemblages. Salinities, however, appear to be low in the gangue mineral assemblages and higher in the assemblages with high amounts of sulfide minerals and sulfosalts. In general the data suggest that each stage of mineralization was accompanied by falling fluid temperatures and increasing salinity (and therefore fluid density). Measurements of sphalerite indicate it occurred during an increase in fluid temperature and salinity.

Figure 22.   Th values for stage 2 banded quartz

HOMOGENIZATION TEMPERATURES
STAGE 2 QUARTZ BANDS
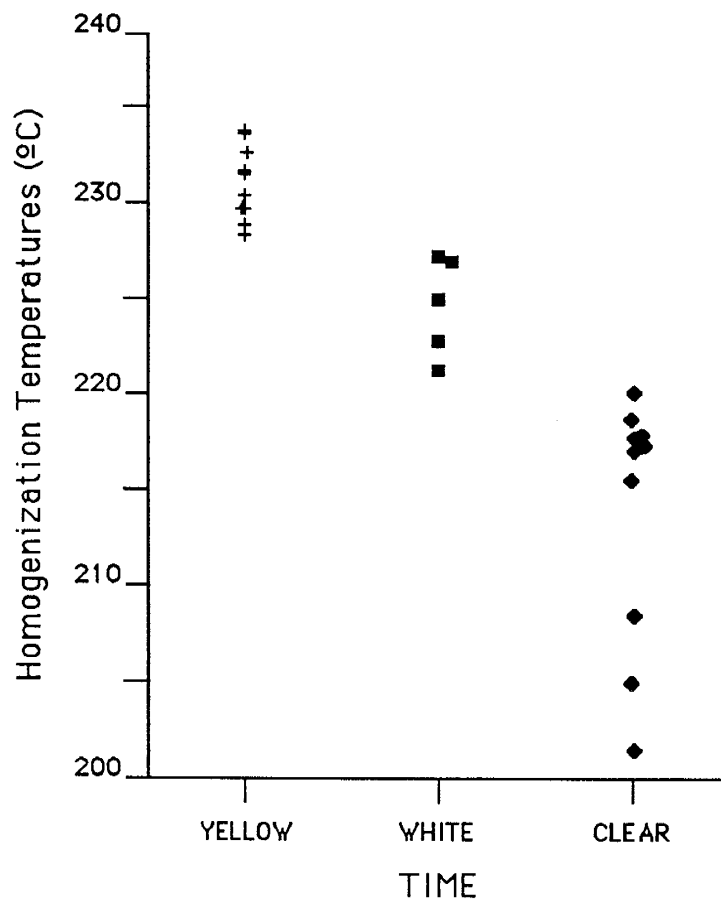
Figure 23.   Fluid inclusion data plotted against the paragenetic

sequence for each level.   Each point represents an

average for one sample.

a. Data for the 320 level.

b. Data for the 425 level.

PARAGENESIS VS. FLUID INCLUSION DATA
320 Level

89
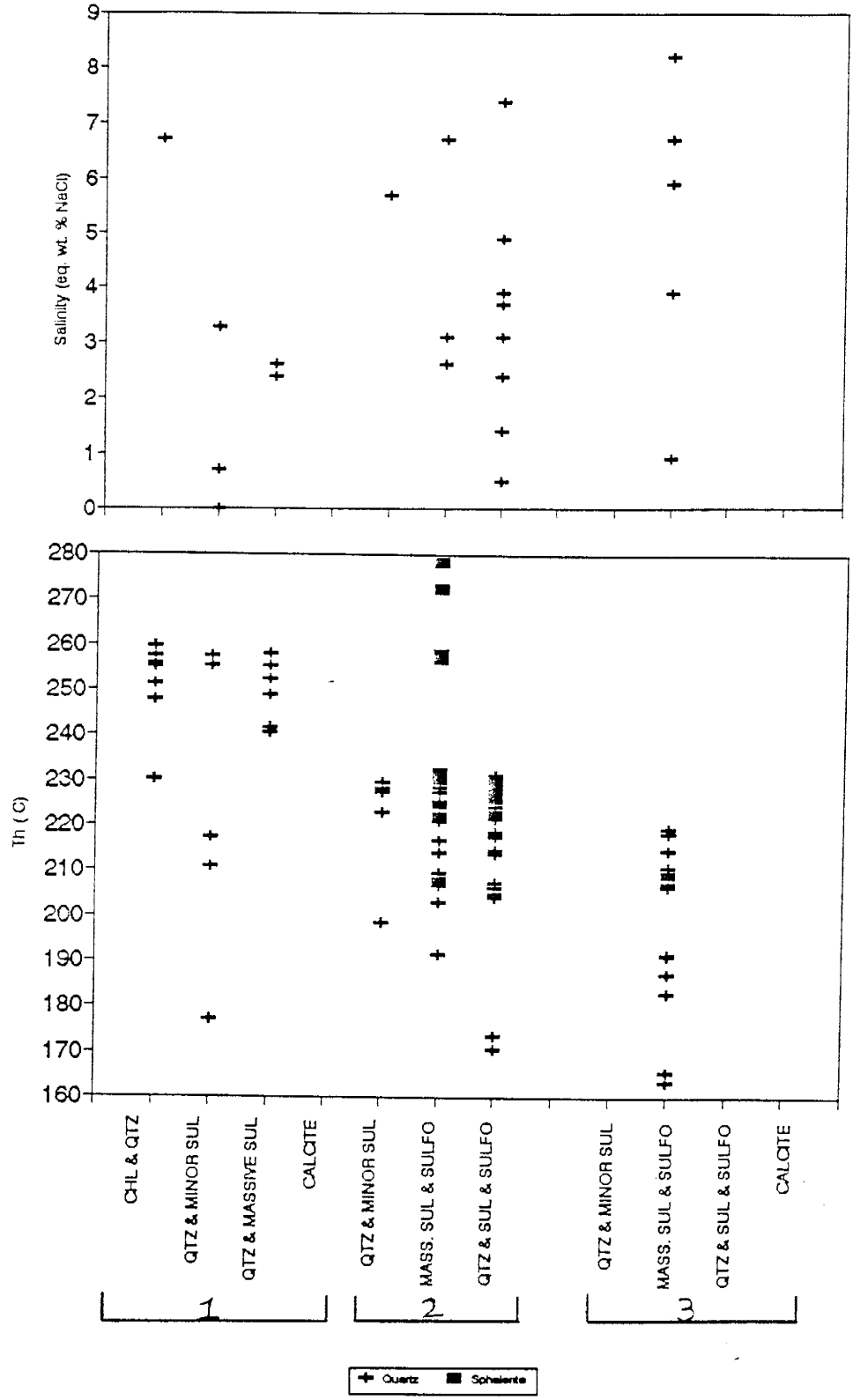
PARAGENESIS VS FLUID INCLUSION DATA
425 Level
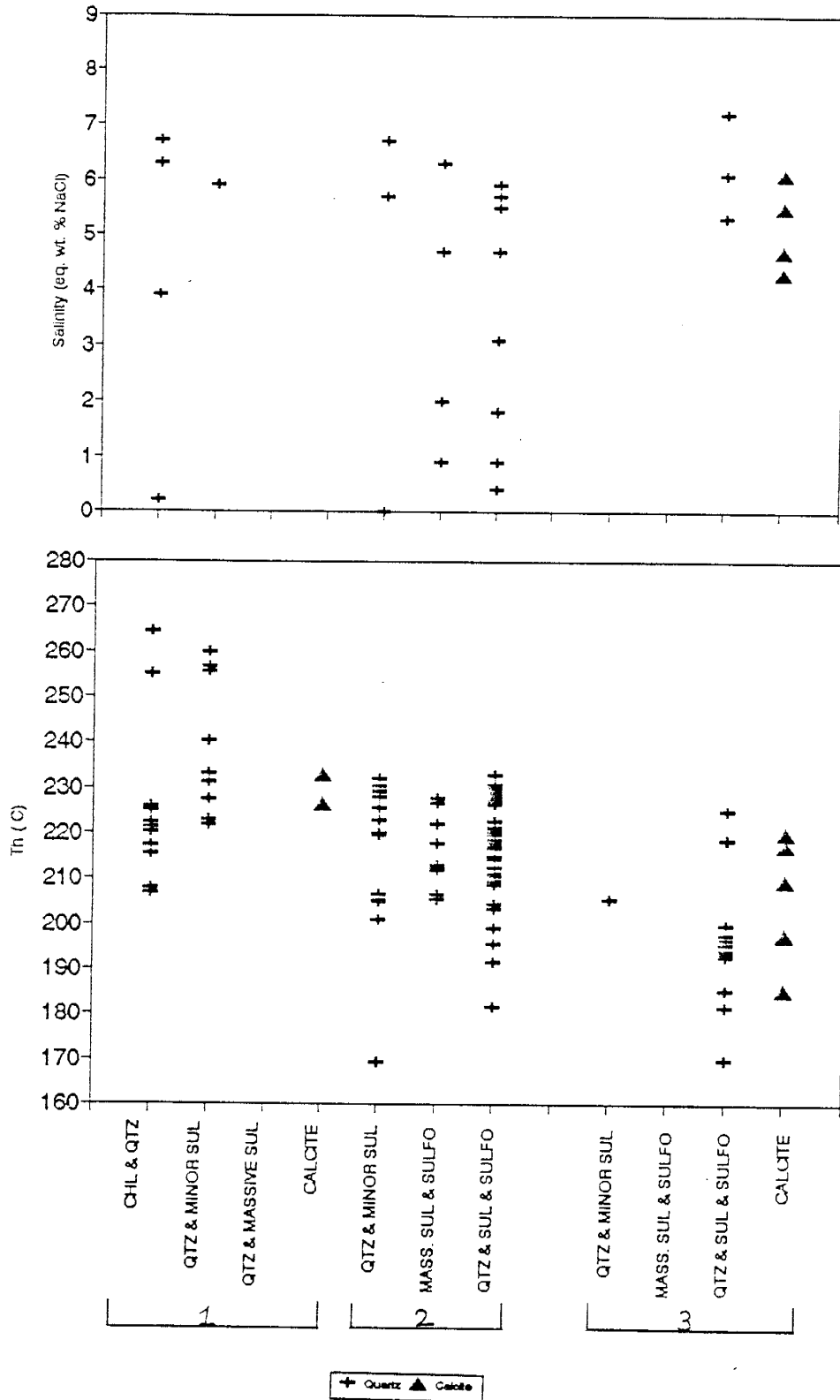
Pressure Regime:

The pressure regime during mineralization was determined by plotting the fluid inclusion histograms against boiling curves for each stage of mineralization (Fig. 24). Histograms were moved up or down the curves until a best fit is obtained with the only constrains being the vertical interval between sample occurrences. It was not clear from the mineralogy during which stage surface mineralization formed. Values for surface samples lie only on the boiling curves for stage 1 data, hence it was assumed surface samples formed during this stage. These plots indicate a total piezometric head decreased of about 300 m; about 200 m. from stage 1 to stage 2 mineralization and another 100 m. decrease during stage 3.

Figure 24. Depth below water table during each stage of
mineralization. Boiling curves are from Simmons
(1986), the upper curve is for pure water, the other
for 5 eq. wt. % NaCl fluid. Horizontal lines indicate
the respective position of surface, 325 m. level, and
the 425 m. level.
a) stage 1 fluid inclusion data
b) stage 2 fluid inclusion data
c) stage 3 fluid inclusion data
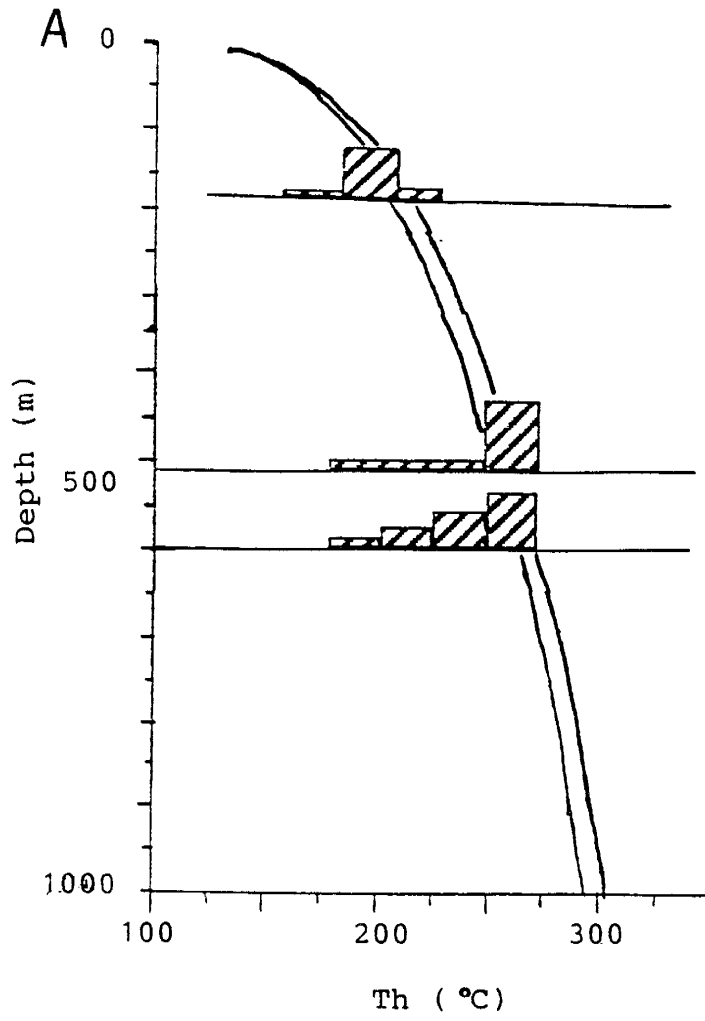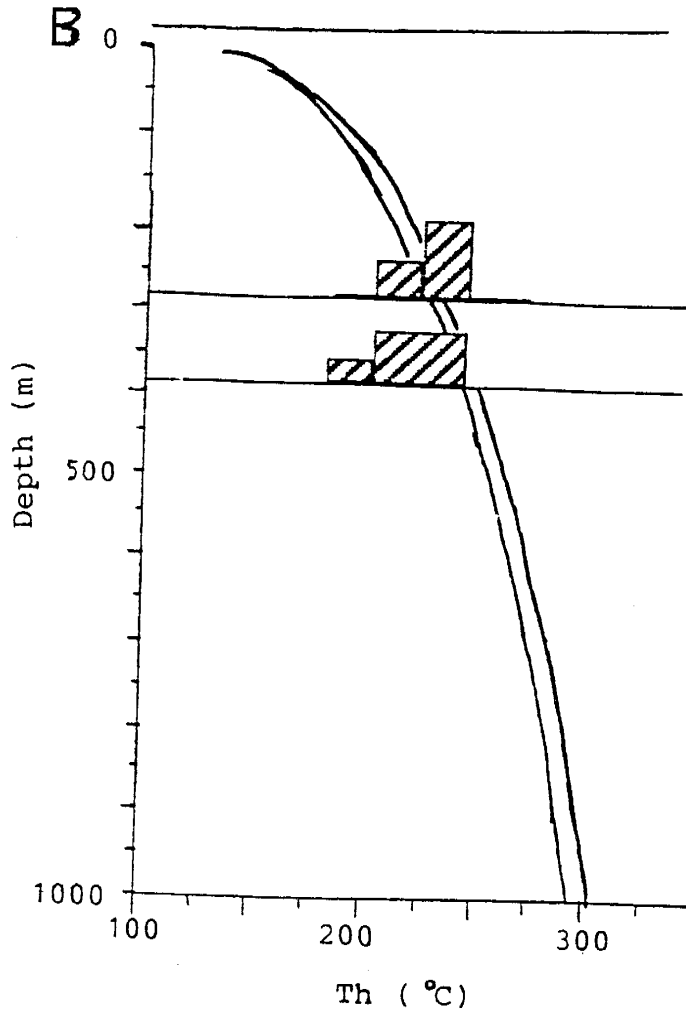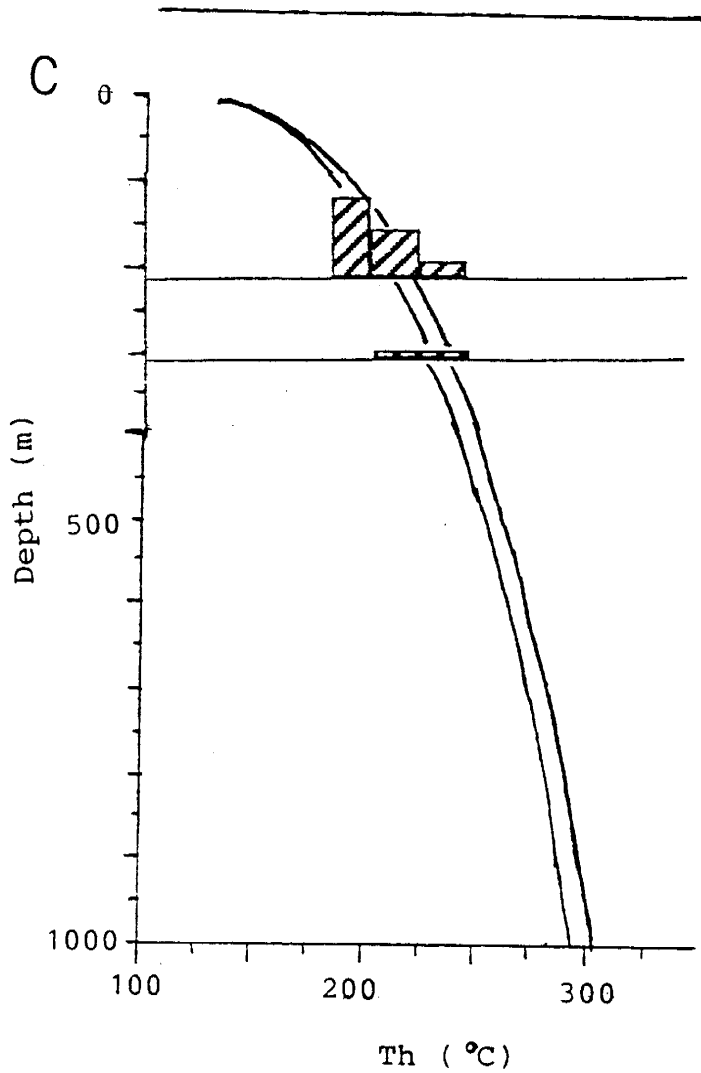
DISCUSSION:

MINERALIZING EVENTS:

The three stages recognized show similar mineral assemblages in the same depositional sequences indicating repeated introduction of similar fluids. Fluid conduits were likely connected both vertically and laterally since all three stages are seen throughout the vein.

Initial opening of the San Mateo vein caused brecciation and space that was filled by stage 1 mineralization. The breccia fragments and surrounding wallrock were propylitically altered. Quartz is seen around the breccia fragments and is abundant. This quartz could have acted as a sealant and prevented later alteration. During stage 2 the vein must have gradually opened again, permitting deposition of finely banded quartz, sulfide minerals and sulfosalts. Stage 3 mineralization is localized into pipelike bodies of brecciated mineralization that can best be explained as hydrothermal breccia pipes perhaps the result of hydrothermal explosion. These are known to occur in active geothermal systems at shallower depths (Kacura, 1968), and hydrothermal breccias would agree with shallower formation of stage 3 mineralization as indicated by fluid inclusion data.

Mineral Deposition:

The assays of base metals correlate with one another, with the best correlation occurring among samples from the 425 m. level. Ag correlates with the base metals in all stages on the 320 m. level and only in stage 2 on the 425 m. level. Au correlates with Pb and Ag in stages 2 and 3 on the 320 m. level as well as Zn and Cu on the 425 m. level. These groups of elements also were seen petrographically to occurred together, such as Ag and Pb in mymerketic intergrowths of galena in pyrargyrite and polybasite. Correlation of the assay values indicate that the elements were deposited in the same area. The implication is that either they were carried together in solution or that the depositional mechanism at each of the high value areas was similar or that ore shoots were areas where more open space was generated. There appears to be no discontinuity in the host rock or changes in the way the minerals were deposited at those locations that would allow for local depositional mechanisms. The paragenesis indicates minerals were deposited in sequence, hence the correlations best indicate zones of open space for mineralization. The indicated mixing, fluid boiling and cooling will cause deposition of base metals and silver from chloride-rich ore solutions (Barnes, 1979). During each stage of mineralization there is a classic paragenesis going from base metals to Ag deposition. The lower levels of Ag in stage 1 could

be the result of stage 1 occurring at higher temperatures and Ag being deposited further out from the San Mateo vein. At Creede Co. bonanza Ag occurred distally in veins and is associated with mixing (Robinson and Norman, 1983).

Mineralization may also be controlled by salinity with sulfide minerals and sulfosalts being deposited from higher salinity fluids as indicated by sphalerite fluid inclusion data. Stage 2 and 3 mineralization started out with higher temperatures than indicated at the close of the preceding stage and temperatures decreased over time. This is especially evident in the stage 2 quartz bands. A fluctuating piezometric head or pressure regime could account for this trend. There is an overall trend of the piezometric head falling with minor fluctuations as each new stage of mineralization began. This falling head may contribute to the abundant metal deposition on the 320 m. level.

CHEMICAL NATURE OF THE FLUIDS:

Evidence for the chemical nature of the ore fluids was derived from the mineralogical, element analysis and fluid inclusion data. Fluid inclusion temperatures of 168 ºC to 278 ºC and mineral assemblages indicate a specific range of log a_{S_2} values as shown in Figure 25. The arsenopyrite field in Figure 25 is preempted by the lack of arsenic and the abundance of pyrite.

Argentite/acanthite appears as a late stage mineral which indicates higher values of log a_{S_2} (Fig. 25). From the mineral assemblages and temperatures of the fluids it can be seen that there is an increase in log a_{S_2} which coincided with a decrease in temperature.

Boiling conditions prevailed throughout the three stages of mineralization which implies that CO_2 escaped and the pH of the system increased. Reed and Spycher (1988) point out that in order to precipitate gold, sulfide must be lost either through boiling, causing a loss of H_2S to a gas phase, or by precipitation of sulfide minerals. The log a_{S_2} increases which means the H_2S gas concentrations must have increased.

The precipitation of sulfide minerals is linked to the salinity of the solutions. Saline waters would carry chlorine complexes of Pb, Zn, and Cu. Silver can be transported by bisulfide complexes but in higher salinity fluids silver can be transported by chloride complexing (Henley, 1988). Seward (1976) showed also, that in dilute sodium chloride waters (Broadlands system), chlorosilver complexes probably account for much of the silver present. In the San Mateo the salinities exhibit a range of values from 0.0 to 8.2 eq. wt. % NaCl. Higher salinity fluids were associated with sulfide and sulfosalt deposition, whereas lower salinity fluids were associated with the gangue mineralization. The metals (Pb, Zn, and Cu) were most likely carried as chloride complexes within this

Figure 25.   Temperature and log a_{S_2} diagram for sulfide and

sulfosalt assemblages (after Gemmel et al., 1988).

Shaded area represents the conditions of deposition

for the San Mateo vein ore deposits.
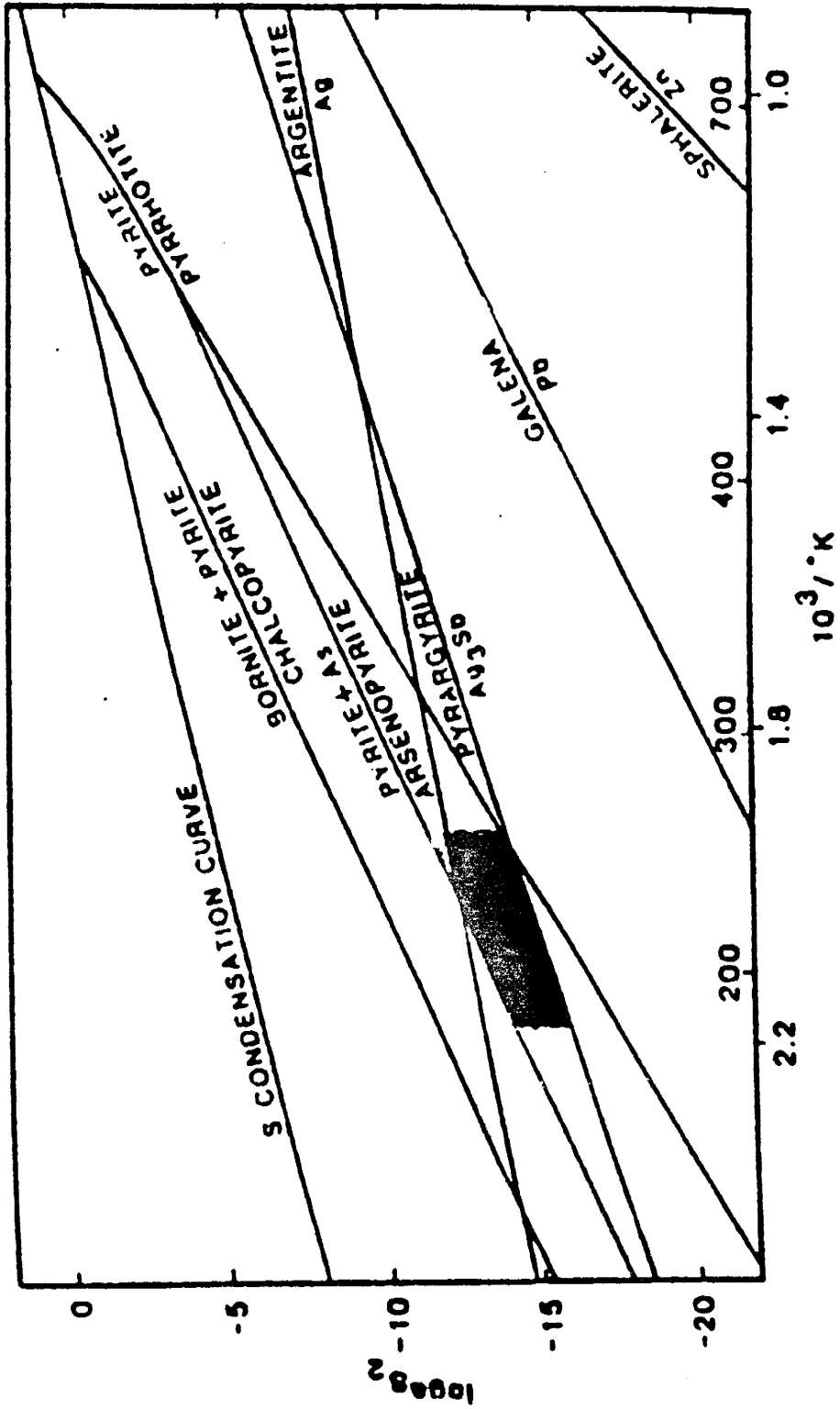
system. Silver can be carried by both chloride complexes and bisulfide complexes. Transportation as a chloride complex is more likely considering the measured fluid salinities and temperatures.

Boiling resulting in an increase of pH which resulted in sulfide and silver sulfosalt deposition. Th-salinity diagrams indicate mixing was accompanied by cooling, suggesting that metal deposition may have been accentuated. As boiling continued in the later periods of each mineralization stage, much of the sulfide in solution had been deposited in sulfide minerals, with remaining sulfide as H_2S gas boiled away. These two sinks for sulfide in solution resulted in silver and gold deposition.

Deposition of quartz occurred over a broad range of temperatures. This scenario was carried out in each of the three stages of mineralization. During the first stage, only sulfide minerals were deposited at high concentrations. The fluid either did not contain gold in solution or not enough sulfur was lost from solution for gold to be precipitated. In the second and third, lower temperature stages sulfide minerals, silver sulfosalts and gold were deposited. A fluid in which the sulfur in solution was depleted by both of the above processes allowed for deposition of silver and gold to occur in these stages as a late stage deposit

Gold occurs in all levels of the San Mateo vein but only below 450 m. in the Santo Niño vein. This may be due to several reasons. Tetrahedrite is concentrated in the banding of stage 3 of the Santo Niño vein. This may indicate that there was not sufficient sulfur

to carry gold in solution as bisulfate Au. If the piezometric head fell throughout the deposition of all stages of mineralization in the San Mateo vein, than the ovserved surface development of the San Mateo vein would indicate upward flowing solutions, allowing for stage 2 and 3 mineralization to be at the higher levels.

RELATIONSHIP TO THE DISTRICT:

Comparisons of the San Mateo vein to the Santo Niño vein are summarized in Table 7. Similarities are readily apparent in the geology, mineralogy and fluid inclusions of the ore bodies. However, there are several differences.

San Mateo vein data indicates there are only three stages of mineralization not four as in the Santo Niño vein (Gemmel, et al, 1988). The first two stages of the Santo Niño vein consist of distinct breccias: stage 1 contains a breccia of unaltered graywacke, while stage 2 consists of a breccia of propylitically altered Chilitos Formation. Stage 1 is volumetrically important, is the richest in ore, and is hosted in the Proaño Group. Stage 2 is lower in the amount of ore minerals. Stage 3 is the second-richest ore-bearing stage and it consists of banded sulfide minerals and quartz. Stage 1 of the Santo Niño does not have a similar analog in the San Mateo vein perhaps due to the host rock. Stage 1 of the San Mateo vein is similar to stage 2 of the Santo Niño vein. They are both low in ore minerals and are comprised of propylitically

Table 7.   Comparisons of the San Mateo and Santo Niño veins.

FEATURE	SANTO NINO VEIN	SAN MATEO VEIN
Structure	N 70º E, dip SE	N 60º E, dip SE
Host Rock	Proano & Chilitos Fms.	Chilitos Fm.
Grade	High Ag, some Au Base Metals < 0.3%	High Ag, some Au Base metals < 0.3%
Mineralogy	Sulfides, sulfosalts, arsenopyrite, tetrahedrite quartz, calcite, chlorite	Sulfides, sulfosalts, native silver & gold quartz, chlorite, minor calcite
Stages	1: breccia Pb-Zn-Ag-As 2: breccia Pb-Zn (Ag) 3: banding 4: massive calcite	1: breccia 2: banding 3: massive mineralization breccia and veins
Fluid Inclusions	Boiling evident	Boiling evident
Homo. Temp.	171-261 ºC	168-278 ºC
Salinities	up to 12 % NaCl, bimodal	up to 8.2 % NaCl

altered breccias of the Chilitos Formation. Stage 2 of the San Mateo vein is similar to stage 3 of the Santo Niño vein. Both are metal rich and consist of banded quartz. Stage 3 of the San Mateo vein is perhaps a local event and has not been reported in the Santo Niño vein. The fourth stage calcite of the Santo Niño vein could be the late calcite seen in the third stage of the San Mateo vein, however the calcite in the San Mateo vein was never massive occurring only as vug filling and thin bands.

There are some significant differences between the veins. Santo Niño vein contains arsenic-rich minerals, such as arsenopyrite, and arsenic rich members of the sulfosalts solid solution series but only in stage 1. The lack of such minerals in the San Mateo vein agrees with the contention that the Santo Niño stage 1 mineralizing event does not occur in the San Mateo vein. Gold was not observed by Gemmel et al, 1988, however it has been noted to occur below the 450 m. level in the Santo Niño vein. In the San Mateo vein, gold was observed on the 320 m. level. Two generations of pyrite are seen in the Santo Niño vein in stage 1 and 2, as well as pyrrhotite, tetrahedrite and stephanite. Only one generation of pyrite in each of the three stages was observed in the San Mateo vein while the other minerals were not observed. Paragenetically, the Santo Niño vein has sulfide minerals occurring first followed by sulfosalts in each stage of mineralization. In the San Mateo vein, the sequence of minerals is the same except that the sulfosalt and native element minerals occurred later in the

paragenesis for each stage.

Fluid inclusion data from both ore bodies suggest similar homogenization temperatures, and pressures for the mineralizing fluids. For the Santo Niño vein, Th's ranged between 171 - 261 ºC (Simmons, et al, 1988). Th values for the San Mateo vein ranged between 168-278 ºC with Th values above 232 ºC mainly in sphalerite. The salinity data for the San Mateo vein indicates a fluid with an average salinity of 3.6 eq. wt. % NaCl. Simmons (1988) found for the Santo Niño vein three distinct fluids with a sphalerite-saturated solutions having salinities of 8.5 to 12 eq. wt. % NaCl, a quartz-saturated fluid with an average salinity of 2 eq. wt % NaCl, and a calcite-saturated fluid. Sphalerite inclusions were observed for the San Mateo vein with one measurement producing a salinity of 16.6 eq. wt. % NaCl. San Mateo fluid inclusion data indicates a continuous range of fluid salinities, and stage 1 data indicates mixing between two fluids one at about 260 ºC, 8 eq wt % NaCl and a second at about 230 ºC, 0-1 eq. wt. % NaCl. Stage 2 data also indicates mixing between two fluids but at a lower temperature. Calcite fluid inclusion data is similar to quartz indicating these were deposited by the same fluid. Boiling was extensive in both veins.

Piezometric head is indicated to have changed approximately 200 m for the Santo Niño vein and about 300 m for the San Mateo vein. This may explain mineral distribution (spatial) in the district. Rock volumes show correspondence between high

temperatures, high salinities and abundant base metals, notably the Cerro Proaño area. The vertical and horizontal metal zonations in the Fresnillo district are similar to Buchanan's (1981) model. Simmons (1991) proposed that fluids responsible for the formation of the Cerro Proaño mineralization flowed laterally outwards forming vein mineralization. Plots of Th versus salinities for the Cerro Proaño, the Santo Niño vein and the San Mateo vein are plotted against lines of constant density suggest that the inclusion fluids associated with all three had about the same density (Fig. 26). Dropping of the piezometric head implies that the system operated at greater relative depths and mineralization was associated with lower temperature fluids. Metals deposited at distal points of the geothermal system (Ag and Au) would be superimposed in time on mineralization associated with deeper, higher temperature part of the system (Fig 27). The precious metals would also be deposited high in the system, topographically above the base metals, as is evident in the San Mateo vein. The base metals are early in the paragenesis and are richer on the 425 m. level. The precious metals are later in the paragenesis and are richest on the 320 m. level. This system could also explain the offset in the stages of mineralization between the veins. Bonanza silver mineralization in the "light" veins at Fresnillo could be the result of fluid mixing and boiling with Au and Ag depositing over a broad vertical range dependent upon the fluctuating piezometric head.

Figure 26.   Th versus salinities for fluid-inclusions from the

Cerro Proaño, the Santo Niño, and the San

Mateo.

DENSITY
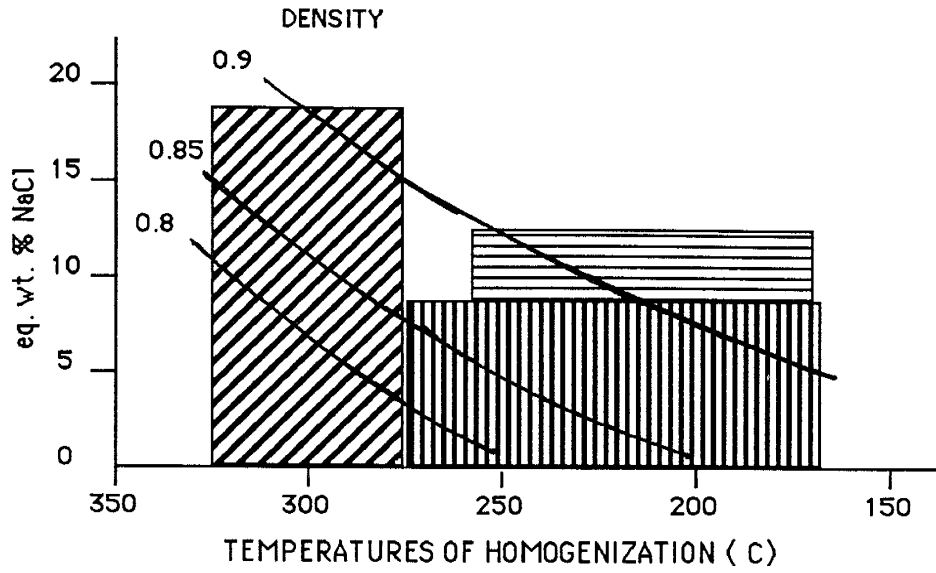
CERRO PROANO

SANTO NINO VEIN

SAN MATEO VEIN

Figure 27.   A system showing the distribution of precious metals and base metals based on Buchanan's model and a fluctuating water table.
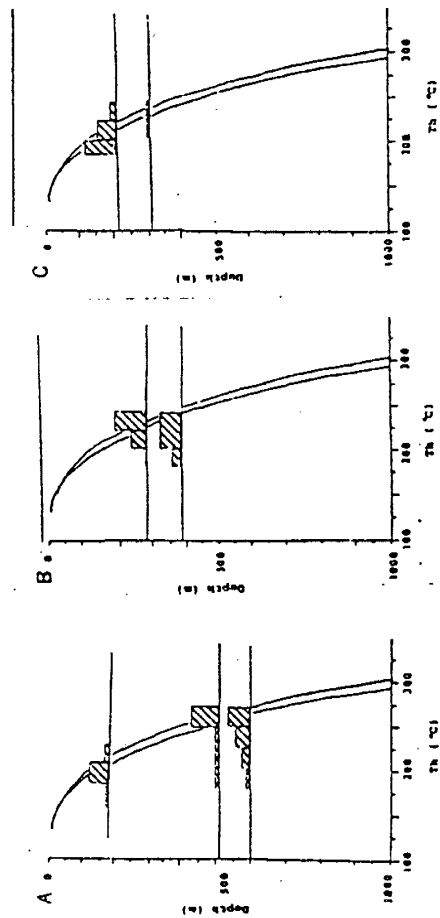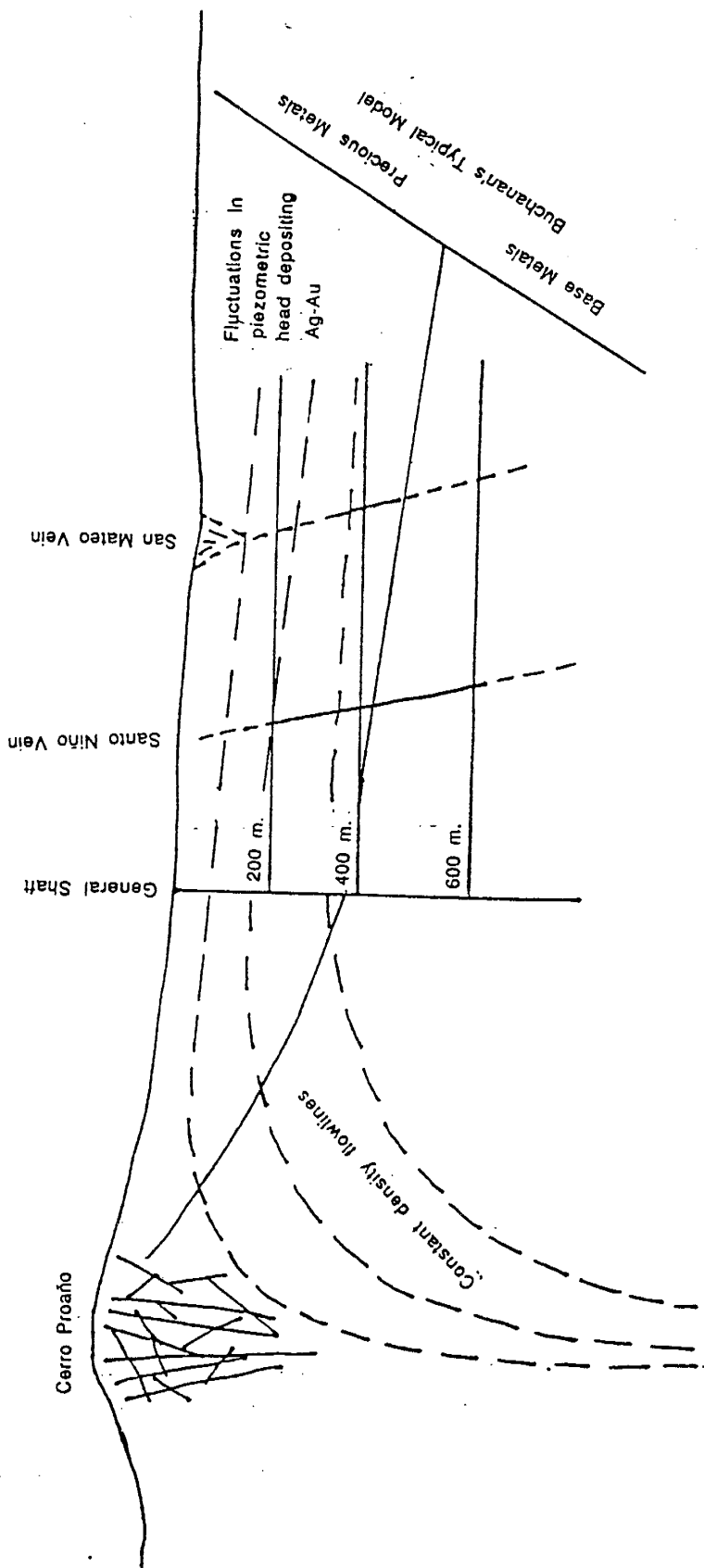
Pressure Regime from fluid Inclusion data.

CONCLUSIONS:

The following conclusions have been drawn from this study:

1. There were three stages of depostion with formation of similar mineral assemblages of quartz and sulfide minerals and sulfosalts. In the later periods of both stages 2 and 3 silver and gold were deposited. These stages are the same as stage 2, 3 and possible stage 4 in the Santo Niño vein.

2. Distribution of silver and gold from assay values correlated with the occurrence of stages 2 and 3 mineralization and indicated that stage 1 and 2 had some gold and stage 1 had minor silver.

3. Statistical analyses of the elements showed that the base metals correlated in all stages while silver correlated significantly with the base metals in most stages. Gold mainly correlated with lead and silver. This indicates that the fluids depositing the 3 different stages were of similar composition and that the precipitation of gold was a later mineralizing event in each stage.

4. Temperatures for mineralization ranged from 168 °C to 278 °C. Boiling conditions existed in all stages of mineralization.

5. Saline-rich fluids were associated with massive sulfide and sulfosalt deposition. Quartz was deposited as temperatures were falling. Mixing between fluids of different salinities occurred. There was rhythmic and repeated deposition of py-sph-gal-Ag and Au in bands of quartz.

6. Boiling, and mixing accompanied by cooling of fluids carring chloride complexes of Ag, Pb, Zn, and Cu and bisulfide complexes of Au allowed for deposition of each of the three stages of mineralization.

7. The San Mateo vein is similar in a gross fashion both in composition and origin to the Santo Niño vein. Minor differences do not preclude invoking a regional model for deposition of the Ag veins.

8. A hydrothermal system under progressive lowering of the piezometric head with laterally flowing fluid of constant density was responsible for the mineralization observed in the Santo Niño and the San Mateo veins and explains the lateral occurrence of Ag and Au minerals deposited by fluids near the distal margins of the heat source.

APPENDIX 1: SAMPLE LOCATIONS AND DESCRIPTIONS

SAMPLE NO.	LEVEL	X (m.)	POSITION	MAIN STAGE	ASSEMBLAGE FOR EACH STAGE
943A	320	0	HW	2	Massive sulfides sulfosalts & qtz
944A	320	4	HW	1	Chlorite & qtz
944B	320	4	FW	1	Chlorite & qtz
9510A	320	8	HW	1	Qtz & minor sulfides
9510B	320	8	FW	1	Qtz & minor sulfides Chlorite & qtz
959A	320	23	HW	2	Qtz & minor sulfides
959C	320	23	Center	2 1	Qtz & sulfides & sulfosalts Chlorite & qtz
958A	320	48	HW	2	Qtz & minor sulfides
958C	320	48	Center	2	Qtz & sulfides & sulfosalts
958B	320	48	FW	2	Qtz & sulfides & sulfosalts
956A	320	72	HW	2 1	Qtz & sulfides & sulfosalts Chlorite & qtz & sulfides
956B	320	72	FW	2 3	Qtz & sulfides & sulfosalts Massive sulfides & sulfosalts & native element minerals
941A	320	85	HW	2	Massive sulfides & sulfosalts
941C	320	85	Center	2 3	Massive sulfides & sulfosalts & qtz Massive sulfides & sulfosalts
941B	320	85	FW	3 2	Massive sulfides & sulfosalts Qtz & sulfides & sulfosalts
942C	320	95	Center	2 1	Qtz & minor sulfides Qtz & chlorite
955	320	100	Center	1	Chlorite
953A	320	113	HW	2	Qtz & sulfides
953C	320	113	Center	2	Qtz & minor sulfides

SAMPLE NO.	LEVEL	X (m.)	POSITION	MAIN STAGE	ASSEMBLAGE FOR EACH STAGE
953B	320	113	FW	2	Massive sulfides & sulfosalts
952A	320	132	HW	1	Chlorite & qtz
952C	320	132	Center	2	Qtz & sulfides & sulfosalts
952B	320	132	FW	3	Qtz & minor sulfides
951A	320	147	HW	1	Chlorite & qtz
951C	320	147	Center	2	Massive sulfides & sulfosalts & qtz
				3	Massive sulfides & sulfosalts
951B	320	147	FW	2	Qtz & minor sulfides
962A	425	6	HW	1	Chlorite & qtz & sulfides
962B	425	6	FW	1	Chlorite & qtz & sulfides
963A	425	12	HW	1	Chlorite & qtz & sulfides
963B	425	12	FW	1	Chlorite & qtz
964A	425	18	HW	1	Chlorite & qtz
964B	425	18	FW	1	Chlorite & qtz
965A	425	24	HW	2	Massive sulfides & sulfosalts
965C	425	24	Center	3	Sulfides & sulfosalts
				2	Qtz & sulfides & sulfosalts
965B	425	24	FW	1	Chlorite & qtz
966A	425	30	HW	3	Qtz & sulfides & sulfosalts
966C	425	30	Center	3	Qtz & sulfides & sulfosalts
				2	Qtz & sulfides & calcite
966B	425	30	FW	2	Qtz & minor sulfides
				1	Chlorite & qtz
961	425	39	Center	2	Qtz & minor sulfides
				1	Qtz & minor sulfides

APPENDIX 2: ASSAY DATA

X m	Y level	length m	width m	Au ppm	Ag ppm	Pb %	Zn %	Cu %
2	320	0.80	0.8	0.6	876	0.10	0.90	0.08
2	320	0.80	1.6	0.1	446	0.10	0.80	0.03
2	320	0.50	2.1	2.6	4186	0.70	1.00	0.12
2	320	0.70	2.8	0.0	92	0.10	0.30	0.04
4	320	0.30	0.3	0.0	6	0.00	0.00	0.01
4	320	0.20	0.5	0.1	474	0.10	0.60	0.06
4	320	1.50	2	0.0	4	0.00	0.10	0.01
4	320	0.30	2.3	0.8	1610	0.20	0.60	0.08
4	320	0.30	2.6	0.0	110	0.10	0.30	0.03
6	320	0.40	0.4	0.0	224	0.10	0.30	0.05
6	320	0.30	0.7	0.0	10	0.00	0.10	0.01
6	320	0.20	0.9	4.4	926	0.10	0.20	0.03
6	320	0.30	1.2	0.0	56	0.00	0.10	0.02
6	320	0.80	2	0.8	1356	0.20	0.90	0.18
8	320	0.50	0.5	0.0	12	0.00	0.10	0.01
8	320	0.30	0.8	1.0	1462	0.20	1.40	0.11
8	320	0.30	1.1	0.0	440	0.10	1.20	0.06
8	320	0.50	1.6	0.9	1290	0.20	0.40	0.08
8	320	0.70	2.3	0.0	314	0.10	0.50	0.05
10	320	0.60	0.6	0.0	34	0.00	0.10	0.01
10	320	0.40	1	2.0	1260	0.60	0.90	0.08
10	320	0.40	1.4	0.1	864	0.10	0.70	0.05
10	320	0.50	1.9	1.8	4440	0.50	1.20	0.14
10	320	0.70	2.6	0.0	60	0.00	0.10	0.01
12	320	0.70	0.7	0.0	96	0.10	0.10	0.04
12	320	0.50	1.2	1.0	2516	0.20	0.70	0.06
12	320	1.00	2.2	0.8	286	0.10	0.40	0.06
14	320	1.00	1	0.0	16	0.00	0.10	0.01
14	320	0.30	1.3	2.2	920	0.10	0.20	0.02
14	320	0.30	1.6	0.6	570	0.10	0.20	0.03
14	320	0.40	2	2.2	1290	0.10	0.50	0.04
14	320	0.50	2.5	0.0	84	0.00	0.20	0.02
16	320	0.90	0.9	0.0	54	0.00	0.10	0.01
16	320	0.40	1.3	0.1	254	0.10	0.40	0.08
16	320	0.70	2	0.1	140	0.10	0.10	0.01
16	320	1.00	3	3.4	1774	0.20	0.60	0.03
18	320	0.80	0.8	0.0	28	0.00	0.10	0.02
18	320	0.30	1.1	0.0	64	0.00	0.20	0.02
18	320	0.40	1.5	0.0	8	0.00	0.10	0.01
18	320	1.00	2.5	0.4	658	0.10	0.40	0.06
18	320	0.40	2.9	1.2	3286	0.30	0.60	0.05
20	320	1.30	1.3	0.0	12	0.00	0.10	0.01
20	320	0.30	1.6	0.3	1360	0.10	1.30	0.05
20	320	0.30	1.9	0.0	120	0.00	0.30	0.02
20	320	0.90	2.8	2.5	5540	0.50	1.60	0.10
22	320	0.30	0.3	0.0	370	0.10	0.20	0.06
22	320	1.30	1.6	0.0	10	0.10	0.00	0.01

X m	Y level	length m	width m	Au ppm	Ag ppm	Pb %	Zn %	Cu %
22	320	0.80	2.4	0.5	12280	0.40	1.90	0.18
22	320	1.10	3.5	0.9	4800	0.10	3.70	0.07
24	320	1.50	1.5	0.0	10	0.00	0.00	0.01
24	320	1.10	2.6	1.6	5820	0.10	1.10	0.07
24	320	1.20	3.8	2.5	2660	0.10	1.70	0.03
26	320	1.50	1.5	0.0	10	0.00	0.00	0.01
26	320	1.80	3.3	3.7	3990	0.20	1.90	0.06
28	320	1.50	1.5	0.0	220	0.10	0.30	0.02
28	320	0.50	2	2.4	7284	0.50	1.00	0.12
28	320	0.70	2.7	0.0	6	0.00	0.00	0.01
28	320	0.70	3.4	4.6	1486	0.10	0.20	0.02
30	320	0.90	0.9	0.0	10	0.00	0.00	0.01
30	320	1.60	2.5	2.9	3030	0.40	1.30	0.04
30	320	1.40	3.9	0.0	8	0.00	0.00	0.01
32	320	0.80	0.8	0.0	10	0.00	0.00	0.01
32	320	1.30	2.1	0.5	3990	0.20	1.90	0.04
32	320	1.00	3.1	0.0	6	0.00	0.00	0.01
34	320	0.35	0.35	0.0	4	0.00	0.00	0.01
34	320	1.00	1.35	1.0	2804	0.30	1.20	0.04
34	320	1.20	2.55	0.0	4	0.00	0.00	0.01
36	320	1.20	1.2	3.6	4060	0.30	1.10	0.03
36	320	1.10	2.3	0.0	4	0.00	0.00	0.01
36	320	0.40	2.7	2.8	338	0.20	0.40	0.04
38	320	0.60	0.6	0.7	1756	0.20	1.40	0.03
38	320	0.50	1.1	0.0	6	0.00	0.00	0.01
38	320	1.00	2.1	14.1	8302	1.20	3.00	0.05
38	320	0.70	2.8	0.0	4	0.00	0.10	0.01
40	320	0.40	0.4	0.3	320	1.00	0.40	0.04
40	320	1.40	1.8	0.0	42	0.00	0.00	0.01
40	320	1.00	2.8	5.0	14377	1.30	2.40	0.15
40	320	0.60	3.4	0.0	6	0.00	0.10	0.01
42	320	1.50	1.5	0.0	4	0.00	0.00	0.01
42	320	1.10	2.6	9.9	12787	1.60	5.70	0.12
42	320	0.40	3	0.0	10	0.00	0.10	0.01
44	320	2.20	2.2	0.0	6	0.00	0.10	0.01
44	320	1.20	3.4	9.3	10531	1.40	3.20	0.01
46	320	2.10	2.1	0.0	4	0.00	0.00	0.01
46	320	1.10	3.2	4.6	13331	1.30	0.30	0.10
48	320	1.40	1.4	0.0	4	0.00	0.00	0.01
48	320	1.80	3.2	5.7	8095	0.90	4.30	0.10
50	320	1.40	1.4	0.0	4	0.00	0.10	0.01
50	320	1.50	2.9	13.9	7811	1.00	3.40	0.05
50	320	0.40	3.3	0.0	20	0.00	0.10	0.01
52	320	1.20	1.2	0.1	750	0.00	0.00	0.01
52	320	1.00	2.2	1.9	5840	0.50	4.80	0.09
52	320	0.80	3	0.0	236	0.00	0.10	0.01
54	320	1.00	1	0.0	6	0.00	0.00	0.01

X m	Y level	length m	width m	Au ppm	Ag ppm	Pb %	Zn %	Cu %
54	320	0.90	1.9	3.6	4063	0.20	1.40	0.03
54	320	1.10	3	0.0	6	0.00	0.00	0.01
56	320	0.40	0.4	0.0	14	0.00	0.00	0.01
56	320	1.10	1.5	1.5	2584	0.10	0.50	0.04
56	320	1.30	2.8	0.0	4	0.00	0.00	0.01
58	320	0.60	0.6	0.0	6	0.00	0.00	0.01
58	320	0.70	1.3	2.6	2782	0.30	1.20	0.04
58	320	1.40	2.7	0.0	120	0.20	0.00	0.01
60	320	0.60	0.6	0.1	710	0.00	0.10	0.01
60	320	0.60	1.2	2.5	3748	0.30	1.00	0.05
60	320	1.80	3	0.0	36	0.00	0.10	0.01
62	320	0.40	0.4	0.0	24	0.00	0.10	0.01
62	320	0.55	0.95	2.0	1448	0.30	1.10	0.09
62	320	1.20	2.15	0.0	80	0.00	0.10	0.01
64	320	0.60	0.6	0.0	40	0.00	0.10	0.01
64	320	0.50	1.1	1.7	950	0.40	1.10	0.06
64	320	1.10	2.2	0.0	34	0.00	0.10	0.01
66	320	0.70	0.7	0.0	12	0.00	0.10	0.01
66	320	0.60	1.3	0.0	22	0.00	0.00	0.01
66	320	0.60	1.9	4.3	4538	0.70	3.60	0.13
66	320	0.70	2.6	0.0	36	0.00	0.10	0.02
68	320	1.10	1.1	0.0	6	0.00	0.10	0.01
68	320	1.20	2.3	2.0	5768	0.80	3.00	0.03
70	320	0.70	0.7	0.0	10	0.00	0.00	0.01
70	320	0.50	1.2	0.1	50	0.10	0.00	0.01
70	320	0.60	1.8	6.7	4318	1.20	4.30	0.10
70	320	0.50	2.3	0.0	6	0.00	0.00	0.01
72	320	0.50	0.5	0.0	14	0.10	0.00	0.01
72	320	0.90	1.4	0.0	40	0.00	0.00	0.01
72	320	0.80	2.2	0.0	40	0.00	0.00	0.01
72	320	0.70	2.9	11.0	919	0.40	1.10	0.03
74	320	1.00	1	0.0	10	0.10	0.00	0.01
74	320	0.70	1.7	8.0	2612	0.80	1.30	0.05
74	320	1.00	2.7	0.0	20	0.10	0.00	0.01
76	320	0.80	0.8	0.0	22	0.10	0.00	0.01
76	320	0.70	1.5	3.8	2267	1.90	1.90	0.04
76	320	1.10	2.6	0.0	30	0.10	0.00	0.02
78	320	0.60	0.6	0.0	16	0.10	0.00	0.01
78	320	0.65	1.25	7.0	2539	1.40	2.20	0.14
78	320	1.00	2.25	0.0	4	0.10	0.00	0.01
80	320	0.35	0.35	0.0	4	0.10	0.10	0.01
80	320	0.40	0.75	0.0	4	0.10	0.00	0.01
80	320	0.50	1.25	5.0	2439	2.90	4.00	0.12
80	320	1.10	2.35	0.0	26	0.10	0.00	0.01
82	320	1.50	1.5	0.0	196	0.10	0.20	0.02
82	320	1.00	2.5	3.2	2469	1.00	1.10	0.04
82	320	0.60	3.1	0.0	26	0.10	0.00	0.01

X m	Y level	length m	width m	Au ppm	Ag ppm	Pb %	Zn %	Cu %
84	320	0.30	0.3	0.1	462	0.10	0.10	0.01
84	320	1.00	1.3	0.0	4	0.10	0.10	0.01
84	320	1.20	2.5	2.9	6270	2.50	2.70	0.12
84	320	0.40	2.9	0.0	26	0.10	0.10	0.01
86	320	0.40	0.4	0.0	78	0.10	0.10	0.02
86	320	0.30	0.7	0.3	1028	0.10	0.70	0.02
86	320	0.60	1.3	0.7	500	0.40	1.10	0.02
86	320	1.30	2.6	2.6	5988	0.60	4.20	0.07
88	320	0.40	0.4	0.0	20	0.10	0.10	0.01
88	320	0.80	1.2	0.1	450	0.10	0.50	0.01
88	320	1.50	2.7	1.3	5350	0.60	4.80	0.08
90	320	1.00	1	0.0	230	0.10	0.10	0.01
90	320	1.70	2.7	0.5	7520	1.90	9.10	0.08
90	320	1.00	3.7	0.0	74	0.10	0.10	0.01
92	320	0.40	0.4	0.8	1004	0.50	1.80	0.02
92	320	2.20	2.6	2.6	4974	1.90	6.50	0.06
92	320	0.90	3.5	0.0	20	0.00	0.10	0.01
94	320	0.60	0.6	0.1	1950	0.20	3.80	0.02
94	320	1.80	2.4	5.5	3485	1.50	5.00	0.05
94	320	0.40	2.8	0.0	180	0.10	0.10	0.01
96	320	1.00	1	1.9	5390	0.90	4.30	0.05
96	320	1.10	2.1	1.9	600	0.10	0.30	0.02
96	320	0.50	2.6	0.1	596	0.10	0.50	0.01
98	320	1.00	1	1.8	5530	4.60	8.20	0.15
98	320	1.00	2	3.4	1090	0.20	0.40	0.01
98	320	0.50	2.5	0.0	817	0.10	0.20	0.01
100	320	1.30	1.3	0.3	15410	4.30	7.00	0.10
100	320	1.30	2.6	9.2	871	0.10	0.30	0.02
100	320	0.60	3.2	0.0	354	0.10	0.20	0.01
102	320	0.50	0.5	0.0	100	0.10	0.10	0.01
102	320	2.10	2.6	2.2	2038	0.10	1.40	0.03
102	320	0.70	3.3	0.0	70	0.00	0.10	0.01
104	320	0.30	0.3	0.1	560	0.10	0.10	0.01
104	320	0.60	0.9	0.0	40	0.10	0.10	0.01
104	320	1.60	2.5	0.5	5200	1.90	3.90	0.08
104	320	0.70	3.2	0.8	1140	0.10	0.40	0.02
106	320	1.60	1.6	0.4	2890	0.10	1.50	0.03
106	320	0.80	2.4	0.0	230	0.10	0.10	0.01
108	320	0.40	0.4	0.0	40	0.00	0.00	0.01
108	320	1.60	2	2.2	1808	0.10	0.60	0.02
108	320	0.50	2.5	1.0	30	0.00	0.10	0.01
110	320	0.30	0.3	0.0	274	0.00	0.10	0.01
110	320	1.50	1.8	1.2	2650	0.20	1.30	0.04
110	320	0.70	2.5	0.3	570	0.10	0.40	0.02
112	320	1.10	1.1	2.2	2292	0.10	0.50	0.03
112	320	0.40	1.5	0.0	58	0.10	0.10	0.02
112	320	0.70	2.2	0.0	88	0.10	0.10	0.02

X m	Y level	length m	width m	Au ppm	Ag ppm	Pb %	Zn %	Cu %
112	320	0.20	2.4	0.1	136	0.10	0.10	0.02
114	320	0.90	0.9	1.9	1076	0.10	0.10	0.04
114	320	0.30	1.2	0.0	42	0.10	0.10	0.01
114	320	0.20	1.4	0.0	62	0.10	0.10	0.06
114	320	0.80	2.2	0.0	24	0.00	0.10	0.01
114	320	0.15	2.35	0.0	164	0.10	0.10	0.01
116	320	0.60	0.6	1.7	824	0.10	0.10	0.03
116	320	1.40	2	0.0	20	0.00	0.00	0.01
116	320	0.20	2.2	0.1	320	0.10	0.10	0.04
116	320	0.80	3	0.0	126	0.10	0.10	0.02
118	320	0.80	0.8	0.1	388	0.10	0.10	0.02
118	320	2.10	2.9	0.0	20	0.00	0.00	0.01
120	320	0.90	0.9	2.9	628	0.10	0.10	0.02
120	320	2.00	2.9	0.0	16	0.00	0.10	0.01
122	320	1.30	1.3	3.2	223	0.10	0.10	0.01
122	320	1.70	3	0.0	12	0.00	0.00	0.01
124	320	0.50	0.5	0.0	38	0.00	0.10	0.01
124	320	0.70	1.2	5.6	703	0.10	0.20	0.03
124	320	2.00	3.2	0.0	32	0.00	0.00	0.01
126	320	1.50	1.5	0.0	28	0.00	0.00	0.01
126	320	0.50	2	5.8	693	0.10	0.10	0.01
126	320	0.30	2.3	0.0	30	0.00	0.10	0.01
126	320	0.35	2.65	11.7	887	0.10	0.10	0.01
126	320	0.40	3.05	0.0	10	0.00	0.10	0.01
128	320	1.50	1.5	0.0	8	0.00	0.00	0.01
128	320	0.80	2.3	13.5	947	0.10	0.10	0.02
128	320	0.40	2.7	0.0	20	0.00	0.10	0.01
130	320	0.70	0.7	0.0	26	0.00	0.00	0.01
130	320	1.00	1.7	1.0	246	0.00	0.10	0.02
130	320	1.00	2.7	6.6	3714	0.20	0.20	0.03
130	320	0.50	3.2	0.0	80	0.00	0.10	0.01
132	320	0.70	0.7	0.0	20	0.00	0.00	0.01
132	320	0.70	1.4	0.8	690	0.10	0.10	0.02
132	320	0.60	2	0.0	40	0.00	0.00	0.01
132	320	0.90	2.9	0.5	2890	0.10	0.10	0.02
132	320	0.70	3.6	0.0	50	0.00	0.00	0.01
134	320	1.20	1.2	0.0	16	0.00	0.10	0.01
134	320	1.10	2.3	0.0	100	0.10	0.20	0.02
136	320	0.80	0.8	0.0	10	0.00	0.00	0.01
136	320	1.00	1.8	2.1	1218	0.10	0.10	0.02
136	320	0.60	2.4	0.0	8	0.00	0.10	0.01
138	320	0.60	0.6	0.0	12	0.00	0.10	0.01
138	320	0.60	1.2	3.5	747	0.10	0.10	0.04
138	320	1.50	2.7	0.0	6	0.00	0.10	0.01
140	320	1.00	1	0.0	8	0.00	0.10	0.01
140	320	0.60	1.6	2.1	708	0.10	0.10	0.02
140	320	1.30	2.9	0.0	14	0.00	0.00	0.01

X m	Y level	length m	width m	Au ppm	Ag ppm	Pb %	Zn %	Cu %
140	320	0.60	3.5	0.0	24	0.00	0.10	0.01
142	320	0.70	0.7	16.9	4884	0.10	0.30	0.04
142	320	1.80	2.5	0.0	60	0.00	0.00	0.01
142	320	0.30	2.8	0.1	380	0.00	0.10	0.01
144	320	1.00	1	60.5	11800	0.20	0.40	0.05
144	320	0.90	1.9	0.0	10	0.00	0.00	0.01
144	320	0.30	2.2	0.9	180	0.00	0.10	0.04
146	320	0.80	0.8	17.5	3703	0.00	1.20	0.04
146	320	0.60	1.4	1.7	456	0.00	0.10	0.03
146	320	0.70	2.1	0.0	76	0.00	0.10	0.01
146	320	0.20	2.3	19.7	2937	0.10	0.50	0.03
146	320	0.50	2.8	0.1	613	0.00	0.10	0.01
148	320	0.80	0.8	3.0	760	0.10	0.20	0.01
148	320	1.20	2	14.2	2076	0.10	0.30	0.01
148	320	1.00	3	0.0	66	0.00	0.10	0.01
150	320	1.50	1.5	0.0	56	0.00	0.00	0.01
150	320	0.70	2.2	7.4	2093	0.10	0.30	0.01
150	320	0.60	2.8	2.9	1038	0.10	0.10	0.01
150	320	0.70	3.5	0.0	20	0.00	0.10	0.01
152	320	0.50	0.5	0.3	470	0.10	0.10	0.01
152	320	1.80	2.3	5.5	1695	0.90	1.50	0.02
152	320	2.20	4.5	0.0	20	0.00	0.00	0.01
152	320	0.40	4.9	0.3	424	0.00	0.10	0.01
154	320	0.50	0.5	0.0	36	0.00	0.00	0.01
154	320	0.90	1.4	1.6	1790	0.10	0.40	0.02
154	320	2.60	4	0.0	20	0.00	0.00	0.01
156	320	0.30	0.3	0.0	12	0.00	0.00	0.01
156	320	1.10	1.4	15.5	3265	0.10	0.10	0.02
156	320	1.80	3.2	0.0	20	0.00	0.00	0.02
158	320	0.30	0.3	0.0	10	0.00	0.00	0.01
158	320	0.90	1.2	0.3	2810	0.10	0.30	0.05
158	320	1.40	2.6	1.0	316	0.00	0.00	0.01
160	320	1.00	1	0.0	70	0.00	0.00	0.01
160	320	1.10	2.1	2.1	618	0.00	0.10	0.01
160	320	1.10	3.2	0.0	260	0.00	0.00	0.01
162	320	1.00	1	0.0	26	0.20	0.30	0.01
162	320	0.80	1.8	2.4	1376	0.40	0.30	0.01
162	320	1.30	3.1	0.0	16	0.40	0.30	0.02
164	320	1.10	1.1	0.0	18	0.00	0.10	0.01
164	320	1.10	2.2	5.6	2761	1.00	1.00	0.01
164	320	1.00	3.2	0.0	26	0.00	0.20	0.02
166	320	1.30	1.3	0.0	12	0.00	0.00	0.01
166	320	0.70	2	13.5	1873	0.10	0.30	0.03
166	320	1.00	3	0.0	28	0.10	0.10	0.07
168	320	1.20	1.2	0.0	12	0.00	0.00	0.01
168	320	0.50	1.7	10.2	1976	0.20	0.70	0.05
168	320	1.20	2.9	0.0	86	0.00	0.00	0.01

X m	Y level	length m	width m	Au ppm	Ag ppm	Pb %	Zn %	Cu %
170	320	2.50	2.5	0.0	12	0.00	0.00	0.01
170	320	0.60	3.1	11.2	3199	0.30	0.50	0.04
170	320	0.40	3.5	0.0	110	0.00	0.00	0.01
172	320	0.30	0.3	0.0	140	0.10	0.10	0.04
172	320	0.50	0.8	4.7	3206	0.40	1.00	0.04
172	320	0.80	1.6	0.0	16	0.00	0.00	0.00
172	320	0.60	2.2	3.0	3628	0.70	1.60	0.07
172	320	0.50	2.7	0.0	80	0.00	0.00	0.01
174	320	0.20	0.2	0.0	8	0.00	0.00	0.01
174	320	0.60	0.8	0.0	30	0.10	0.50	0.04
174	320	1.40	2.2	0.0	20	0.00	0.00	0.01
174	320	0.20	2.4	0.8	790	0.10	0.10	0.02
174	320	0.30	2.7	0.0	20	0.00	0.00	0.01
176	320	0.60	0.6	0.0	8	0.00	0.00	0.01
176	320	0.50	1.1	8.9	3228	0.70	0.80	0.05
176	320	2.70	3.8	0.0	16	0.00	0.00	0.01
176	320	0.20	4	2.1	3548	0.20	0.70	0.06
0	425	0.60	0.6	0.0	40	0.10	0.10	0.02
0	425	0.90	1.5	0.1	210	0.90	1.50	0.11
0	425	1.30	2.8	0.0	26	0.10	0.10	0.02
2	425	0.70	0.7	0.0	10	0.00	0.10	0.02
2	425	1.00	1.7	0.0	180	0.40	1.30	0.13
2	425	1.10	2.8	0.0	30	0.00	0.10	0.01
4	425	0.60	0.6	0.0	6	0.10	0.10	0.05
4	425	0.80	1.4	0.3	306	0.10	0.40	0.03
4	425	0.80	2.2	0.0	4	0.00	0.00	0.01
6	425	0.60	0.6	0.0	6	0.00	0.00	0.01
6	425	1.00	1.6	0.1	206	0.00	0.40	0.05
6	425	0.70	2.3	0.0	4	0.00	0.00	0.01
8	425	0.70	0.7	0.0	4	0.00	0.00	0.01
8	425	1.10	1.8	0.1	204	0.10	0.40	0.06
8	425	0.60	2.4	0.0	90	0.00	0.00	0.01
10	425	2.00	2	0.0	60	0.00	0.10	0.01
10	425	1.00	3	0.1	246	0.20	0.60	0.06
10	425	0.70	3.7	0.0	90	0.10	0.20	0.02
12	425	0.50	0.5	0.1	260	0.00	0.10	0.08
12	425	1.10	1.6	0.0	70	0.10	0.60	0.05
12	425	0.70	2.3	0.0	16	0.00	0.00	0.01
14	425	0.60	0.6	0.1	126	0.00	0.10	0.01
14	425	0.80	1.4	1.3	284	0.30	0.60	0.04
14	425	1.00	2.4	0.0	96	0.10	0.10	0.03
16	425	0.80	0.8	0.0	26	0.00	0.00	0.01
16	425	0.70	1.5	1.3	950	0.50	2.30	0.10
16	425	1.00	2.5	1.3	286	0.10	1.00	0.05
16	425	0.50	3	0.0	16	0.00	0.00	0.01
18	425	0.50	0.5	0.0	50	0.00	0.00	0.01
18	425	0.90	1.4	0.1	180	0.10	0.70	0.05

X m	Y level	length m	width m	Au ppm	Ag ppm	Pb %	Zn %	Cu %
18	425	0.80	2.2	0.1	130	0.10	0.20	0.03
20	425	0.50	0.5	0.0	16	0.00	0.00	0.01
20	425	0.90	1.4	2.2	354	0.10	0.70	0.03
20	425	0.70	2.1	0.0	140	0.00	0.00	0.01
22	425	0.30	0.3	0.0	6	0.00	0.00	0.01
22	425	1.10	1.4	1.3	378	0.10	0.30	0.02
22	425	1.30	2.7	0.0	8	0.00	0.00	0.01
24	425	1.15	1.15	1.9	428	0.40	1.10	0.04
24	425	1.20	2.35	0.0	12	0.00	0.00	0.02
26	425	0.60	0.6	2.0	960	0.40	2.10	0.06
26	425	0.70	1.3	0.0	12	0.00	0.00	0.05
26	425	0.40	1.7	1.6	592	0.50	0.70	0.11
26	425	0.60	2.3	0.0	62	0.00	0.00	0.01
28	425	1.20	1.2	1.7	1338	0.30	1.60	0.07
28	425	1.30	2.5	0.7	252	0.10	0.20	0.02
30	425	0.30	0.3	0.0	12	0.00	0.00	0.00
30	425	0.60	0.9	0.1	182	0.30	1.10	0.05
30	425	1.40	2.3	0.0	34	0.00	0.00	0.01
32	425	0.40	0.4	0.0	8	0.00	0.00	0.01
32	425	0.90	1.3	0.1	388	0.10	0.10	0.04
32	425	1.30	2.6	0.0	24	0.00	0.10	0.02
34	425	0.40	0.4	0.5	206	0.00	0.00	0.01
34	425	1.10	1.5	3.2	2803	0.60	1.70	0.05
34	425	0.70	2.2	0.1	906	0.10	0.00	0.02
36	425	0.70	0.7	0.0	170	0.00	0.00	0.01
36	425	0.70	1.4	4.4	2310	0.70	1.70	0.07
36	425	0.90	2.3	0.0	64	0.00	0.00	0.01

APPENDIX 3: FLUID INCLUSION DATA

SAMPLE	TYPE	STAGE	Th	Tm	Eq.Wt.%
941A	QTZ	2	191.7		
941A	QTZ	2	206.8		
941A	QTZ	2	209.4		
941A	QTZ	2	216.9		
941A	QTZ	2	221.7	-3.5	6.7
941A	QTZ	2	222.7	-1.7	3.1
941A	QTZ	2	224.2		
941A	QTZ	2	229.6		
941A	QTZ	2	257.2		
941B	QTZ	3	163.5	-3.5	6.7
941B	QTZ	3	165.6	-4.2	8.2
941B	QTZ	2	170.6	-3.8	7.4
941B	QTZ	2	223.4		
941B	QTZ	1	255.3		
941C	QTZ	3	129.2		
941C	QTZ	3	129.2		
941C	QTZ	3	139.7		
941C	QTZ	3	139.8	-2.4	4.5
941C	QTZ	3	139.8		
941C	QTZ	3	148.5		
941C	QTZ	3	156.5		
941C	QTZ	3	161.7		
941C	QTZ	3	161.7		
941C	QTZ	3	163.8		
941C	QTZ	3	165.2		
941C	QTZ	3	169.5		
941C	QTZ	3	183		
941C	QTZ	3	187.3		
941C	QTZ	3	191.7		
941C	QTZ	3	206.7	-0.5	0.9
941C	QTZ	3	207.5	-2.1	3.9
941C	QTZ	3	209	-3.1	5.9
941C	QTZ	3	209.9		
941C	QTZ	3	210.8		
941C	QTZ	3	214.8		
941C	QTZ	3	214.8		
941C	QTZ	3	219.4		
941C	QTZ	3	219.4		

SAMPLE	TYPE	STAGE	Th	Tm	Eq.Wt.%
941C	QTZ	2	222.2		
941C	QTZ	2	222.2		
941C	QTZ	2	227.4		
941C	QTZ	2	230.2		
942C	QTZ	2	228.3		
942C	QTZ	2	228.3		
942C	QTZ	2	229.7		
942C	QTZ	1	257.6	-3.5	6.7
9510A	QTZ	1	159	0	0
9510A	QTZ	1	177	-0.4	0.7
9510A	QTZ	1	210.8		
9510A	QTZ	1	217.3		
9510A	QTZ	1	257.6	-1.8	3.3
951A	QTZ	3	191.5		
951A	QTZ	3	208.7		
951A	QTZ	2	214.2		
951A	QTZ	3	218.3		
951A	QTZ	2	221.1		
951A	QTZ	2	224.7		
951A	QTZ	2	225.2		
951A	QTZ	1	230.2		
951A	QTZ	1	247.7		
951A	QTZ	1	251.3		
951A	QTZ	1	255.1		
951A	QTZ	1	255.8		
951A	QTZ	1	259.8		
951C	SPH	2	272.6		
953A	QTZ	2	221.7		
953A	QTZ	2	226.4		
953B	QTZ	2	203	-1.4	2.6
953B	QTZ	2	207.7		
953B	QTZ	2	208.6	0	0
953B	QTZ	2	209.3		
953B	QTZ	2	224.9		
953B	QTZ	2	228.5		
956A	QTZ	2	214.5		
956A	QTZ	2	217.5		
956A	QTZ	2	218.5		

SAMPLE	TYPE	STAGE	Th	Tm	Eq.Wt.%
956A	QTZ	2	222.1		
956A	QTZ	2	222.5	-2.1	3.9
956A	QTZ	2	226.2	-1.3	2.4
956A	QTZ	2	226.7		
956A	QTZ	2	226.8		
956A	QTZ	2	227.8	-1.7	3.1
956A	QTZ	2	228.5		
956A	QTZ	2	228.7		
956A	QTZ	2	229		
956A	QTZ	2	229.7		
956A	QTZ	2	229.7		
956A	QTZ	2	229.9		
956A	QTZ	2	230.4		
956A	QTZ	2	231.2		
956A	QTZ	1	240.7	-1.3	2.4
956A	QTZ	1	241.8		
956A	QTZ	1	241.8	-1.4	2.6
956A	QTZ	1	248.9		
956A	QTZ	1	252.4		
956A	QTZ	1	255.3		
956A	QTZ	1	258.1		
956A	SPH	2	278.3		
956B	QTZ	2	204.3	-0.8	1.4
956B	QTZ	2	204.8		
956B	QTZ	2	206.2	-2	3.7
956B	QTZ	2	207.5		
956B	QTZ	2	213.9	-2.6	4.9
956B	QTZ	2	218.3		
956B	QTZ	2	218.6		
956B	QTZ	2	221.6		
956B	QTZ	2	224.5		
956B	QTZ	2	225.3	-0.3	0.5
956B	QTZ	2	226.2		
956B	QTZ	2	226.4		
956B	QTZ	2	226.5	-2	3.7
956B	QTZ	2	227.6		
956B	QTZ	2	227.9	-2.6	4.9
956B	QTZ	2	227.9		

SAMPLE	TYPE	STAGE	Th	Tm	Eq.Wt.%
956B	QTZ	2	230.8		
956B	SPH	2	231.7	-7.8	16.6
956B	SPH	2	256.9		
956B	SPH	2	258.1		
958C	QTZ	2	228		
958C	QTZ	2	229.7		
958C	QTZ	1	257.3		
959A	QTZ	2	198.5		
959A	QTZ	2	222.8		
959A	QTZ	2	227.3	-3	5.7
959C	QTZ	2	173.6	-0.8	1.4
959C	QTZ	2	223.3		
961	QTZ	2	169.4		
961	QTZ	1	227.5		
963A	QTZ	2	210.6		
963A	QTZ	2	218.6	-3	5.7
963A	QTZ	2	220.4		
963A	QTZ	2	221.3		
963A	QTZ	1	221.8		
963A	QTZ	1	222.9		
963A	QTZ	1	255.6		
963A	QTZ	1	256.7		
963A	QTZ	1	259.9		
963A	QTZ	1	259.9		
964A	QTZ	2	181.7		
964A	QTZ	2	214.3		
964B	QTZ	2	191.7	-3.1	5.9
964B	QTZ	2	195.6		
964B	QTZ	1	206.8		
964B	QTZ	1	207.9		
964B	QTZ	1	215.4	-0.1	0.2
964B	QTZ	1	217.3	-2.1	3.9
964B	QTZ	1	220.3	-3.3	6.3
964B	QTZ	1	221.5		
964B	QTZ	1	222.4	-2.1	3.9
964B	QTZ	1	225		
964B	QTZ	1	225.8	-3.5	6.7
965A	QTZ	2	205.6		

SAMPLE	TYPE	STAGE	Th	Tm	Eq.Wt.%
965A	QTZ	2	206.7		
965A	QTZ	2	212		
965A	QTZ	2	212.9	-2.5	4.7
965A	QTZ	2	213.1	-0.5	0.9
965A	QTZ	2	217.9	-1.1	2
965A	QTZ	2	222.1		
965A	QTZ	2	226.7	-3.3	6.3
965A	QTZ	2	227.8		
965C	QTZ	2	147.7		
965C	QTZ	2	222.6		
965C	QTZ	2	228.3		
965C	QTZ	2	230.8		
965C	QTZ	2	232.7		
966A	QTZ	3	185.4	-3.2	6.1
966A	QTZ	3	192.9	-3.7	7.2
966A	QTZ	3	197.7		
966A	QTZ	3	197.7		
966A	QTZ	3	199.8		
966A	QTZ	2	200.9		
966A	QTZ	2	201		
966A	QTZ	2	204.8		
966A	QTZ	2	205.1	-3.5	6.7
966A	QTZ	2	205.1	0	0
966A	QTZ	3	205.6		
966A	QTZ	2	208.7		
966A	QTZ	2	209.6		
966A	QTZ	2	212.6		
966A	QTZ	2	217		
966A	QTZ	2	217.4		
966A	QTZ	2	217.8	-1.7	3.1
966A	QTZ	2	217.8		
966A	QTZ	3	218.7		
966A	QTZ	2	219.7		
966A	QTZ	2	219.8	-2.5	4.7
966A	QTZ	2	220.9		
966A	QTZ	3	225		
966A	QTZ	2	226.5	-2.5	4.7
966A	QTZ	2	226.5	-2.5	4.7

SAMPLE	TYPE	STAGE	Th	Tm	Eq.Wt.%
966A	QTZ	2	227.2		
966A	QTZ	2	227.5	-0.2	0.4
966A	QTZ	2	233	-2.9	5.5
966B	QTZ	2	206.7		
966B	QTZ	2	219.6		
966B	QTZ	2	219.9		
966B	QTZ	2	222.9		
966B	QTZ	2	225.7		
966B	QTZ	2	228.1		
966B	QTZ	2	228.1		
966B	QTZ	2	229.1	-3	5.7
966B	QTZ	2	229.3		
966B	QTZ	2	229.8		
966B	QTZ	2	230.4		
966B	QTZ	2	232.1		
966B	QTZ	1	255.1		
966B	QTZ	1	264.4		
966C	QTZ	3	169.8	-2.8	5.3
966C	QTZ	3	181.7		
966C	CAL	3	185.4	-3.2	6.1
966C	QTZ	3	193.3	-4	7.8
966C	QTZ	3	194.2		
966C	QTZ	3	195.7		
966C	QTZ	2	196.5		
966C	CAL	3	197.5	-2.9	5.5
966C	QTZ	3	197.7		
966C	CAL	3	197.7	-2.5	4.7
966C	QTZ	2	199.1		
966C	QTZ	2	203.3	-1.7	3.1
966C	QTZ	2	203.5	-0.5	0.9
966C	QTZ	2	204.4	-1	1.8
966C	QTZ	2	209		
966C	CAL	3	209.6	-2.3	4.3
966C	QTZ	2	211.2		
966C	QTZ	2	215		
966C	QTZ	2	217.3		
966C	CAL	3	217.4	-2.5	4.7
966C	QTZ	2	218.2		

SAMPLE	TYPE	STAGE	Th	Tm	Eq.Wt.%
966C	CAL	3	219.8		
966C	QTZ	2	221.5		
966C	CAL	1	226.5		
966C	CAL	1	226.5		
966C	QTZ	2	227.2		
966C	QTZ	2	228.9		
966C	QTZ	2	229.1		
966C	QTZ	2	230		
966C	QTZ	2	230.4		
966C	QTZ	1	231.3		
966C	CAL	1	233		
966C	QTZ	1	233.2		
966C	QTZ	1	240.5	-3.1	5.9
SURF	CAL		167.8	-1.5	2.8
SURF	CAL		178		
SURF	CAL		178.2	-1.5	2.8
SURF	CAL		184		
SURF	CAL		187.8		
SURF	CAL		192.2		
SURF	CAL		194.8		
SURF	CAL		198		
SURF	CAL		199.2		
SURF	CAL		199.7		
SURF	CAL		202.9	-0.7	1.3

REFERENCES

Albinson, T. F., 1988, Geologic reconstruction of paleosurfaces in the Sombrerete, Colorada, and Fresnillo districts, Zacatecas State Mexico: Econ. Geol., v. 83, p. 1647-1667.

Benton, L.D., 1991, Composition and source of the hydrothermal fluids of the Santo Niño vein, Fresnillo, Mexico as determined from $^{87}Sr/^{86}Sr$, stable isotope, and gas analyses: Unpub. M.S. thesis, N.M. Institute of Mining and Technology, 55 p.

Barton, P.B, Jr., Bethke, P.M., and Roedder, E., 1977, Environment of ore deposition in the Creede mining districts, San Juan Mountains, Colorado: Econ. Geol., v. 72, p. 1-24.

Bodner, R. J., Reynolds, T. J., and Kuehn, C. A., 1985, Fluid inclusions systematics in epithermal systems: Rev. Econ. Geology, v. 2, p. 73-98.

Buchanan, L. J., 1981, Precious metal deposits associated with volcanic environments in the southwest: Geol. Soc. Arizona Digest, v. 14, p. 237-261.

Campa, M. F., and Coney, P. J., 1983, Tectono-stratigraphic

terranes and mineral resource distributions in Mexico: Canadian Jour. Earth Sci., v. 20, p. 1040-1051.

Chico, E., 1986, Mineralogy, paragenesis, and fluid inclusion studies in three veins of the Fresnillo mining district, Zacatecas, Mexico: Unpub. M.S. thesis, Dartmouth College, 115 p.

Clark, K. F., Foster, C. T., and Damon, P. E., 1982, Cenozoic mineral deposits and subduction-related magmatic arcs in Mexico: Geol. Soc. America Bull., v. 93, p. 533-544.

Cumming, G. L., Kesler, S. E., and Krstic, D., 1979, Isotopic composition of lead in Mexican mineral deposits: Econ. Geol., v. 74, p. 1395-1407.

de Cserna, Z., 1976, Geology of the Fresnillo area, Zacatecas, Mexico: Geol. Soc. America Bull., v. 87, p. 1191-1199.

Garcia, E. M., Querol, F. S., and Lowther, G. K., 1991, Geology of the Fresnillo mining district, Zacatecas: in The Geology of North America, v. P-3, Economic Geology, Mexico, The Geological Society of America, p. 383-394.

Gemmel, J. B., Simmons, S. F., and Zantop, H., 1988, The Santo Nino silver-lead-zinc vein, Fresnillo, Zacatecas, Mexico: Part 1. Structure, vein stratigraphy, and mineralogy: Econ. Geol., v. 83, p. 1597-1618.

Hayba, D. O., Bethke, P. M., Heald, P., and Foley, N. K., 1985, Geologic, mineralogic and geochemical characteristics of volcanic-hosted epithermal precious-metal deposits: Rev. Econ. Geology, v. 2, p. 129-168.

Kacura, G., 1968, Genesis of mineral and thermal waters: Report of the 23rd Session of Int. Geological Congress, 212 p.

Lang, B., Steinitz, G., Sawkins, F. J., and Simmons, S. F., 1988, K-Ar age studies in the Fresnillo silver district, Zacatecas, Mexico: Econ. Geol., v. 83, p. 1642-1646.

MacDonald, A. J., Kreczmer, M. J., and Kesler, S. E., 1986, Vein, manto, and chimney mineralization at the Fresnillo silver-lead-zinc mine, Mexico: Canadian Jour. Earth Sci., v. 23, p. 1603-1614.

Querol, F., and Palacios, H., 1990, Geology of the Fresnillo mining district, Zacatecas: Unpub. in house Rept.,

Compania Fresnillo, S.A. de C.V., 15 p.

Reed, M. H., and Spycher, N., 1985, Boiling, cooling, and oxidation in epithermal systems: a numerical modeling approach: Rev. Econ. Geology, v. 2, p. 249-272.

Robinson, R.W., and Norman, D.I., 1984, Mineralogy and fluid inclusions study of the Southern Amethyst Vein System, Creede mining district, Colorado: Econ. Geol., v. 79, p. 439-447.

Ruvalcaba-Ruiz, D., and Thompson, T., 1988, Ore deposits at the Fresnillo mine, Zacatecas, Mexico: Econ. Geol., v. 83, p. 1583-1596.

Seward, T.M., 1976, The stability of chloride complexes of silver in hydrothermal solutions up to 350 $^\circ$C: Geochim. et Cosmochim. Acta, v. 40, p. 1329-1341.

Shepherd, T. J., Rankin, A. H., and Alderton, D. H. M., 1985, A practical guide to fluid inclusion studies: Blackie and sons, 239 p.

Simmons, S. F., 1986, Physico-chemical nature of mineralizing

solutions for the Santo Nino vein: Results from fluid inclusion, hydrogen, oxygen, and helium studies in the Fresnillo district, Zacatecas, Mexico: Unpub. Ph.D. thesis, Univ. Minnesota, Minneapolis, 204 p.

-------1991, Hydrologic implications of alteration and fluid inclusion studies in the Fresnillo district, Mexico: Evidence for a brine reservoir and a descending water table during the formation of hydrothermal Ag-Pb-Zn orebodies: Econ. Geol., v. 86, no. 8, p. 1579-1600.

-------, Gemmel, J. B., and Sawkins, F. J., 1988, The Santo Nino silver-lead-zinc vein, Fresnillo district, Zacatecas, Mexico: Part 2. Physical and chemical nature of ore-forming solutions: Econ. Geol., v. 83, p. 1619-1641.

Stone, J. B., and McCarthy, J. C., 1942, Mineral and metal variations in the veins of Fresnillo, Zacatecas, Mexico: Am. Inst. Mining Metall. Petroleum Engineers Trans., v. 178, p. 91-106.

Welton, J.E., 1984, SEM petrology atlas: AAPG publication, 237 p.

This thesis is accepted on behalf of the faculty
of the Institute by the following committee:

_____
                    Adviser

_____

_____

_____

_____

_____
                    Date